Igor Acoob Varagilal
Licenciado em Ciências de Engenharia Civil

Stability analysis of gravity dams for the maximum design earthquake

Dissertação para obtenção do Grau de Mestre em
Engenharia Civil – Perfil de Estruturas

Orientador: João Rocha de Almeida, Professor Associado, Faculdade de Ciências e Tecnologia da Universidade Nova de Lisboa

Co-orientador: Nuno Monteiro Azevedo, Investigador Auxiliar, Departamento de Barragens de Betão, Laboratório Nacional de Engenharia Civil

Presidente: Professor Doutor Daniel Aelenei

Arguente: Doutor Sérgio Martins Oliveira

Vogal: Professor Doutor João C. G. R. Almeida

FACULDADE DE CIÊNCIAS E TECNOLOGIA
UNIVERSIDADE NOVA DE LISBOA

Maio 2018

Igor Acoob Varagilal
Licenciado em Ciências de Engenharia Civil

Stability analysis of gravity dams for the maximum design earthquake

Dissertação para obtenção do Grau de Mestre em
Engenharia Civil – Perfil de Estruturas

Orientador: João Rocha de Almeida, Professor Associado, Faculdade de Ciências e Tecnologia da Universidade Nova de Lisboa

Co-orientador: Nuno Monteiro Azevedo, Investigador Auxiliar, Departamento de Barragens de Betão, Laboratório Nacional de Engenharia Civil

Maio 2018

Stability analysis of gravity dams for the maximum design earthquake

ACKNOWLEDGEMENTS

The completion of this thesis is the final chapter of my academic life, that lasted 5 years full of hard-work and dedication that would not have been possible without the following people:

Dr. João Rocha de Almeida, thesis supervisor, for his guidance during my academic life. His notes and advices were often fundamental to improve my work. I would also like to thank him for providing me this exceptional experience to work in LNEC, where I learned valuable academic and personal lessons.

Dr. Nuno Monteiro Azevedo, thesis co-advisor, for his tireless pursue of excellence and his never-ending availability to clarify any existing doubts about the program he himself created and developed. Without his extra efforts this thesis would not exist.

Dr. Maria Luísa Braga Farinha, for her invaluable guidance and for always providing me every material I needed to fully understand the problems ahead. Her continued encouragement and kindness, no matter the circumstances, were always a good incentive to keep pushing forward.

I would like to thank LNEC for granting me the means to develop this thesis within the framework of the research project "DAMFA: Cutting-edge solutions for sustainable assessment of concrete dam foundations" which has been carried out jointly by the National Laboratory for Civil Engineering (LNEC) and NOVA.ID.FCT – Associação para a Inovação e Desenvolvimento da Faculdade de Ciências e Tecnologia (FCT) da Universidade Nova de Lisboa".

I would also like to thank the EDP – *Energias de Portugal* and *Agência Portuguesa do Ambiente* (APA) representatives who allowed me to follow an inspection visit to Pocinho dam, explaining me all the details I wished to know in my first inspection visit to a dam.

I would also like to thank the master and doctoral students and researchers from the Concrete Dams Department of LNEC for their laugh and friendship throughout these six months: Patrícia Reis, Cláudia Manco, André Alegre, Miguel Rodrigues, David Pereira, Pedro Miranda and Renato Pereira.

To my university colleagues and friends that accompanied me during my journey. You are too many to enumerate but I hope you know how much your support and warm words meant to me.

To my partner, Zuzana Marešová for her unquestionable support and friendly shoulder in the right moments. Her patience and love were always a source of energy for me.

Lastly, I would like to thank my mom and my dad for always being my foundation rock. They are the role-models of what I aspire to be every day, a strong, motivated and independent person. Thank you is not enough.

RESUMO

Neste trabalho é realizada uma análise de estabilidade de barragens gravidade considerando o sismo máximo de projeto. Tem-se em conta a interação entre o comportamento mecânico e hidráulico do maciço rochoso de fundação das obras.

Apresentam-se os aspetos mais relevantes relativos a barragens gravidade e as principais causas de rotura. São referidas recomendações atualmente em vigor, consideradas pelo Comité de Segurança Sísmica da Comissão Internacional das Grandes Barragens (ICOLD). Os principais fundamentos de aplicação sísmica nos modelos numéricos desenvolvidos são também apresentados, nomeadamente o modelo de massas associadas, que de forma simplificada representa a interação dinâmica entre o reservatório e o paramento de montante da barragem, as condições de fronteira adequadas para um método explícito e as hipóteses de amortecimento.

São analisadas duas barragens de altura diferente, fundadas em maciços rochosos de geometria idêntica com descontinuidades horizontais e verticais. Considera-se a existência de cortina de impermeabilização e de sistema de drenagem na fundação das obras. É efetuada uma análise bidimensional considerando um modelo descontínuo usando o programa Parmac2D-FFlow. Os deslocamentos na base da barragem, tanto no pé de montante como no pé de jusante, são comparados para a hipótese de amortecimento de Rayleigh e para o amortecimento considerando somente o termo de massa. Em todos os casos estudados são consideradas duas situações de comportamento da fundação: i) comportamento não-linear da junta barragem/fundação e comportamento elástico da zona da fundação fraturada e ii) comportamento não-linear da junta barragem/fundação e da zona fraturada da fundação. Os resultados apresentados permitem analisar o efeito da aceleração de pico e tirar conclusões sobre o efeito da rigidez normal das interfaces no comportamento de barragens gravidade sob ações sísmicas.

Palavras-chave: barragem gravidade, fundação rochosa, modelação numérica, comportamento hidrodinâmico, deslizamento, amortecimento de Rayleigh.

ABSTRACT

This thesis presents a two-dimensional hydrodynamic stability analysis of gravity dams for the maximum design earthquake. The coupled mechanical and hydraulic behavior of the dam's rock mass foundation is taken into account.

The main aspects concerning gravity dams are presented along with their main failure causes. The safety rules currently in use and approved by the International Commission on Large Dams (ICOLD) Seismic Committee are presented. The fundamental elements of seismic application relevant for the models used in this work are also presented, such as the dynamic interaction between the reservoir and the upstream face of the dam, adequate boundary conditions for an explicit method and different damping hypotheses.

Two dams of different height are numerically analysed. Both dams have rock mass foundations with identical geometry, with horizontal and vertical discontinuities, and the grout and drainage curtains are simulated. Analysis is carried out with a discontinuum model, Parmac2D-FFlow. The displacements at the base of the dam, both on the dam's heel and the dam's toe, are compared for the Rayleigh damping hypothesis and the mass proportional term damping. In every case studied two different situations regarding the dam foundation behavior are considered: i) non-linear behavior of the dam/foundation interface and elastic behavior of the fractured rock mass area and ii) non-linear behavior of both the dam/foundation interface and the joints in the fractured rock mass area. The results presented allow the analysis of the effect of the peak ground acceleration to be carried out. Conclusions are drawn regarding the effect of joint normal stiffness on the behavior of gravity dams due to seismic loads.

Keywords: gravity dam, rock mass foundation, numerical modelling, hydrodynamic behavior, shear sliding, Rayleigh damping.

TABLE OF CONTENTS

LIST OF FIGURES

LIST OF TABLES

LIST OF SYMBOLS

[C]	damping matrix [-]
[K]	stiffness matrix [-]
[M]	mass matrix [-]
a	fracture aperture [L]
A	cross section area [L^2]
a_h	hydraulic aperture [L]
A_i	area of the influence of the nodal point [L^2]
a_{max}	maximum hydraulic aperture [L]
a_{min}	minimum hydraulic aperture [L]
a_o	fracture aperture free of normal stresses [L]
b	width [L]
C	cohesion [$L^{-1}MT^{-2}$]
c	damping constant [-]
C_{cr}	critical damping [-]
C_p	pressure wave propagation velocity through a continuous medium [LT^{-1}]
C_s	shear wave propagation velocity through a continuous medium [LT^{-1}]
E	Young's modulus [$L^{-1}MT^{-2}$]
f	frequency [T^{-1}]
F_{int}	internal forces [LMT^{-2}]
g	acceleration of gravity [LT^{-2}]
G	shear modulus [$L^{-1}MT^{-2}$]
H	height of the reservoir [L]
h	dam height [L]
H'	height of the water downstream from the dam [L]

H_2	function of the dam height [L]
i	two-dimensional hydraulic gradient [LL^{-1}]
I	moment of inertia [L^4]
K	foundation bulk modulus [$L^{-1}MT^{-2}$]
k	permeability factor [L^2]
k_{ce}	seepage channel permeability factor [$LM^{-1}T$]
k_f	fractured hydraulic conductivity [LT^{-1}]
k_n	interface normal contact stiffness [$L^{-2}MT^{-2}$]
k_s	interface shear contact stiffness [$L^{-2}MT^{-2}$]
k_w	water bulk modulus [$L^{-1}MT^{-2}$]
l	length [L]
m	mass [M]
M	bending moment [$M\ L^2\ T^{-2}$]
m_i	mass associated with nodal point i [M]
p	applied uniform load [$M\ L^{-1}\ T^{-2}$]
q	flow rate per unit length [L^3T^{-1}]
Q	flow rate [$L^3\ T^{-1}$]
R	function of the safety factor [$L^{-1}MT^{-2}$]
s	seconds [T]
s_f	safety factor [-]
t	time [T]
u_n	joint normal displacement (aperture and closing) [L]
v	velocity of the fluid in a certain point, velocity [LT^{-1}]
v_{hist}	history value velocity [LT^{-1}]
v_p	pressure wave velocity [LT^{-1}]
v_{ref}	reference velocity [LT^{-1}]

v_s	shear wave velocity [LT^{-1}]
y_i	elevation [L]
z	distance from a compressed or tensioned fiber to the neutral axis [L]
α	mass proportional damping ratio [-]
α_{fr}	viscous boundary damping ratio [-]
β	stiffness proportional damping ratio [-]
γ_c	unit weight of concrete [$L^{-2}MT^{-2}$]
γ_r	unit weight of the rock mass foundation [$L^{-2}MT^{-2}$]
γ_w	unit weight of the water [$L^{-2}MT^{-2}$]
δ	displacement [L]
Δa	variation in the aperture [L]
Δt	timestep [T]
θ	inclination of the upstream face of the dam [-]
v_k	kinematic viscosity of the fluid [L^2T^{-1}]
ξ	relative damping ratio [-]
ρ	density [$L^{-3}M$]
ρ_c	concrete density [$L^{-3}M$]
ρ_f	foundation density [$L^{-3}M$]
ρ_w	water density [$L^{-3}M$]
σ	stress [$L^{-1}MT^{-2}$]
σ_0	function of the safety factor [$L^{-1}MT^{-2}$]
σ_c	compressive stress [$L^{-1}MT^{-2}$]
σ_i	principal stress “i“ [$L^{-1}MT^{-2}$]
σ_n	normal stress [$L^{-1}MT^{-2}$]

σ'_n	effective normal stress [$L^{-1}MT^{-2}$]
σ_t	tensile stress [$L^{-1}MT^{-2}$]
τ	shear stress [$L^{-1}MT^{-2}$]
τ_{ref}	reference shear stress [$L^{-1}MT^{-2}$]
υ	Poisson's ratio [-]
Φ	total head, hydraulic potential, hydraulic head, piezometric head, head [L]
φ	friction angle [-]
ω	fundamental natural frequency [T^{-1}]

OFFICIAL BODIES

APA	Agência Portuguesa do Ambiente
DBB	Departamento de Barragens de Betão
EDP	Energias de Portugal
FCT/UNL	Faculdade de Ciências e Tecnologia da Universidade Nova de Lisboa
ICOLD	International Commission on Large Dams
INAG	Instituto da Água
LNEC	Laboratório Nacional de Engenharia Civil
NOVA.ID.FCT	Associação para a Inovação e Desenvolvimento da FCT

ABBREVIATIONS

2D	2 dimensions
3D	3 dimensions
CE	construction earthquake
DBE	design basis earthquake
EAP	emergency action plans

FEM	finite element method
HN	hydraulic node
JE	joint element
MC	Mohr-Coulomb
MCE	maximum credible earthquake
MDE	maximum design earthquake
OBE	operating basis earthquake
PGA	peak ground acceleration
PSHA	probabilistic seismic hazard analysis
RCC	roller-compacted concrete
SC	seepage channel
SEE	safety evaluation earthquake

1 INTRODUCTION

1.1 Background

Dams are built on rivers or water streams with the purpose of storing water. The need to construct dams all over the world is not recent and goes back 5 000 years, proving to be a necessary element for populations to adapt and improve their quality of life. However, more than half of the dams that exist today were built in the past 50 years due to the steadily increasing demand for water resources and to technology advances (INAG, 2001).

According to the International Commission on Large Dams (ICOLD), the world population has increased by a factor of 8 in the past century and the demand for water resources naturally followed this tendency. Moreover, hydropower production which is generated without polluting the atmosphere is a major advantage that pushes technology advances for dams.

A dam with a height greater than 15 metres measured from the lowest foundation to the crest, or a dam between 5 and 15 metres high with a reservoir storage of more than 3 million cubic metres is considered a large dam (ICOLD, 2017). When a large dam is constructed, it can be a single-purpose or it can be a multi-purpose dam. Nowadays, according to ICOLD, there are 28 614 single-purpose large dams and 9 930 multipurpose large dams. Irrigation accounts for almost 50 % of the single purpose dams, but hydropower, water supply and flood control are among other main purposes for a dam (ICOLD, 2017). Figure 1.1 shows the distribution for each purpose of single-purpose dams and the distribution for purposes of multipurpose dams.

The most common way to characterize a dam is based on the material used to construct it. Dams can be built of earth or rocks and be called embankment dams or be built of concrete or masonry. The concrete or masonry dams are of three main types: gravity dams, arch dams and buttress dams. Each of these three different types has a different structural behavior. Figure 1.2 shows the highest dams of each one of these types. The Grande Dixence dam (Figure 1.2 a)) is a concrete gravity dam for energy production, situated in Switzerland, with a maximum height of 285 m. Jinping 1 dam (Figure 1.2 b)), in China, concluded in 2013, is a 305 m high double curvature arch and is now the highest dam of the world, being designed to supply energy, improve flood protection and prevent erosion. Roselend dam (Figure 1.2 c)) is a buttress dam with a maximum height of 150 m, located in France. This dam is mainly destined to energy production.

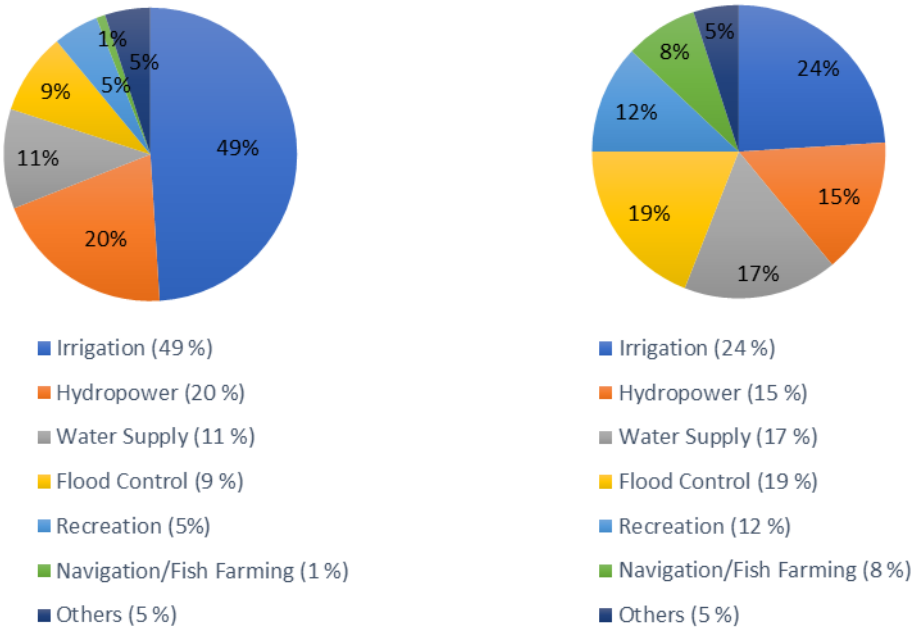

a) Single-purpose dams b) Multi-purpose dams

Figure 1.1 – Single-purpose and multi-purpose dams' distribution

Concrete and masonry dams have their foundations in rock masses, which are made of rock blocks separated by discontinuities that result from natural events. Thus, the foundation structure is discontinuous, anisotropic and heterogenous. Rock masses on which dams are built are usually treated with the purpose of improving their mechanical and hydraulic characteristics.

In case of an accident, the social, economic and environmental damage can be very significative; therefore, dams are considered as very high-risk structures. To minimize the risk, there is a growing concern in designing and constructing a dam and very strict monitoring plans are followed for safety control. Following accidents in the Malpasset dam (France 1959) and the Vajont dam (Italy 1963) (Anderson, Mohorovic, Mogck, Cohen, & Scott, 1998), the importance of the mechanical and hydraulic characteristics of the foundation rock mass was highlighted. In a dam foundation, there is continuous passage of water through the rock masses discontinuities from the reservoir towards downstream.

a) Grande Dixence dam (www.swissinfo.ch/eng)

b) Jinping 1 dam (www.chinadaily.com.cn)

c) Roselend dam (www.structurae.net)

Figure 1.2 – The world's highest gravity, arch and buttress dams

The mechanical and hydraulic behaviors are not independent: alterations in the stress state of the rock mass lead to the opening or closing of the dam foundation discontinuities, changing the paths through where the water flows. At the same time, these alterations in the hydraulic behavior change the stress field.

Although there are no recorded life losses so far following a concrete dam's failure caused by an earthquake, there are several reports of local cracks that reduce the structure safety. Consequently, seismic action must be taken into account when designing new dams as well as when reassessing the safety of operating dams.

The study of the coupled hydromechanical behavior taking into account hydrodynamic components requires numerical tools with a certain degree of complexity. In addition to being necessary the use of heavy calculation programs, it is required to fully know the mechanical and hydraulic characteristics of the rock mass, as well as its geometry, which can be very difficult to characterize due to its heterogeneity. Therefore, it is not easy to develop a realistic model. To evaluate the seismic action, data from a real earthquake is required, such as velocity or stress history records, in order to simulate the structural response.

The numerical models used to perform seismic stability evaluation of dams can be of two types: continuum equivalent models or discontinuous models. The main difference between these two approaches is the representation of the rock mass discontinuities. The choice between the continuum or discontinuum approach depends on many specific factors, namely the joint pattern, the spacing of the discontinuities and their influence on the overall behavior. These two distinct types of models may be combined and used simultaneously.

The numerical investigation presented here was developed as part of the research project "DAMFA: Cutting-edge solutions for sustainable assessment of concrete dam foundations" which has been carried out jointly by the National Laboratory for Civil Engineering (LNEC) and *NOVA.ID.FCT – Associação para a Inovação e Desenvolvimento da Faculdade de Ciências e Tecnologias* (FCT) *da Universidade Nova de Lisboa"*.

1.2 Objectives and methodology

The main objective of this research is to assess the stability of a concrete gravity dam for a shear sliding failure scenario under the maximum design earthquake (MDE) loading, taking into account the coupled hydromechanical behavior of the dam foundation.

The numerical investigation is carried out with two dams of different height and foundations with the same joint pattern. The effect of the dam/foundation interface stiffness on shear sliding displacements is evaluated. The results obtained using two different damping approaches are discussed and compared.

1.3 Thesis outline

The thesis is divided into 6 chapters. The first chapter presents the subject of the thesis and the main goals that are set to be achieved. Chapter 2 presents the main characteristics of gravity dams. Reference is made to the current state of safety aspects and earthquake safety, not only of existing dams but also of dams that are to be constructed. A brief description of the visit to Pocinho dam that occurred in the follow up of this work is also presented. The next two chapters, 3 and 4, present the theoretical and practical elements for the hydromechanical and hydrodynamic studies. In the end of each of these chapters one example of a computer simulation carried out with the program Parmac2D-FFlow is presented. Chapter 5 presents the numerical models of two gravity dams of different height and the results of the correspondent dynamic stability analyses which were carried out. Parametric studies were done in order to assess the influence of the dam/foundation interface stiffness on sliding displacements. The final chapter presents the main conclusions of this thesis and some suggestions for further developments.

2 GRAVITY DAMS

Gravity dams, as previously mentioned, are one of the main types of concrete or masonry dams, along with buttress and arch dams. The studies in this thesis focus only on the behavior of concrete gravity dams during an earthquake.

In the case of concrete gravity dams, the seismic evaluation should consider the maximum design earthquake, MDE, and the possibility of sliding along the dam/foundation interface. The structural behavior and the main failure causes of these constructions are presented. In addition, the safety aspects for concrete gravity dams against earthquakes considered at the design stage and during the dam operation are mentioned. A reference is made to the monitoring plans designed for structural safety control during the dam's life span and to emergency plans in case of failure. Lastly, a brief description of the visit to Pocinho dam is presented.

2.1 Structural stability

Gravity dams are designed and built to rely entirely on their self-weight to balance the pressure on the dam caused by the water stored in the reservoir, transferring the actions to the foundation. The typical cross section of a gravity dam is a triangle and the base width is, normally, 80 % of the height, as shown in Figure 2.1 (INAG, 2001).

In plan, gravity dams can be straight or with a slight curvature. Gravity dams are suited for wide valleys and require sound rock masses as foundation. The first gravity dams were constructed with masonry blocks, but since the 19th century their main material is mass concrete or roller compacted concrete, RCC.

The main forces to consider while designing gravity dams are presented in Figure 2.2: hydrostatic pressure on both upstream and downstream sides of the dam, self-weight and the uplift pressure caused by the presence of water in the rock mass discontinuities. When a dynamic analysis is carried out, both hydrodynamic pressure and inertia forces must be considered. Thermal variations are only relevant during the construction and result from heat release from the cement. Seepage through the foundation may give rise to other problems, such as erosion of the rock mass.

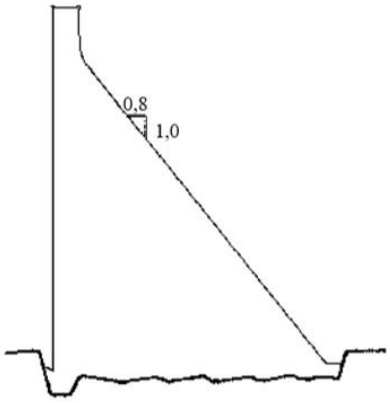

Figure 2.1 - Gravity dam. Typical cross section (adapted from INAG, 2001)

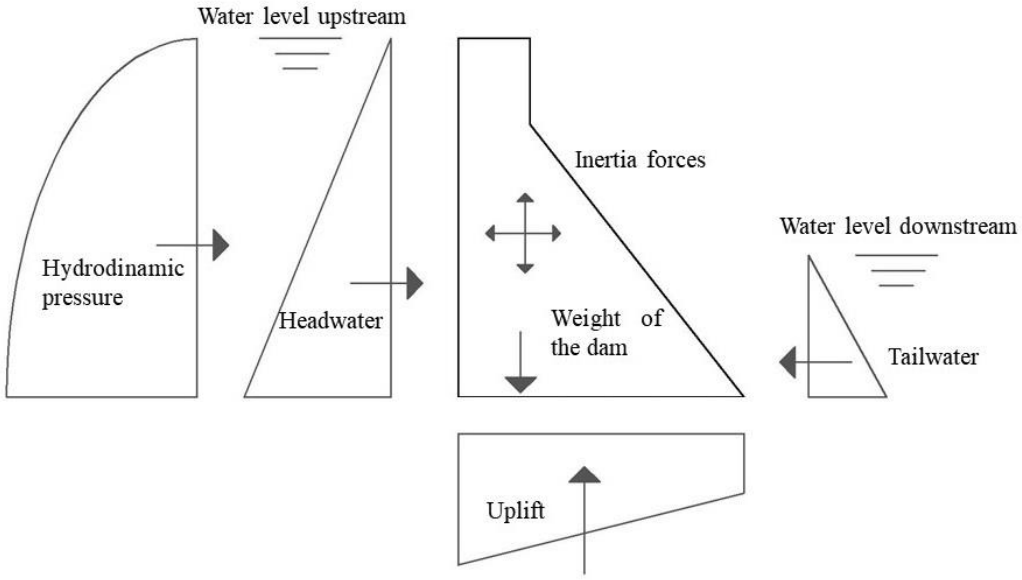

Figure 2.2 – Main forces acting on a concrete gravity dam (adapted from www.hydroworld.com)

When designing and assessing the safety of a gravity dam, it is very important to ensure safety against sliding. On the contrary, overturning around a left abutment/right abutment axis is not usually considered. Nevertheless, earthquakes can cause sliding of a gravity dam and high tensile stresses may build up close to the crest of the dam.

It is very important to ensure that a dam continues to be structurally stable during and after an earthquake, as the consequences of a failure can be catastrophic. After the Wenchuan earthquake in China in May 12, 2008, the problem of dam stability after an earthquake was highlighted. The earthquake had the epicenter near the city of Dujiangyan at a depth of 19 km below the surface and

a magnitude of 7.9 in the Richter scale. Due to the earthquake, around 69 000 people were killed, 80 % of the city buildings were destroyed and 403 hydropower plants were damaged. The Committee on Seismic Aspects of Dam Design of ICOLD has recently addressed the state of the seismic design and safety aspects of large dams (Wieland, 2016; ICOLD, 2016).

2.2 Main failure causes

The main problems that can occur in gravity dams are:

i) lack of shear resistance in the dam/rock mass foundation interface or in the rock mass discontinuities;

ii) loss of connection to the rock mass foundation due to high tensile stresses;

iii) high quantities of water that flow through the dam foundation.

In a rock mass, failure is frequently controlled by the presence of discontinuities such as faults, shear zones, bedding planes and joints (Hoek, 2017). Due to lack of shear resistance of the discontinuities, deformation and failure are caused by sliding along individual discontinuity surfaces or along other planes such as the interface between the dam and the rock mass. The failure of the intact rock is rarely a problem. Because the area of the interface between the dam and the rock mass is very large, the uplift pressure is substantial, acting as an opposite force to the self-weight. The water pressure at the upstream face of the dam can also be harmful to the dam if the construction joints in the dam's body are, by some reason, altered.

The loss of connection with the foundation at the heel of the dam is a problem that can occur in concrete gravity dams. The hydrostatic pressure on the upstream face of the dam transmits tensile stresses to the heel of the dam and to the rock mass foundation. The cycle of filling and emptying a reservoir creates stresses and deformation cycles in the foundation, opening and closing horizontal and sub-horizontal discontinuities, eventually producing new cracks and increasing the length of the existent ones.

The identification and analysis of the main accident scenarios that have taken place in concrete dams has been the subject of numerous groups. Some studies, carried out by several ICOLD committees, have concluded that for concrete dams most of the recorded failures were due to problems in the foundation rock mass.

Weathering processes due to erosion and dissolution actions in rock masses normally leads to the loss of strength of the foundation, ultimately causing the failure of a dam. Another factor that underlines the importance of the rock mass foundation of a dam is the lack of shear resistance in rock masses along weak planes of unfavorable direction.

The first filling of a reservoir corresponds to the first loading test of a dam. Therefore, it is extremely important to follow the structural behavior during this phase. As an example, the Austin dam in Austin, Pennsylvania, USA, collapsed in January 1911 due to a structural failure with foundation sliding during unusually heavy rains. The dam was 15 m high and 165 m long and was constructed on horizontally bedded sandstone with interbedded layers of shale and disintegrated sandstone. The failure occurred when the foundation slid in one of its weaker layers (Anderson et al., 1998). Figure 2.3 shows Austin dam after the accident.

Figure 2.3 - Austin dam ruins (pabook2.libraries.psu.edu/palitmap/AustinDam.html)

2.3 Dam safety against earthquakes

The seismic design criteria and methods of dynamic analysis of dams have undergone substantial changes since the 1930's when earthquake action was introduced in the design of large concrete dams. In fact, large dams were the first structures to be systematically designed against earthquakes (Wieland, 2016).

When selecting the seismic parameters, the type of dam and the possible modes of failure must be considered, along with the site hazard and the structure risk rating (Bozovic, 1989). In the case of gravity dams, both stress and stability assessments need to be performed, as well as additional assessments related to appurtenant structures, foundation and reservoir bank (Darbre, 2004).

Several types of analysis can be performed, either preliminary or more elaborate. For straight concrete gravity dams, a two-dimensional model is generally sufficient for a simplified analysis. For a more complex analysis, a finite element method (FEM) analysis is usually performed, which for the case of gravity dams, can also be planar. Dynamic finite element response analyses may be performed using either response spectra or acceleration time histories. If linear elastic behavior is assumed, both procedures are considered appropriate. However, if non-linear analysis is contemplated, acceleration time histories must be used exclusively (Darbre, 2004).

One of the most well-known incidents of a gravity dam subjected to an earthquake, which showed that earthquake safety requires proper attention, happened in December 1967 in Koyna dam, in India. The dam is located on the river Koyna and stands 103 m high and 853 m long (Figure 2.4). Although the structure of the dam was only designed to withstand seismic accelerations of 0.05 g, one accelerograph located in the gallery of one of the dam's monoliths recorded peak ground accelerations as high as 0.63 g in the horizontal direction parallel to the dam axis. The dam safely withstood the seismic activity, but the reservoir had to be lowered for inspection and the entire dam was locally repaired and strengthened.

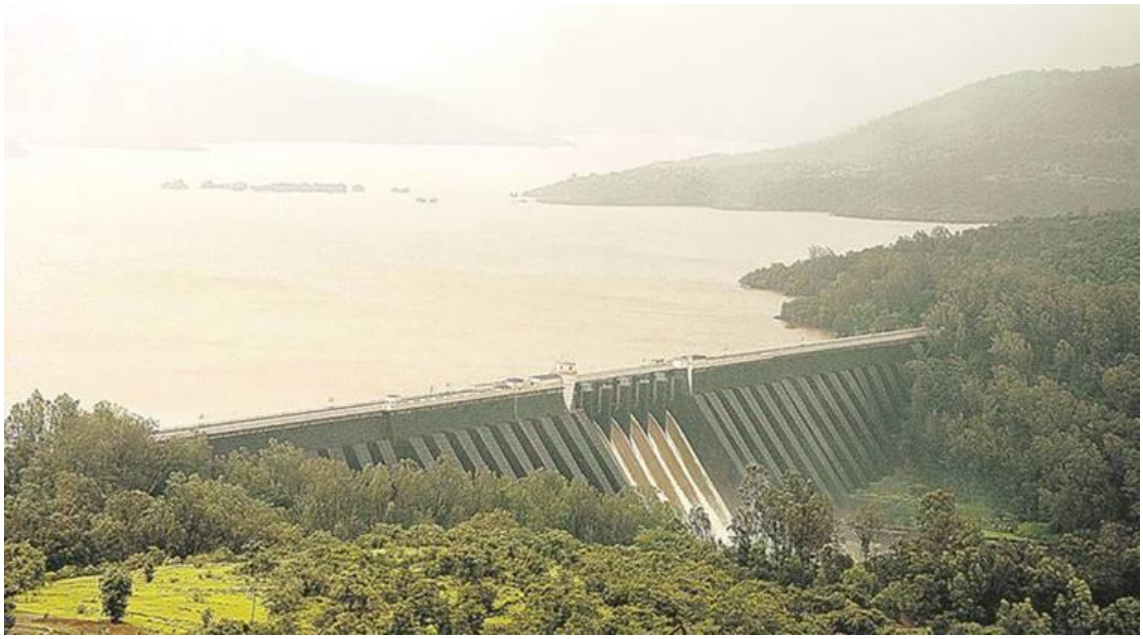

Figure 2.4 - Koyna dam view (adapted from http://indianexpress.com/article/india/studying-seismic-activity-epicentre-zone-shifting-towards-warna-reservoir-4950512/)

The two main goals of every safety concept for large storage dams and infrastructure projects are the minimization of all risks and the mastering of the remaining risk in the best conceivable way. Therefore, for sustainable storage dams emphasis must be placed on the long-term safety of the dam. To reach these goals, a comprehensive safety concept is adopted, comprising the following key elements (Wieland, 2012):

i) structural safety;

ii) dam safety monitoring;

iii) operational safety;

iv) emergency planning.

A brief review of each of these items is presented below.

2.3.1 Structural safety

Structural safety is the main prerequisite for the safe operation of any structure. A large dam must be designed according to internationally accepted criteria against natural environment, man-made

environment and project and site-specific hazards. The design must be carried out assuming the dam may become exposed to the worst possible scenarios.

In the past, the seismic coefficient used to represent ground shaking had no clear physical relation to the design ground motions and the seismic hazard at the dam site. The dynamic response was not correctly determined because it was based in a pseudo-static analysis (Wieland, 2012). Today the seismic design criteria, last revised in 2010 by ICOLD, are clear and methods of dynamic analyses have been developed which allow the calculation of the inelastic seismic response of concrete dams (Wieland, 2014).

2.3.2 Dam safety monitoring

Dam safety monitoring is a key activity in dam safety management and includes two main activities:

i) visual inspections of the entire dam and appurtenant structures;

ii) monitoring of different physical quantities such as deformations, pressure, flow and temperature.

The monitoring data is used to assess the status of both the dam and its foundation. Monitoring includes both the equipment and the methodologies used to collect and collate the data.

The main advantage of monitoring is that it provides a rational insight into the safety of the dam-foundation system. Modern automatic data acquisition systems allow real-time developing deficiencies and rapidly changing conditions to be timely detected. Piezometers, plumb lines, foundation extensometers and seepage weirs are some examples of equipment usually installed in large dams to measure the structure's response. It is also necessary to install equipment to measure external data such as hydrostatic pressure, meteorological parameters and seismic events.

There are still many old dams in operation which have inadequate or even nonexistent monitoring facilities. Nowadays, if a dam does not comply with current safety and monitoring standards and shows an unusual behavior, the most effective means of reducing the risk is by reducing the reservoir level. However, this measure may have significant economic consequences.

2.3.3 Operational safety

The importance of operational safety of dams is still overlooked and often seen as not fundamental. When it comes to long-term safety, maintenance is the key factor and it includes operational guidelines for the reservoir for the usual, unusual and extreme conditions, training of personnel, experienced and technically qualified dam maintenance staff and dam maintenance procedures. If a dam designed for 100 years is not maintained, it can become unsafe within a very short period of time (Wieland, 2014).

2.3.4 Emergency planning

In the emergency planning concept, it is assumed that every dam can fail or be destroyed. Therefore, the consequences of a dam failure causing an uncontrolled release of water from the reservoir must be analysed. The main objective of emergency planning is to save lives by alarming and evacuating people on time (Wieland, 2016).

The worst failure case of a dam is with a full reservoir. Extreme flood events with overtopping of the dam and extreme water levels downstream of the dam may also be a dangerous scenario. No failure probabilities are considered for these scenarios. The safety-relevant elements of a dam are spillway gates and bottom outlets which must be operational after an earthquake in order to control the water level in the reservoir so that, in case of damage, the dam can be repaired and/or strengthened (Wieland, 2012).

Emergency Action Plans (EAP) are intended to help dam owners, operators and emergency officials to minimize the consequences of flooding or the uncontrolled release of water from the reservoir. The EAP will guide the responsible personnel in identifying, monitoring, responding to and mitigating emergency situations, answering questions like “who does what, where, when and how”. The EAP should be updated regularly and after important emergency events (Wieland, 2014).

2.4 Seismic hazard

Earthquakes can cause multiple hazards in large storage dam projects, such as:

- ground shaking causing vibration in dams, appurtenant structures and equipment, and their foundation;

- fault movements in the dam foundation or discontinuities in the dam foundation near major faults which can be activated during strong nearby earthquakes, causing structural distortions;

- fault displacement in the reservoir bottom, causing water waves in the reservoir;

- rockfalls with large rocks causing damage to gates, spillway piers, retaining walls, surface powerhouses, electro-mechanical equipment, etc.;

- mass movements into the reservoir causing impulse waves, increase of the reservoir level and overtopping of dams;

- project and site-specific hazards (ground deformations, seepage, liquefactions, etc.)

The main seismic hazard addressed in codes and regulations is the earthquake ground shaking, which can cause stresses, deformations, cracking, sliding and overturning in the dam's body (Wieland, 2016). However, movements in a joint of a concrete dam can be more critical than ground shaking, as any of these movements would cause a complicated crack pattern, which cannot be reliably predicted in numerical models.

Every time a strong earthquake occurs, the design guidelines have to be reviewed as new phenomena appear, which may have been overlooked. Usually, seismic hazard analyses are only concerned with the estimation of ground motion parameters such as peak ground acceleration (PGA) and response spectrum. Ground motion parameters can be determined by a probabilistic and/or deterministic seismic hazard analysis (Wieland, 2012).

2.5 Seismic design criteria

The following design earthquakes are needed for the seismic design of the different structures and elements of a large dam project (Wieland, 2016): safety evaluation earthquake (SEE), design basis earthquake (DBE), operating basis earthquake (OBE) and construction earthquake (CE).

- The SEE is the earthquake ground motion a dam must be able to resist without the uncontrolled release of the reservoir. The SEE is the governing earthquake ground motion for the safety assessment and seismic design of the dam and safety-relevant components, which must remain functioning after the SEE.

- The DBE, with a return period of 475 years, is the reference design earthquake for the appurtenant structures. The DBE ground motion parameters are estimated based on a probabilistic seismic hazard analysis (PSHA).

- The OBE is expected to occur during the life span of a dam and no loss or damage of service should happen. It has a probability of happening of about 50 % during a service life of 100 years. The ground motion parameters are also estimated based on a PSHA.

- The CE is to be used for the design of temporary structures such as coffer dams and takes into account the service life of these temporary structures.

The SEE ground motion can be obtained from a probabilistic and/or deterministic seismic hazard analysis:

- The maximum credible earthquake (MCE) is the event that produces the largest ground motion expected at the dam site based on the seismic history and the seismotectonic setup in the region. It is estimated based on deterministic earthquake scenarios.

- The maximum design earthquake (MDE) is used in the analysis presented in this thesis and the ground motion parameters are estimated on a PSHA. For large dams, the return period is taken as 10 000 years but for smaller, more limited damage potential, shorter return periods can be specified.

The different design earthquakes are characterized by the PGA horizontal and vertical components and the acceleration response spectra of horizontal and vertical earthquake components, typically for 5 % damping and obtained from the PSHA (mean values) for the MDE. In case of fault movements, similar seismic parameters are required but it is quite difficult for a dam designer to obtain quantitative estimates because the seismic analyses are mainly concerned with ground shaking.

2.6 Visit to Pocinho dam

According to current Portuguese regulations, inspection visits to a dam are made during the construction, before, during and after the first filling, and during its exploitation. In the period of exploitation there are three types of visual inspection visits: routine, specialty and exceptional visits. Routine inspection visits are made by local teams, responsible to explore the dam's monitoring

system. Specialty and exceptional visits involve the dam owner, the authority (*APA – Agência Portuguesa do Ambiente*) and LNEC, as an external consultor of the authority. Routine visual inspection visits are usually carried out monthly, specialty visits every two years and exceptional visits only after a flood, an earthquake or when there is an emptying and subsequent filling of the reservoir. The main purpose of these visits is to search for eventual signs of deterioration and to check if the observation system is working properly.

While developing this thesis, it was possible to follow a specialty inspection visit to Pocinho dam. The visit took place in the beginning of February of 2018.

Pocinho dam is a concrete gravity dam located on the river Douro national section. The main purposes of the dam are production of energy and navigation. Figure 2.5 shows a scheme of location and storage capacity of the different dams in the river Douro drainage basin, where Pocinho dam is highlighted.

The project of the dam was finished in 1974 and work was concluded in 1982. The developer of the construction was *EDP – Energias de Portugal.*

Pocinho dam is the most upstream construction in national soil of the hydraulic infrastructure of hydroelectric exploitation made by EDP in river Douro. The hollow gravity overflow dam has a straight axis, with a large gallery at the base. The spillway formed by four openings was designed for a considerable flood flow. A navigation lock is adjacent to the dam on the right bank, and the powerhouse, on the left bank, is equipped with 3 units. A fish lock of the Borland type is located in the powerhouse-dam wall (Portuguese National Committee on Large Dams, 1992). Figure 2.6 presents views from both upstream and downstream of the construction.

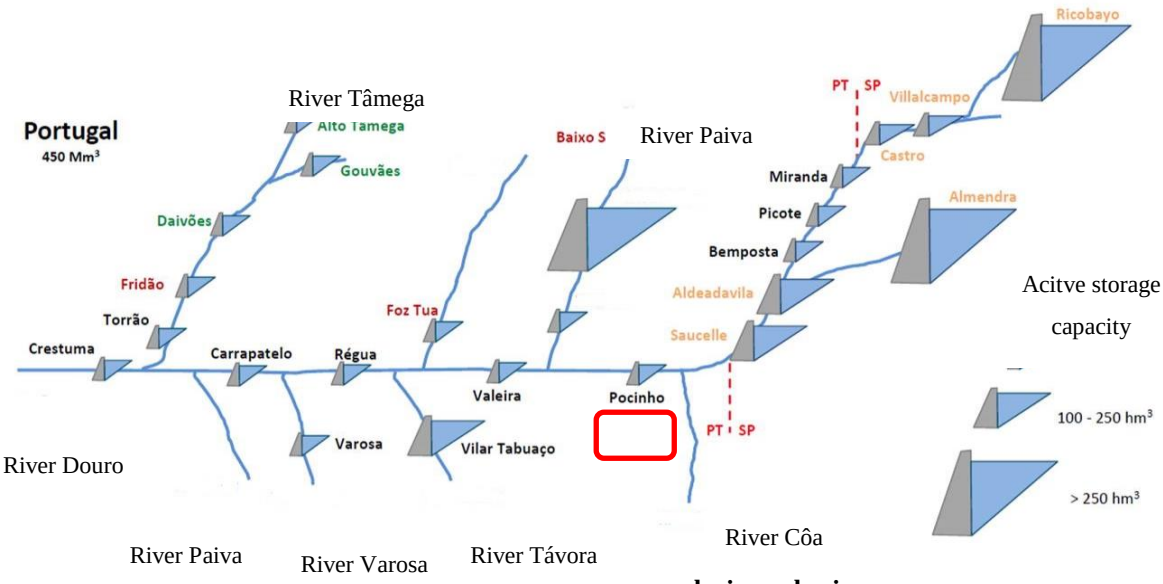

Figure 2.5 – Dams in river Douro drainage basin

Figure 2.6 - Upstream and downstream views of Pocinho dam

The dam is 49 m high and the total length of the crest is 430 m. In the crest there is a road that connects both banks. The dam has also an auxiliary half-bottom spillway. The normal top water level is 125.5 m and the maximum water level is 134.5 m. Figure 2.7 shows the dam cross-section.

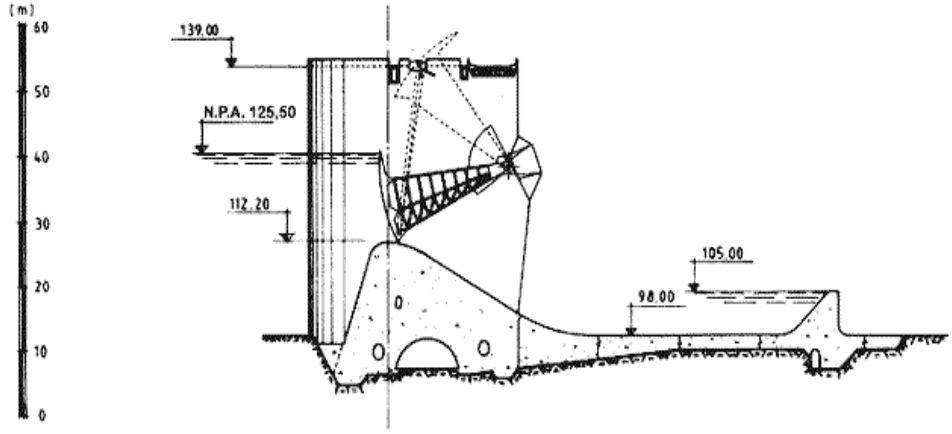

Figure 2.7 - Cross-section of Pocinho dam
(http://cnpgb.apambiente.pt/gr_barragens/gbportugal/Pocinhodes.htm)

During the visit it was possible to walk through the inspection galleries and observe different monitoring equipment installed in the dam. This equipment allows measurement data to be taken, such as displacements, movements of cracks, movement of the dam joints or volume of drained water. This data is stored in an informatic system called GestBarragens that allows the engineers responsible to review the safety of the dam to analyse its behavior. Some of the equipment observed during the visit were piezometers installed upstream and downstream of the drainage curtain to measure the water pressure and its variation over time, plumb lines and inverted plumb lines that measure the horizontal displacement in two orthogonal directions, foundation extensometers that allow measurement of the relative displacement between two pre-defined points. According to the current protocol, in the end of the visit a meeting took place with all the entities responsible for the safety of the dam (APA, EDP and LNEC) to further analyse the results.

Figure 2.8 a) shows one of the inspection galleries where it is possible to walk and watch the gallery walls and the equipment. Figure 2.8 b) shows the gallery at the dam's foundation. The foundation consists predominantly of dark grey phyllite, a schistous rock with some metagreywacke intercalations. Figure 2.8 c) and Figure 2.8 d) show a plumb line and a piezometer.

a) Inspection gallery in Pocinho dam

b) Gallery close to the dam foundation

c) Plumb line in Pocinho dam

d) Piezometer installed upstream from the drainage curtain in Pocinho dam

Figure 2.8 – Inspection galleries and some monitoring equipment

3 HYDROMECHANICAL BEHAVIOR OF CONCRETE DAM FOUNDATIONS

3.1 Hydromechanical interaction

The mechanical and hydraulic processes in rock masses are interdependent. Changes in the water flow influence the mechanical behavior due to variations in seepage forces and in the hydraulic uplift. Changes in these mechanical loads cause changes in the stress field of the rock mass, generating deformations. These deformations, in turn, cause variations in permeability hence changes in water flow. This is called a coupled hydromechanical process.

With the purpose of understanding the hydromechanical behavior of concrete dam foundations it is essential to understand how fluid flows through rock joints. This complex phenomenon has been the subject of extensive research since the 1960's (Snow, 1965; Louis & Maini, 1970 and Brown, 1987). The most commonly applied conceptual model and the one considered in this work is the parallel plate model. This model is made to describe the flow in a void space (without filling material) between two parallel smooth plates (Louis, 1969).

For a steady state laminar incompressible flow in such fracture geometry, the solution for the mean velocity is given as:

$$\boldsymbol{v = k_f\, i} \tag{3.1}$$

where *i* [m/m] is the hydraulic gradient and k_f [m/s] is the fracture hydraulic conductivity, given by:

$$\boldsymbol{k_f = \frac{a^2 g}{12 \nu_k}} \tag{3.2}$$

where *a* [m] represents the fracture aperture and ν_k [m^2/s] is the kinematic viscosity of the fluid.

The flow rate per unit width of the aperture is given by the following cubic law:

$$q = v\,a = \frac{a^3 g}{12v} i \tag{3.3}$$

According to this cubic law, the flow of parallel-plate openings is proportional to the cube of the aperture, meaning that it is extremely sensitive to a variation in the aperture.

Laboratory experiments have shown that the roughness and the aperture of a rock joint are the key factors governing fluid flow through a joint (Barton & de Quadros, 1997). The cubic law based on the parallel plate model considers only the influence of the aperture because of the impossibility of measuring the roughness parameter directly in a flow process. However, some studies were carried out trying to establish whether the parallel plate model is adequate for prediction of flow in natural fractures. Some authors have introduced an additional empirical correction factor that considers fracture roughness.

Barton, Bandis, & Bakhtar, (1985) suggested that a rock fracture has both a mechanical and hydraulic aperture. The mechanical joint aperture (a) is defined as the average point-to-point distance between two rock joint surfaces, perpendicular to a selected plane, as shown in Figure 3.1. A single average value can be used to define the aperture, but it can also be described stochastically. The aperture distribution of a joint is only valid at a certain state of rock stress and pore pressure. The mechanical aperture is usually determined from a two-dimensional, (2D) joint section, which is only a part of the real tridimensional (3D) surface and is geometrically measured with epoxy injection. The hydraulic aperture (a_h) is measured by analysis of the fluid flow and can be determined both from laboratory fluid-flow experiments and borehole pump tests in the field (Olsson & Barton, 2001).

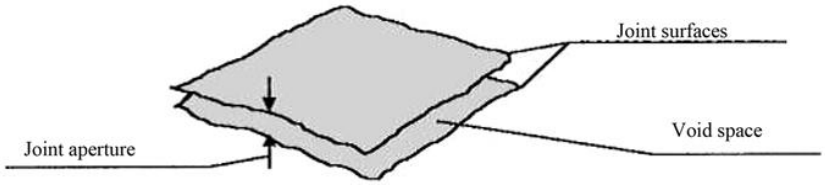

Figure 3.1 - Definition of mechanical aperture

The hydraulic aperture depends on the joint normal displacement, u_n.Three different apertures may be considered: a_0, a_{min} and a_{max}, where a_0 is the hydraulic aperture value for a joint element free of imposed normal stress (σ_n) by external actions, a_{min} is the minimum hydraulic aperture and a_{max} is the maximum hydraulic aperture.

The values of these model parameters may be calibrated in order to obtain water pressures and flows close to those recorded in situ. When the joints of a rock mass are highly compressed, the value of a_{min} is used, ensuring it is always possible to calculate a residual permeability. For very high values of hydraulic aperture, a_{max} is used in order to limitate the joint permeability up to a maximum value. Figure 3.2 is the graphical representation of the physical meaning of the three input model parameters that define the hydraulic aperture.

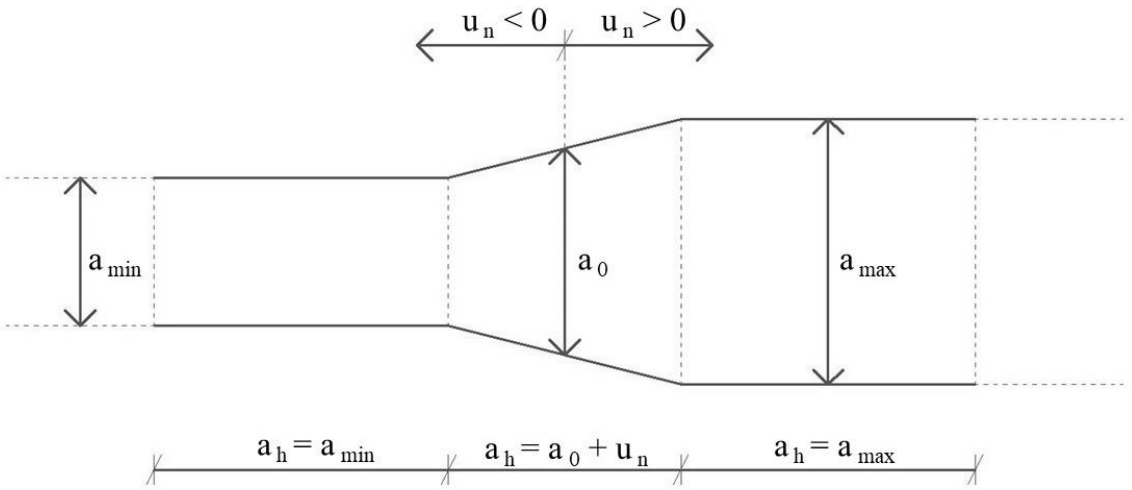

Figure 3.2 - Hydraulic aperture

According to the scheme presented in the code program UDEC (Itasca, 2004), and in the program Parmac2D-FFlow (Monteiro Azevedo & Farinha, 2015, Monteiro Azevedo, Bretas, & Lemos, 2012), used in this work, the hydraulic aperture associated with each integration point (far points of each SC) is given by:

$$a_h = \begin{cases} a_{min} & \text{If } u_n + a_0 < a_{min} \\ u_n + a_0 & \text{If } a_{min} \leq u_n + a_0 \leq a_{max} \\ a_{max} & \text{If } u_n + a_0 > a_{max} \end{cases} \quad (3.4)$$

3.2 Concrete dam foundations

Gravity dams are usually built on rock masses. These rock masses have always a complex structure and it is very difficult to fully know their geology, geomechanics and hydromechanical characteristics. It is necessary to undergo a well-designed and comprehensive site and laboratory study program to acquire enough knowledge to assist with the design of the super-structure and the

foundation treatment. Such detailed programs are conducted for one or more of the following reasons (Wyllie & Mah, 2004):

- The consequences of failure of a dam are usually very severe and can result in loss of life and property damage;
- The loads on dams can be higher than other structures and non-vertical;
- The loads are cyclic due to fluctuations in the reservoir level and the foundation must be able to withstand these changing stress conditions;
- High hydraulic gradients and water pressures are developed in the dam foundation.

Rock masses where concrete dams are built are discontinuous, heterogeneous and anisotropic. A foundation treatment is normally performed for large dams. This treatment consists in: i) consolidation grouting; ii) grout curtains; iii) drainage systems. The main objective of this treatment is to improve both the mechanical and hydraulic characteristics of the rock mass.

Consolidation grouting strengthens the uppermost strata of the foundation rock mass, that due to excavation works and initial loading is more fractured and altered than the rock mass at higher depth.

Seepage through the rock mass in a concrete dam foundation is a crucial factor. In the context of a project, the uplift pressures must be acceptable. By reducing the uplift pressures, the effective stresses are greater, consequently leading to increased safety. For economic reasons, it is also necessary to guarantee low values of percolated flow.

Local permeability reduction is executed through grout curtains. A cement-based injection of grout fills the holes oriented accordingly to the localization and orientation of the rock mass discontinuities. The holes are usually drilled from a drainage gallery. These grout curtains are vertical or sub-vertical surfaces situated close to the upstream face of the dam that penetrate the rock mass until a determined depth, which generally varies from 0.35 to 0.75 H, where H is the height of the reservoir above the top of the grout curtain, reducing the flow values and speed in the intersected discontinuities by reducing the rock mass permeability in that area.

The uplift pressure is a result of the presence of water in the dam's foundation. Its effect is contrary to the equilibrium effect of the dam's own-weight. As a way of reducing the uplift pressure values, drainage curtains are built. The drainage curtain is usually a line of boreholes drilled downstream of the grout curtain and, as a general rule, its length is one third to half of the grout curtain. The main objective is to collect and control seepage under the dam. Drainage boreholes are drilled after the grouting of the curtains is complete to avoid the filling of the holes with grout. The boreholes are usually located 3 m apart and their diameter is usually 76 mm. The drain boreholes can be uncoated, if the rock mass where they are drilled is sound rock, or coated with perforated plastic casing when the rock mass is fractured, to allow the hole opening and avoid the rock becoming loose from the hole walls. Figure 3.3 presents a gravity dam cross section, indicating the location of both the grout curtain and the drainage system.

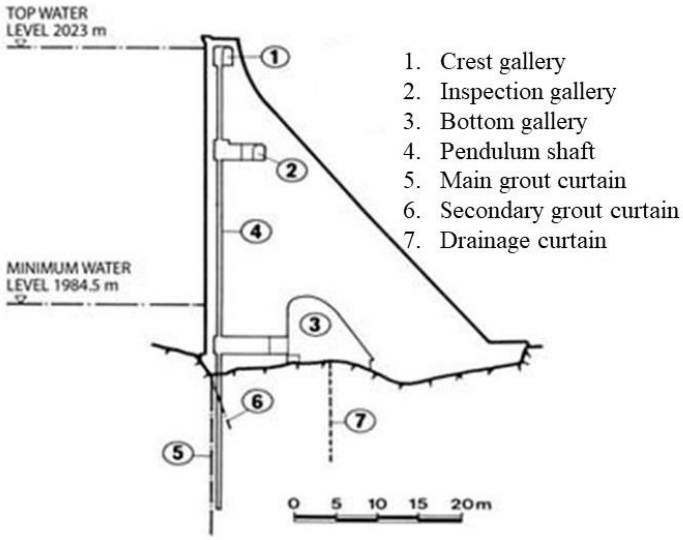

Figure 3.3 - Gravity dam cross section, indicating the location of grout curtain and drainage system (http://www.icold-cigb.net/GB/dams/dams.asp)

Drainage in concrete dam foundations is always relevant, especially when the discontinuities of rock masses have a very small aperture, which leads to an increase in water pressure over time. When there is no drainage system, the uplift pressure diagram is approximately linear between the upstream and downstream faces. Figure 3.4 presents a typical uplift pressure diagram for a dam with and without drainage system. During the dam's life span it is important to control the efficiency of the grout and drainage curtains, measuring uplift pressures and water flows.

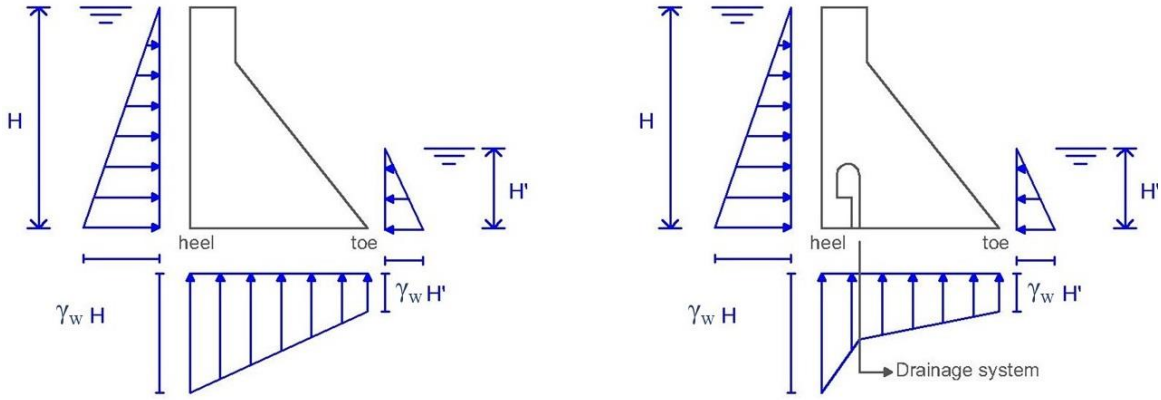

Figure 3.4 – Uplift pressure diagram in a concrete gravity dam without and with drainage system

3.3 Numerical modelling

3.3.1 Continuum equivalent and discontinuum models

To simulate the complex hydromechanical coupled behavior of fractured rock masses, it is possible to replicate the dam's foundation using continuum equivalent models or considering the rock mass fracture networks. The choice between continuum or discontinuum models depends on many case-specific factors, but the main one is the size and spacing of the discontinuities, when compared to the size of the problem.

In equivalent continuum models, the rock mass physical behavior needs to be properly represented by adjusting the materials' properties. To simulate the fluid flow in the foundation, different rock mass areas are identified and the local equivalent permeability is estimated by in-situ Lugeon type tests. The seepage forces induce deformations in the continuous medium, which in turn alters the permeability. This type of analysis requires correlations between stress or strain and permeability to be previously established (Farinha, 2010).

In fractured flow models the discontinuities are explicitly represented, with their individual hydromechanical properties. It is assumed that the water only flows through the rock mass joints. The joint water pressure gives rise to changes in joint apertures and, consequently, alters the flow rates. This modelling approach requires field, hydraulic and mechanical characterization data, such as orientation and spacing of discontinuities, joint normal and shear stiffnesses, joint apertures and residual apertures (Farinha, 2010).

3.3.2 Discontinuum analysis with Parmac2D-FFlow

Because rock masses are naturally discontinuous, they may be modelled using the discrete element method. In the discrete element method, blocks interact between each other, representing the rock mass discontinuities. The mechanical characteristics of the model depend not only on the element properties, such as Young's modulus or Poisson's ratio, but also on the interface properties, such as the normal and shear stiffnesses, the friction angle, the cohesion and the maximum resistance to tensile and compressive stresses. In the case of non-linear analysis, the model's behavior is ruled by the interface properties (Bretas, 2012). These properties follow a given constitutive model. The one adopted in this thesis is the Mohr-Coulomb constitutive law with a tensile cut off (Figure 3.5).

As a pre-processing tool, the block generation modulus of the program UDEC (Itasca, 2004) is used to define the block system of the different model examples presented in this work. UDEC is a bi-dimensional numerical code which simulates discontinuous media such as rock masses under static or dynamic actions. The domain is represented as a block system, where a rigid or deformable behavior can be adopted, and the discontinuities are the boundary conditions between blocks.

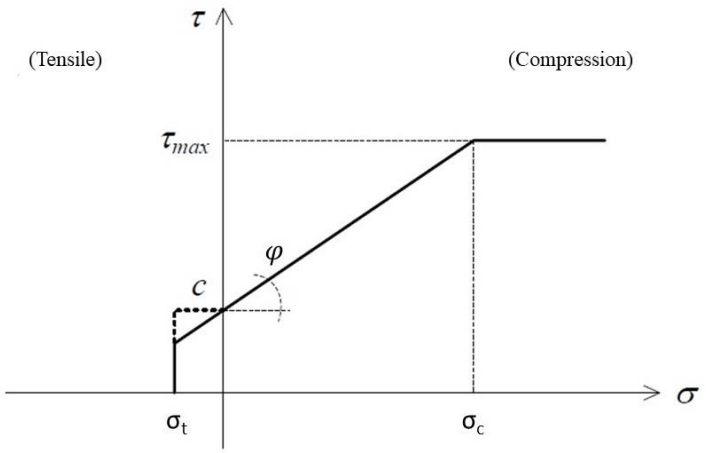

Figure 3.5 - Mohr-Coulomb constitutive law for the interfaces (adapted from Bretas, 2012)

The models here presented are implemented in the program Parmac2D-FFlow, which has been adopted for dam stability studies under static and dynamic loading. The coupled seepage-stress couple model proposed in this work is based on an edge-to-edge contact between blocks in which the hydraulic model is defined in a consistent way with the mechanical model. This allows the water pressure and contact forces to be calculated at the same mesh points adopted in the

stress/displacement field modelling. However, the model requires a thorough pre-processing stage in order to ensure that the interactions between the blocks are always edge to edge.

3.3.2.1 Mechanical model

The mechanical model used in Parmac2D-FFlow is a model of discrete nature and uses an explicit solution algorithm based on the centered difference method, Monteiro Azevedo, (2003). It is possible to take into account the deformability of the blocks by, after dividing the domain into several blocks, divide internally every block into a mesh of triangular shape elements. Figure 3.6 shows the calculation cycle of the explicit mechanical model.

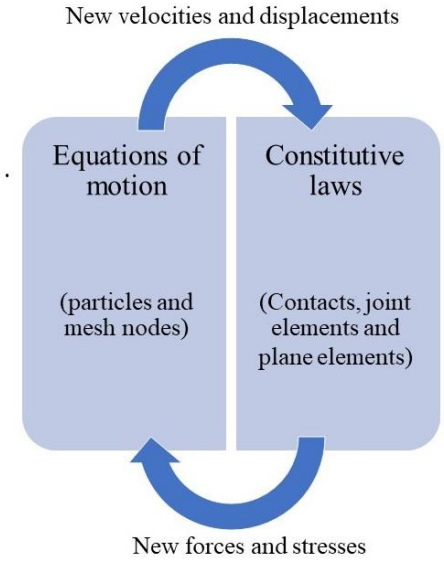

Figure 3.6 - Calculation cycle of the mechanical model

In this work, the interaction between blocks is done by edge-to-edge joint finite element methods which require each block's finite element mesh to be compatible and are in general adequate for small displacement analysis. Farinha, Monteiro Azevedo, & Candeias, (2017) show that the hypothesis of small displacements is valid for the analysis of the seepage-stress coupled behavior of concrete dam foundations and for stability analysis in both static and dynamic conditions. In the joint finite elements, as there is perfect compatibility of the displacement field along the interfaces, a more accurate representation of the stress distribution along the joints is obtained compared to the solutions obtained with traditional discrete elements with similar discretization.

Figure 3.7 shows the interaction between block B1 and blocks B2 and B3, based on joint elements.

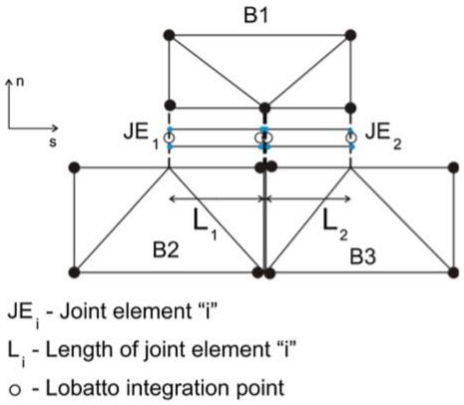

Figure 3.7 - Joint element model (Monteiro Azevedo & Farinha, 2015)

As previously mentioned, it is necessary that the internal finite element mesh of each block is compatible, in order to ensure that the interactions are always edge-to-edge. To achieve this, it is necessary to implement a pre-processing procedure that guarantees that each edge of a block coincides with an edge of the adjacent block.

3.3.2.2 Hydraulic model

The hydraulic model is compatible with the mechanical model (Figure 3.8 a) because, as the processing operation generates a perfectly compatible mesh of plane triangular elements, the hydraulic nodes (HNs), represented in Figure 3.8 b), coincide with the nodal points from the mesh which have the same coordinates at the beginning of the numerical analysis and the seepage channels of the hydraulic model (SC), Figure 3.8 b), coincide with the midplane of the joint elements. Throughout the calculation process moving occurs and the changes for the nodal points from its initial position to the new one is only possible thanks to the independent mechanical behavior of the nodal points.

The coordinates of each hydraulic node are given by the average coordinates of the group of nodes of the associated mechanical model. The volume of each SC is obtained considering the mechanical apertures measured on the nodal points of the joint element associated with the SC. As shown in Figure 3.8 c), the water pressures are defined on the hydraulic nodes and the discharges are calculated in the seepage channels.

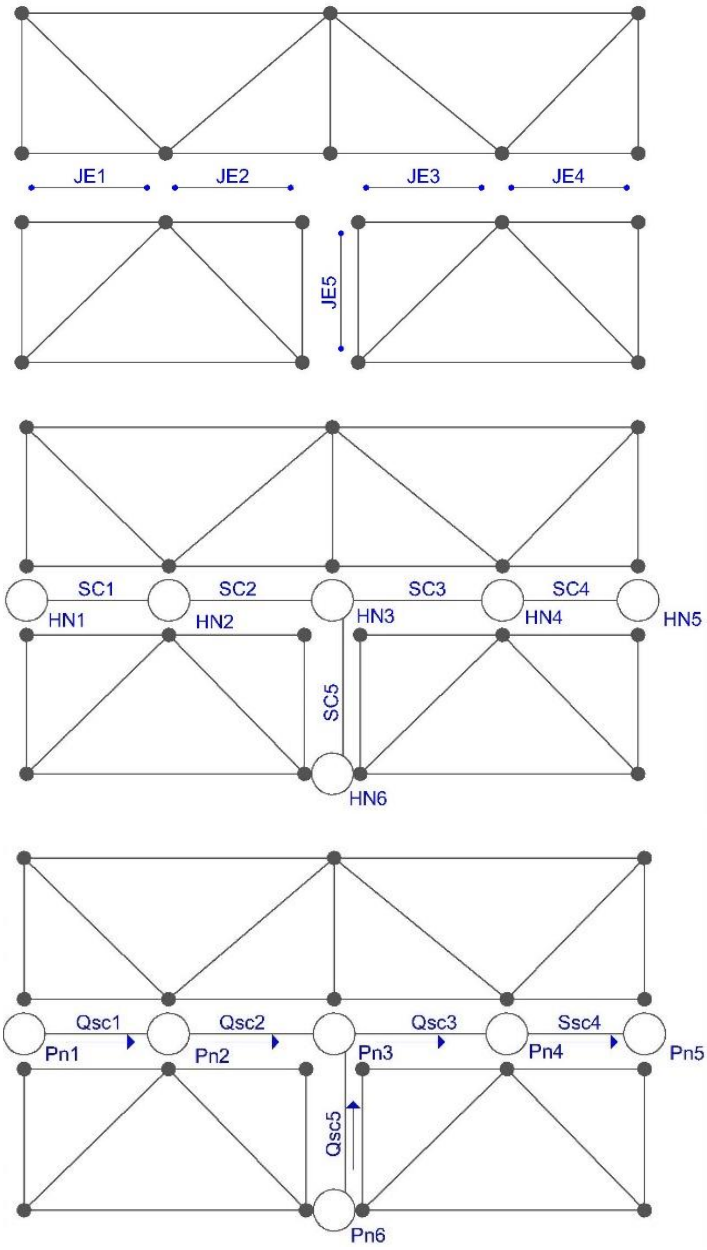

a) Mechanical model

b) Hydraulic model: hydraulic nodes (HNs) and seepage channels (SC)

c) Hydraulic model: pressures on the hydraulic nodes (P) and discharges in seepage channels (Q)

Figure 3.8 - Superposition of hydraulic and mechanical models

The model proposed in Farinha et al. (2017) ensures that the water pressures are continuous where various seepage channels converge, that is, in the HNs. These HNs, where the water pressure is calculated, are in the same location as the mechanical nodes. Thus, the mechanical and hydraulic models are perfectly compatible which ensures greater precision, for the same discretization, than when the numerical analysis is carried out using models not perfectly compatible.

The hydraulic aperture (a_h) is defined at the seepage channel endpoints. As each SC coincides with a joint element (mechanical model), the joint normal displacement (u_n) at the integration points (two Lobatto points at the joint end points) is also known.

At each timestep, taking into account the relative position of the blocks, the mechanical apertures of the joint are known. From these values it is possible to know the hydraulic aperture, the hydraulic conductivity in the SC, the hydraulic head (Φ) and the discharge. Knowing the discharges calculated in each SC, it is possible to establish the discharge associated with each HN so that the new water pressure at the nodes is obtained. Figure 3.9 shows the hydraulic calculation cycle.

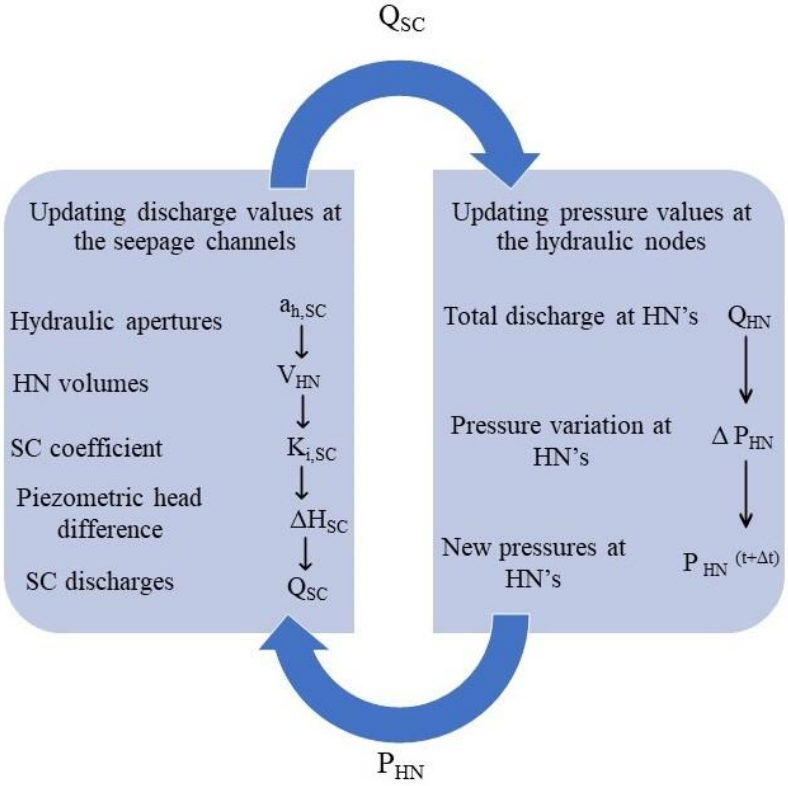

Figure 3.9 - Hydraulic calculation cycle

3.3.2.3 Hydromechanical model

The seepage-stress coupled model results from the coupling between the mechanical model and the hydraulic model. The models interact adopting a timestep similar in both models, the lowest timestep value associated to each domain. Given an initial hydraulic aperture, which is set given the initial joint element normal displacement, the water pressures are calculated in the hydraulic

model. The water pressures are then transferred to the mechanical model and considered in the calculation of the internal forces at the joint elements representing the discontinuities (effective stresses). The hydromechanical calculation cycle is presented in Figure 3.10.

When only a steady state equilibrium position is required, a unitary timestep is adopted on both domains. As a way to guarantee numerical stability, the hydraulic volumes associated with the hydraulic nodal points and the masses associated with the nodal points of the mechanical model are scaled accordingly.

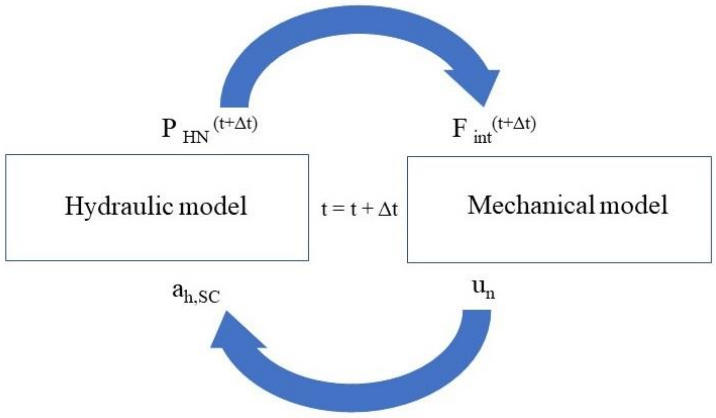

Figure 3.10 - Hydromechanical calculation cycle

3.4 Hydromechanical behavior of gravity dam foundations

As an example of the possible results and analyses performed in Parmac2D-FFlow, a gravity dam was analysed. The water pressure distribution along the dam/foundation interface and the nodal horizontal displacement at the dam upstream face is represented.

The results obtained were compared for different water levels downstream from the dam for:

i) linear elastic analysis and non-linear elastic analysis based on a Mohr-Coulomb constitutive law with a tensile cut-off criterion;

ii) dam foundation with and without grout curtain and drainage holes.

3.4.1 Geometry

Figure 3.11 presents the geometry of the model used in this example and in the examples presented in chapter 5, to numerically model the foundation. Is this figure, *H* represents the height of the dam and *l* is the length of the crest. The initial block model geometry including the foundation discontinuities was generated in UDEC.

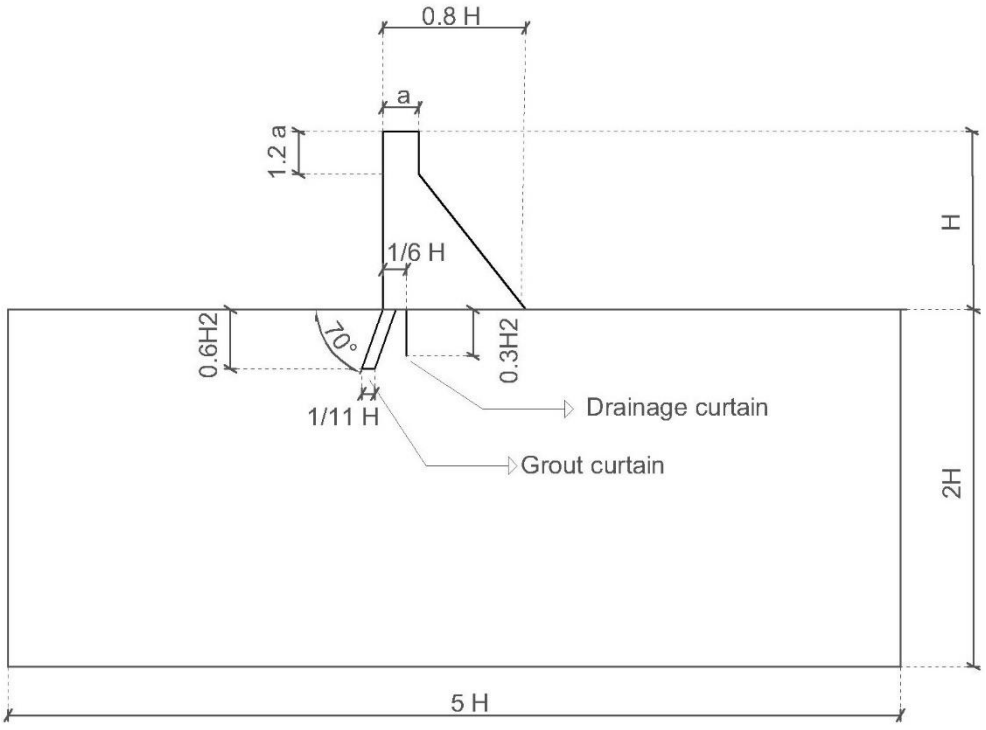

Figure 3.11 – Model geometry: dam and foundation

The grout curtain, when considered, starts at the heel of the dam and its width is approximately 1/11 of the dam height. The inclination of the grout curtain is 70º towards upstream and its depth is 0.55 H_2, where H_2 is the height of the dam minus 2 m, considering the top water level. The drainage curtain is situated at 1/6 H from the heel of the dam and at a depth of 0.3 H_2.

Figure 3.12 shows the geometry adopted for the dam model and the water pressure applied on the upstream face. In this model the existence of the grout curtain and of the drainage system is neglected. It is considered that nodal points at the left and right sides of the foundation rock mass, and at the base of the model, are fixed in both the horizontal and vertical directions. The foundation model has horizontal and vertical discontinuities, perpendicular between each other and separated by 5 m with a standard deviation of 1 m.

Figure 3.13 shows the geometry of the model, considering now the grout curtain and the drainage boreholes. Figure 3.14 presents the same geometry of the dam's structure, considering there is water downstream from the dam, with a level equal to 10 m.

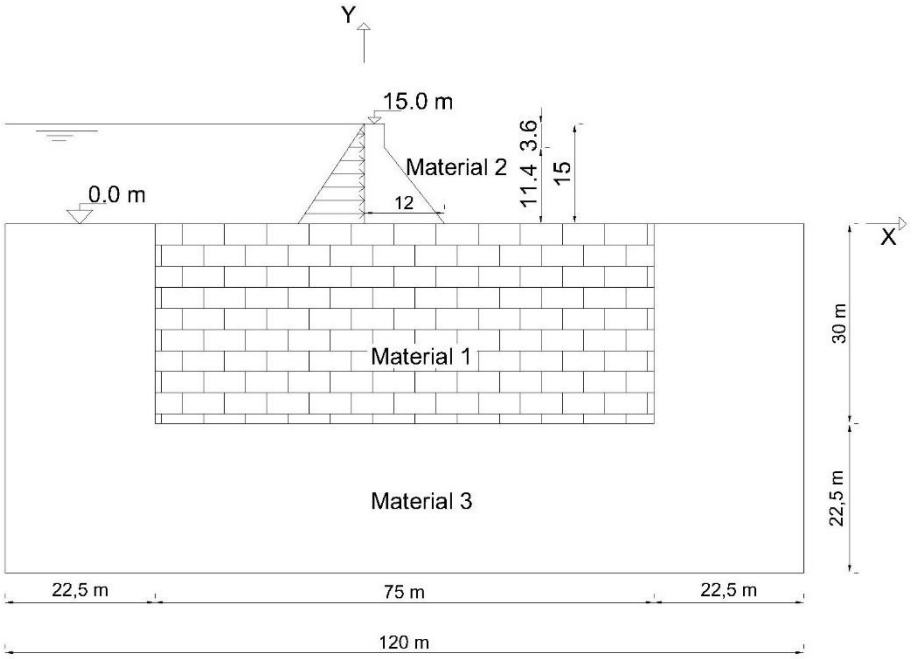

Figure 3.12 – Model geometry of the dam

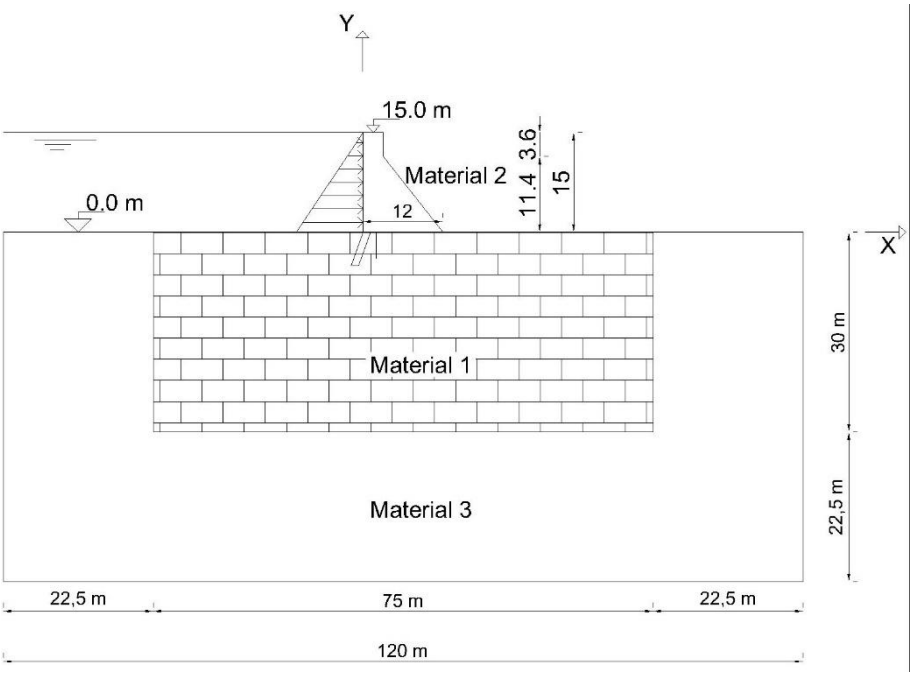

Figure 3.13 – Model geometry of the dam considering grout curtain and drainage system

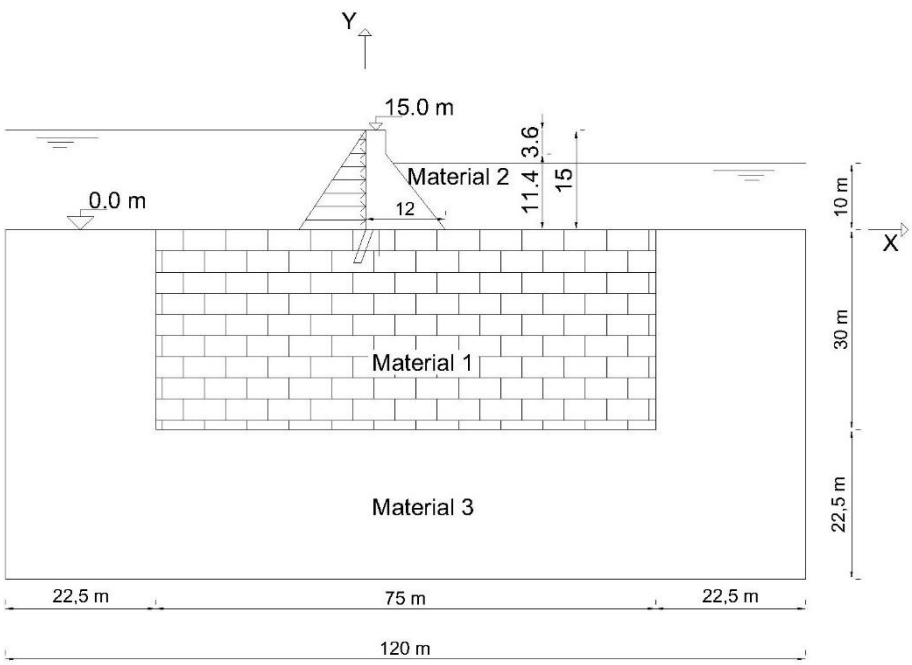

Figure 3.14 - Model geometry of the dam considering a water level downstream from the dam

3.4.2 Material properties

The fractured rock mass foundation is assigned to material 1, the body of the dam is assigned to material 2 and the homogeneous and continuum foundation is assigned to material 3. The mechanical characteristics adopted for all the materials that are part of the numerical model are presented in Table 3.1.

Table 3.1 - Mechanical characteristics for the dam model

Mechanical Characteristics	Material 1	Material 2	Material 3
E [GPa]	12.0	20.0	10.0
ν	0.2	0.2	0.2
ρ [kg/m^3]	2650.0	2400.0	2650.0
g [m/s^2]	10.0	10.0	10.0

Two different constitutive models were adopted for the joint elements behavior: i) linear elastic behavior and ii) non-linear elastic behavior following a Mohr-Coulomb constitutive law without cohesion for material 1, fractured rock interfaces, and with cohesion for material 2, dam/foundation interface. A shear stiffness equal to 0.4 of the normal stiffness is adopted. The interface characteristics for non-linear elastic behavior are presented in Table 3.2. For the interfaces between

the continuum and the fractured areas of the foundation, linear elastic model is adopted considering the elastic properties set for material 2.

Table 3.2 - Mohr-Coulomb constitutive law

Interfaces between materials	Material 1	Material 2
Kn [GPa/m]	24.0	24.0
Ks [GPa/m]	9.6	9.6
Cohesion [MPa]	0	2.0
Tensile Strength [MPa]	0	2.0

Table 3.3 shows the hydraulic characteristics of the seepage channels. The values used are based on Farinha, (2010).

Table 3.3 - Hydraulic characteristics of each material assigned to the interfaces

Hydraulic characteristics	Material 1	Material 2	Material 3
K_{ce} [$\times 10^5$ MPa^{-1} s^{-1}]	0.8300	0.4150	0.8300
K_w [GPa]	2.1	2.1	2.1
a_0 [mm]	1.668	1.668	1.668
a_{min} [mm]	$1/3 \times a_0$	$1/3 \times a_0$	$1/3 \times a_0$
a_{max} [mm]	$5 \times a_0$	$5 \times a_0$	$5 \times a_0$

When the grout curtain is considered, the permeability factor of the seepage channels that are intersected by the grout curtain are reduced. For the fractured foundation, the permeability factor of the intersected seepage channels is reduced to 0.327×10^5 kPa^{-1} s^{-1} and the permeability of the seepage channels of the dam/fractured foundation interface is reduced to 0.164×10^5 kPa^{-1} s^{-1}.

As for the hydraulic nodes in the vicinity of the drainage holes, the water pressure is set equal to 2/3 of the water pressure at the dam's heel. The drainage holes contribute to the overall control of the uplift water pressure. The water body acceleration is 10 m/s^2 and specific mass is equal to 1 kN/m^3.

3.4.3 Numerical models

The domain was discretized using triangular plane finite elements with an average edge length of 1,0 m in the dam and fractured foundation and of 3 m in the homogeneous and continuum foundation. The Parmac2D-FFlow mechanical model has 5587 triangular plane elements,

corresponding to a total of 3998 nodal points and 1001 interfaces between materials. The hydraulic model has 895 hydraulic nodes and 976 hydraulic seepage channels.

Figure 3.15 presents the block model generated in UDEC program and Figure 3.16 and Figure 3.17 show the mechanical and hydraulic modes. In the hydraulic model, the dam construction joints are shown in black, which means they are impervious. The fractured foundation has the seepage channels shown in red and the points in blue mean that they have a certain water pressure associated.

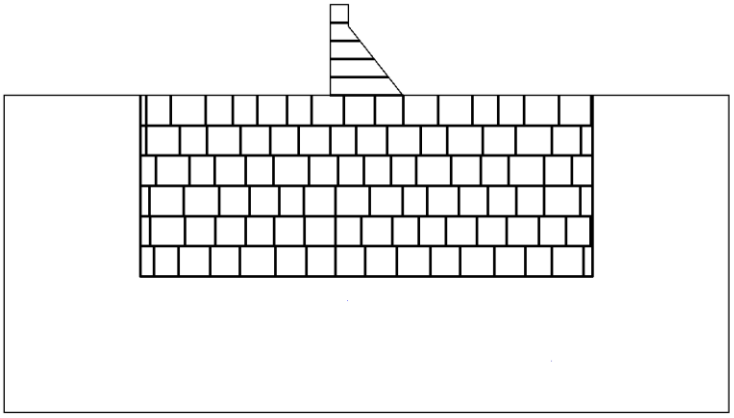

Figure 3.15 - Block model

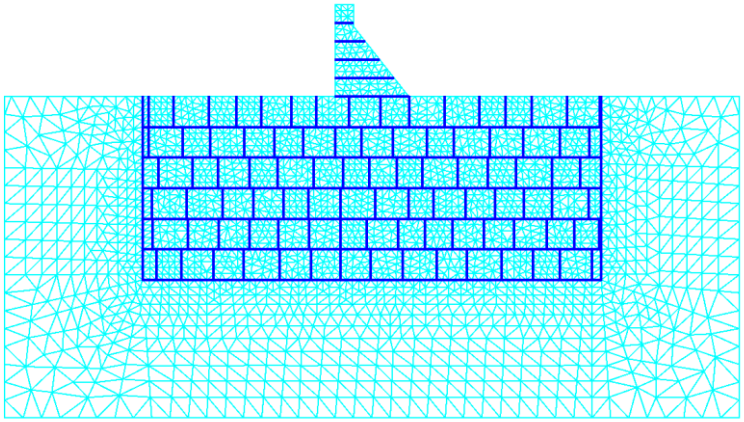

Figure 3.16 – Mechanical model

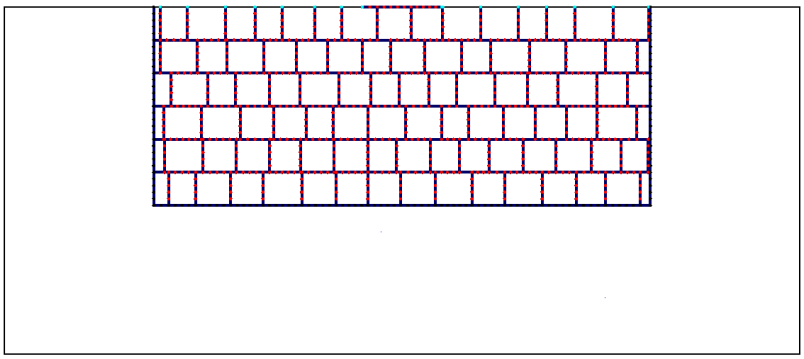

Figure 3.17 - Hydraulic model

3.4.4 Analysis sequence

In the initial stage, coupled hydromechanical calculation is carried out, taking into account the dam's self-weight. For the foundation, an initial stress state of 26.5 kPa along the y axis, corresponding to the rock self-weight and a relation between the vertical and horizontal stresses of $0.7 \times \sigma_v$, is considered. The water table is initially considered to be at the foundation surface.

The hydrostatic pressure at the upstream face and at the upstream foundation surface is then applied considering linear elastic behavior at the joint elements. The non-linear elastic behavior is only considered after the equilibrium is reached.

3.4.5 Results analysis

The water pressure distribution along the dam/foundation joint and the displacements of the upstream face are assessed. The results are compared for different foundation models: i) elastic fractured foundation and ii) non-linear behavior.

Figure 3.18 compares the water pressure distribution with and without the grout curtain and drainage system. The results presented in Figure 3.18 a) correspond to the elastic analysis and the results presented in Figure 3.18 b) correspond to the non-linear behavior. Given the presence of the drainage boreholes at 2 metres distance from the dam's heel, the water pressure at the intersected hydraulic nodes is set equal to 50 kPa.

Figure 3.19 compares the results of elastic and non-linear interface models at the water pressure distribution with drainage system (Figure 3.19 a) and without drainage system (Figure 3.19 b). The water pressure distributions are very similar for the elastic and non-linear behavior. None of the examples has a perfect linear water pressure distribution thanks to different mechanical apertures along the dam/fractured foundation interface. However, it can be seen that the uplift pressure distribution is approximately linear when there is no drainage system and it is approximately bi-linear in the presence of a drainage system, which is in agreement with the distributions usually adopted at the design stage.

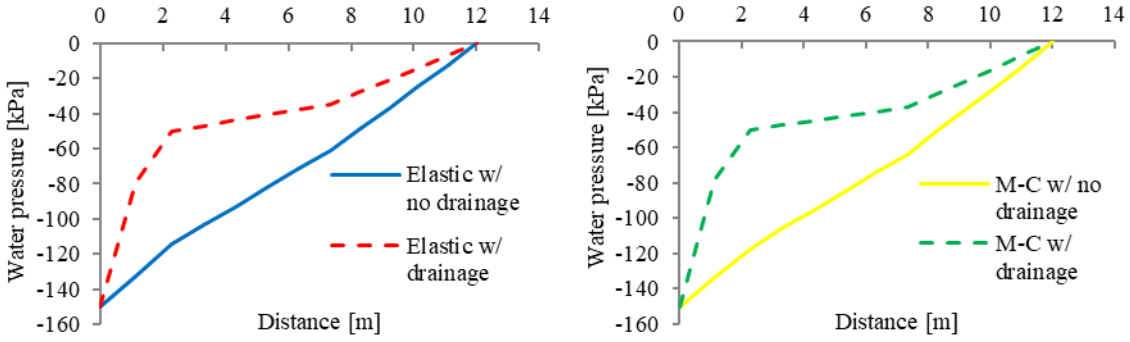

a) Elastic behavior b) Mohr-Coulomb behavior

Figure 3.18 - Water pressure along the base of the dam for two interface models without water downstream from the dam

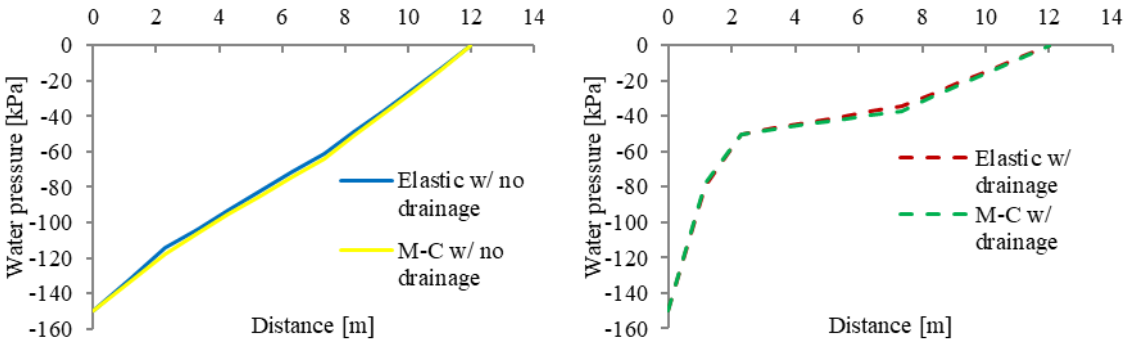

a) Dam without drainage system b) Dam with drainage

Figure 3.19 – Water pressure along the base of the dam with and without drainage system without water downstream from the dam

The obtained horizontal displacements at the upstream face are presented in Figure 3.20 and Figure 3.21 for the different interface models adopted with and without drainage system. Figure 3.20 compares the results of the upstream face displacement for elastic behavior interfaces, with and without drainage system. As seen, the upstream face horizontal displacement are similar with and without drainage system. The upstream face of the dam works as a cantilever where the loads applied are the hydrostatic and the uplift pressure. This results on a slightly curved deformed shape.

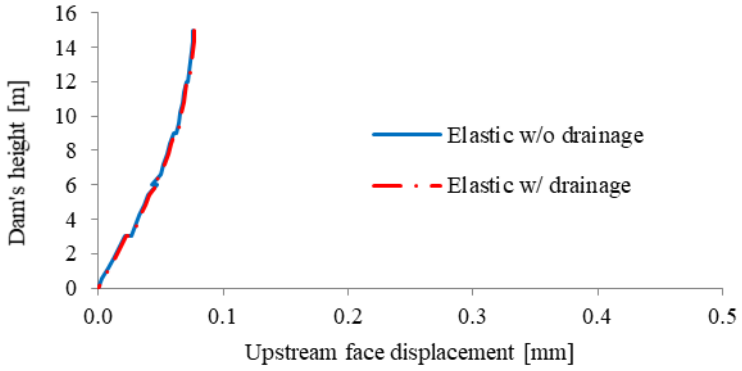

Figure 3.20 – Upstream face displacement for elastic behavior, with and without drainage system and without water downstream from the dam

When non-linear interface models are adopted at the dam/foundation interface and at the fractured foundation, the displacements obtained in the presence of a drainage system are lower than those without the drainage system as seen in Figure 3.21.

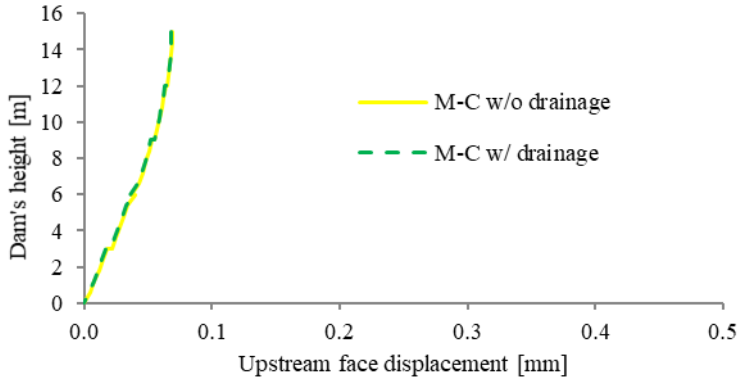

Figure 3.21 – Upstream face displacement for Mohr-Coulomb behavior, with and without drainage system and without water level downstream

Figure 3.22 and Figure 3.23 present the hydraulic head distribution within the fractured area of the dam foundation, when a non-linear Mohr-Coulomb criterion is considered. Results presented in Figure 3.22 are obtained without grout curtain and drainage system whilst Figure 3.23 shows the results taking into account the existence of grout curtain and drainage system.

It is possible to observe that upstream of the dam the hydraulic head is equal to the water level, 15 m. The hydraulic head downstream from the is equal to zero dam for the two models. When the grout curtain and the drainage system are considered, the hydraulic head values present a significant reduction, equaling the values imposed in the drainage system.

Figure 3.24 and Figure 3.25 show the percentage of hydraulic head contours within the dam foundation (percentage of hydraulic head is the ratio of the water head measured of a given level, expressed in metres of height of water, to the height of water in the reservoir above that level). It can be seen that without grout curtain and drainage system, Figure 3.24, the water pressure decreases steadily from upstream towards downstream. When the grout curtain and drainage system are simulated, there is a significant loss of hydraulic head between the heel of the dam and the drainage area.

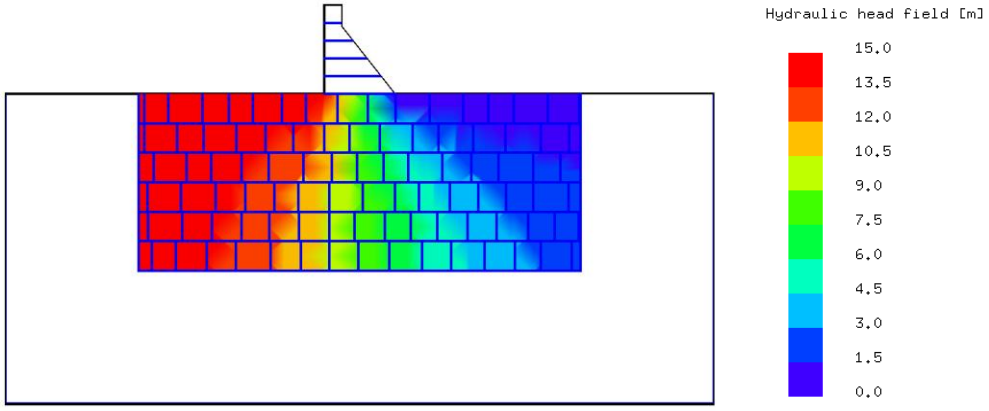

Figure 3.22 - Hydraulic head in the dam foundation (without grout curtain and drainage system)

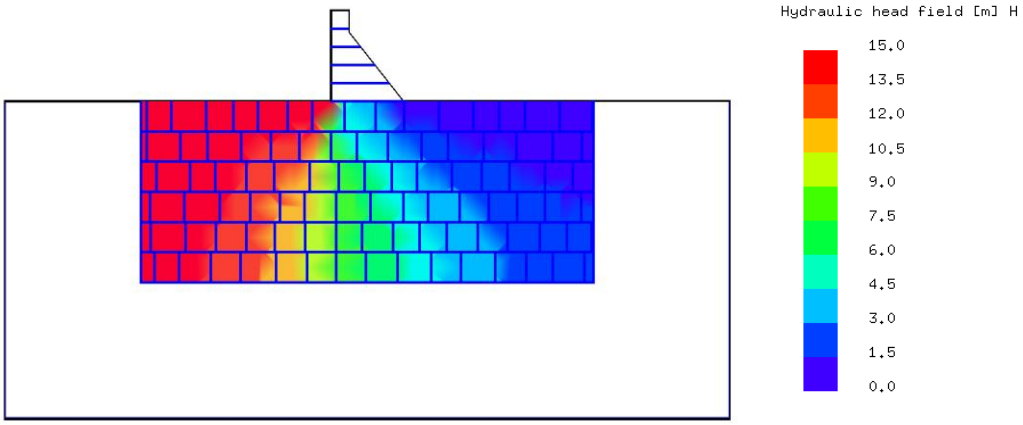

Figure 3.23 - Hydraulic head in the dam foundation (with grout curtain and drainage system)

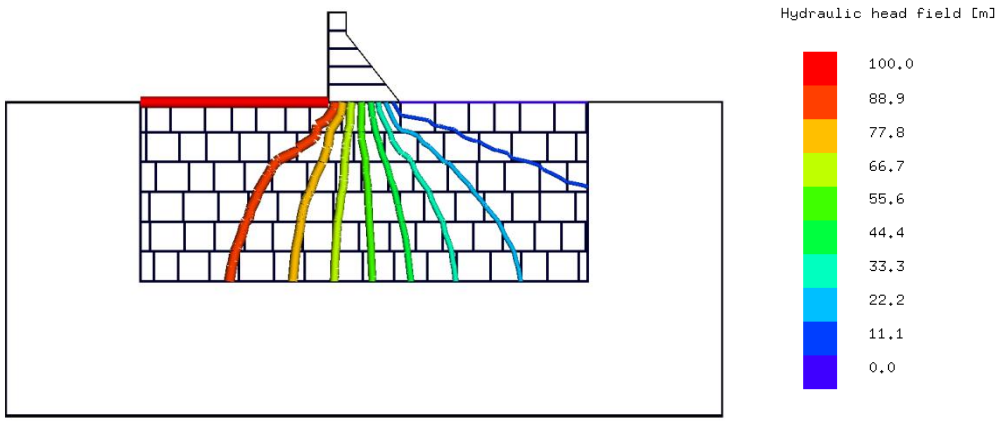

Figure 3.24 – Percentage of hydraulic head in the dam foundation (without grout curtain and drainage system)

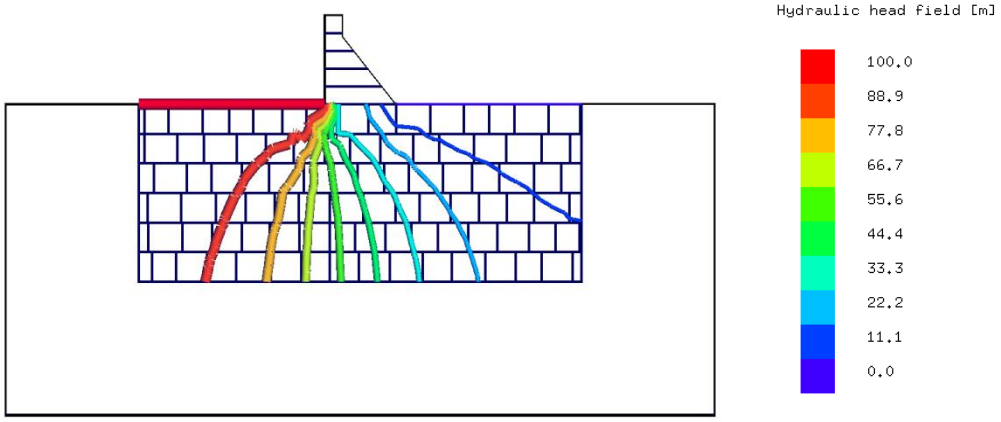

Figure 3.25 - Percentage of hydraulic head in the dam foundation (with grout curtain and drainage system)

4 SEISMIC EVALUATION OF CONCRETE GRAVITY DAMS FOR SHEAR SLIDING FAILURE SCENARIOS

4.1 Introduction

Several methods are adopted for the dynamic analysis of concrete gravity dams, varying in degree of difficulty and applicability. One of the most straight forward methods, the pseudo-static analysis, determines the inertia forces caused by the earthquake, given by the product of the dam mass and horizontal acceleration, considering also in addition the hydrodynamic water pressures of the reservoir. A more sophisticated approach is based on the finite element method and on the structural modal analysis. The latter procedure can be defined through a response spectrum or an acceleration history, using Duhamel's integral (Bretas, 2012).

The seismic evaluation of concrete gravity dams should consider the possibility of sliding on the horizontal foundation joint for the maximum design earthquake, MDE. The maximum shear sliding displacement should be lower than a predefined value in order to ensure that global dam safety is verified. The static loads that should be considered are the same as in the hydromechanical model (self-weight of the dam and foundation, hydrostatic pressure on the upstream face of the dam and hydromechanical pressures).

During an earthquake, due to its short duration, the hydraulic apertures do not change, causing the water pressure and the flows to be kept constant during the MDE loading and thus the fluid flow coupling is not performed (Lemos, Cundall, & Dasgupta, 1999).

For the definition of the MDE, two accelerations records are required, for the horizontal and vertical components. The vertical seismic component is given by scaling with a factor of 2/3 the horizontal acceleration records. Considering a vertical component of the earthquake may lead to greater values of displacement and stresses, making the analysis even safer.

4.2 Hydrodynamic pressure

During an earthquake, there is a dynamic interaction between the dam and the water reservoir that causes a water pressure variation. Westergaard (1933) developed a model that simulates this interaction. In order to determine the water pressure diagram, Westergaard proposed a solution

including a series of sines, earthquake-imposed function of accelerations, the water density, the reservoir level, water Young's modulus and the fundamental natural frequency of the structure. The same author proposed a simplified solution that resembles this effect with a water volume moving together with the dam during the earthquake, originating inertia forces. The shape of this diagram is a parabola (Figure 4.1), similar to the original water pressure diagram, given by:

$$\boldsymbol{m_{h,i} = \frac{7}{8}\,\rho_w \sqrt{H\,y_i}\,A_i} \tag{4.1}$$

where $m_{h,i}$ is the horizontal mass associated with nodal point *i* (kg), ρ_w is the water density (kg/m^3), y_i is the vertical height, measured from the reservoir surface to the nodal point *i* (m), *H* is the reservoir level (m) and A_i is the area of influence of nodal point *i* (m^2).

This solution was developed for a dam with a vertical upstream face and a horizontal seismic action, thus perpendicular pressures to the upstream face. In order to generalize to inclined upstream dam faces, equation 4.1 must be corrected to (Priscu, Popovici, Stematiu, & Stere, 1985):

$$\boldsymbol{m_{h,i} = \frac{7}{8}\,\rho_a \sqrt{H\,y_i}\,A_i \cos^2\theta} \tag{4.2}$$

$$\boldsymbol{m_{v,i} = \frac{7}{8}\,\rho_a \sqrt{H\,y_i}\,A_i \cos^2(90-\theta)} \tag{4.3}$$

in which $m_{v,i}$ is the vertical mass associated with nodal point *I* (kg) and θ is the upstream face inclination (º), as shown in Figure 4.1.

Generally, upstream faces have very low inclination angles, thus the vertical component is not relevant for the dynamic behavior of the structure. Then, the additional mass equivalent to the hydrodynamic pressure is added to the real mass at each upstream face nodal point.

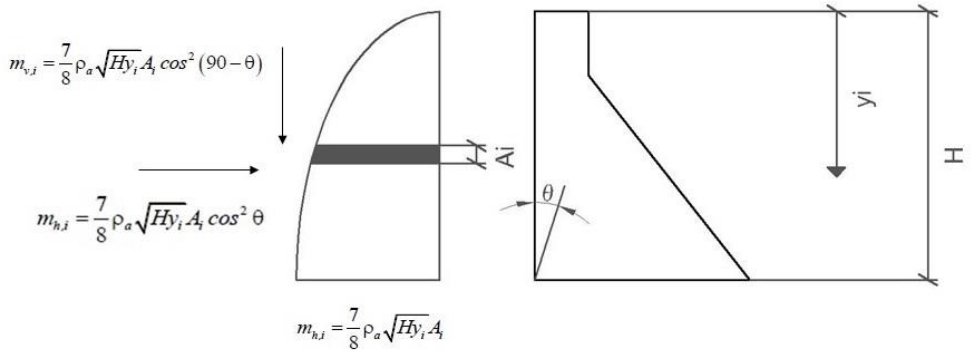

Figure 4.1 - Associated masses - Westergaard simplified solution (adapted from Westergaard, 1933)

There are more complex models available to simulate the interaction between the water in the reservoir and the dam's upstream face such as an Euler formulation for the fluid, (Cervera, Oliver, & Faria, 1995) or a Lagrangian fluid formulation, (Wilson & Khalvati, 1983), but for 2D gravity dams the added mass approach is known to give a very good agreement with the recorded behavior of a dam under seismic loading.

4.3 Earthquake equivalent loading and boundary conditions

With the purpose of applying the seismic action in the computational model, three different definitions of boundary conditions can be considered, under explicit solution algorithms. For rigid foundations the seismic action is applied through velocity history records. When the foundation is deformable, the seismic action may be imposed through a stress wave history on top of the viscous boundary that is included to absorb the reflected waves. When the foundation is considered to be deformable, the seismic action can be defined in both horizontal and vertical directions by adopting free-field conditions at the lateral boundaries.

4.3.1 Rigid rock mass foundation and seismic application using a velocity history record

The seismic action is applied through a velocity history record. This procedure can be adopted when only one component of the earthquake is considered or when both components are considered. For example, a velocity history record may be associated with the horizontal direction (x), while the vertical direction (y) is assumed as zero (Figure 4.2 a). The same procedure can be applied when the vertical component of the earthquake is not zero and the horizontal component does not exist. For this case, the velocity history record is imposed on the vertical direction (Figure 4.2 b). Generally, an earthquake presents both components, thus the velocity history record is applied in both directions. In these cases, the velocity history records can be different for each direction (Figure 4.2 c).

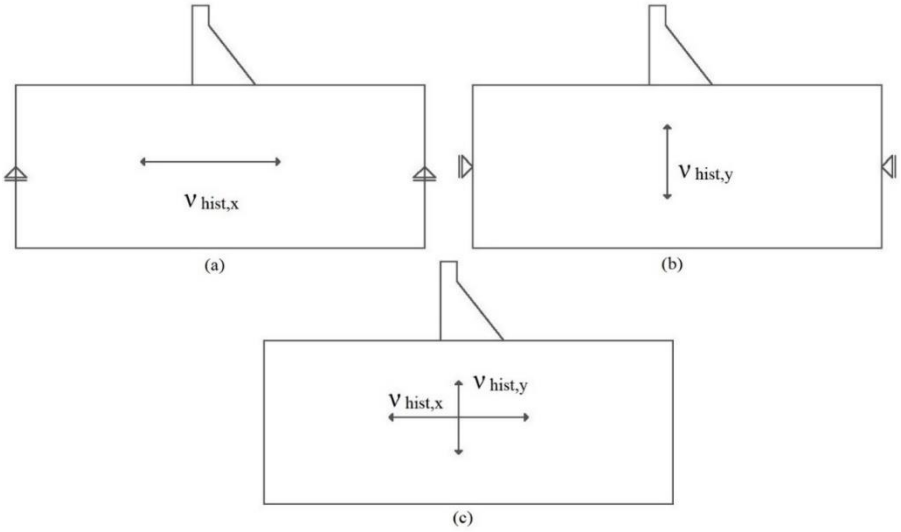

Figure 4.2 - Rigid rock mass foundation and application of the seismic action through velocity history records

4.3.2 Deformable rock mass foundation and seismic application using stress wave history

When the rock mass foundation is deformable, the seismic loading under explicit solutions procedures is applied trough a shear (τ) and/or pressure (σ) stress wave history, determined from the velocity history, according to (Bretas, 2012):

$$\boldsymbol{\tau = \rho_f C_s v_s} \tag{4.4}$$

$$\boldsymbol{C_s = \sqrt{\frac{G}{\rho_f}}} \tag{4.5}$$

$$\boldsymbol{\sigma = \rho_f C_p v_p} \tag{4.6}$$

$$\boldsymbol{C_p = \sqrt{\frac{K + \left(\frac{4}{3}\right) G}{\rho_f}}} \tag{4.7}$$

where τ is the shear stress (N/mm^2), σ is the normal stress (N/mm^2), ρ_f is the foundation density (kg/m^3), v_s is the shear wave velocity (m/s), v_p is the pressure wave velocity (m/s), C_s is the shear wave propagation velocity through a continuous medium (m/s), C_p is the pressure wave propagation velocity through a continuous medium (m/s), G is the foundation shear modulus (Pa) and K is the foundation bulk modulus (Pa).

When this procedure is adopted, it is only possible to apply one of the seismic action components. If a stress wave is imposed in the *x* direction, the lateral foundation boundaries must be fixed in the *y* direction. A viscous boundary is applied in the horizontal direction at the base of the model (Figure 4.3 a). If a pressure wave is imposed in the *y* direction, the lateral foundation boundaries must be fixed in the *x* direction. In this case, a viscous boundary is applied in the vertical direction at the base of the model (Figure 4.3 b).

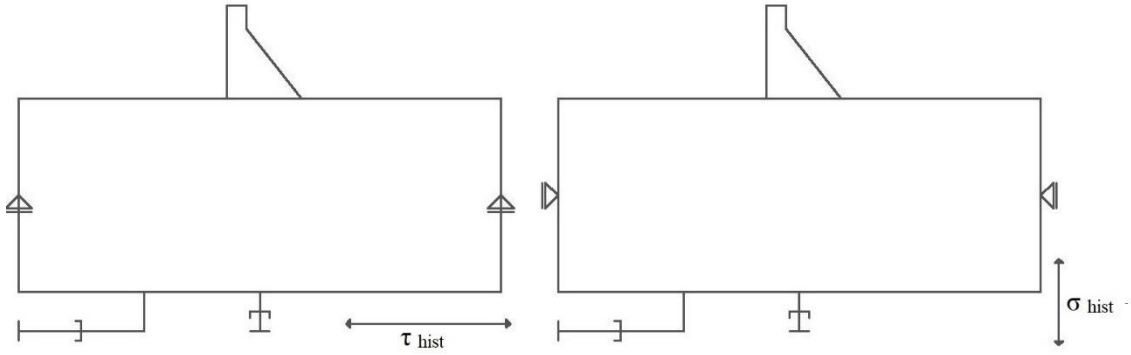

Figure 4.3 – Deformable rock mass foundation and application of the seismic action through stress wave history

For numerical implementation in the computational program, in the case of the shear wave, a reference shear stress (τ_{ref}) is initially applied, derived from the initial reference velocity (v_{ref}), according to (Bretas, 2012):

$$\boldsymbol{\tau_{ref} = \rho_f C_s v_{s,ref}} \quad \textbf{(4.8)}$$

where τ_{ref} is the initial reference shear stress (Pa) and $v_{s,ref}$ is the initial reference shear velocity (m/s).

The equation of movement in every nodal point is normally established and takes into account the force resulting of the shear stresses along this degree of freedom. This resulting force is updated at every step of the calculation, accordingly to the velocity history record. Hence:

$$\boldsymbol{\tau = \tau_{ref} v_{hist}} \quad \textbf{(4.9)}$$

The v_{hist} value is updated by interpolation of the velocity history record in every step of the calculation program, because the history step normally does not coincide with the calculation step.

If $v_{s,ref}$ is equal to 1 m/s, the velocity history record must be adapted for the maximum velocity wanted. Otherwise, $v_{s,ref}$ can be considered as a scale factor.

This solution assumes the existence of viscous boundaries that are able to absorb the reflected waves from the free surfaces and the structure (Lysmer & Kuhlemeyer, 1969). Viscous boundaries can be imposed in the normal and tangential directions of the surface and their restrictions are established in the *x* and *y* directions.

$$\alpha_{fr,n} = \frac{\rho_f \, C_p \, A_i}{m} \tag{4.10}$$

$$\alpha_{fr,s} = \frac{\rho_f \, C_s \, A_i}{m} \tag{4.11}$$

where $\alpha_{fr,n}$ is the viscous boundary damping ratio in the normal direction, $\alpha_{fr,s}$ is the viscous boundary damping ratio in the tangential direction, A_i is the influence area of the nodal point (m^2), *m* is the nodal point mass (kg).

4.3.3 Deformable rock mass foundation and seismic application using free-field boundary conditions

If the earthquake loading is applied on both directions, free-field conditions at the lateral boundaries have to be adopted. The free-field represents an artificial boundary which simulates the existence of an infinite medium that absorbs the reflected waves by the free surface and the structure and applies equivalent stresses. A Free-field model is added to the main model (dam and rock mass foundation) and consists of two columns, one in each lateral boundary of the foundation, with unit width and with the same height as the foundation medium. The boundary conditions and dynamic actions applied in the free-field are the same as those applied at the base of the main model (Figure 4.4 a).

The free-field lateral boundaries allow not only simultaneous application of the earthquake shear and the pressure component of the waves but also the absorption of the reflected waves by the lateral sides of the foundation model.

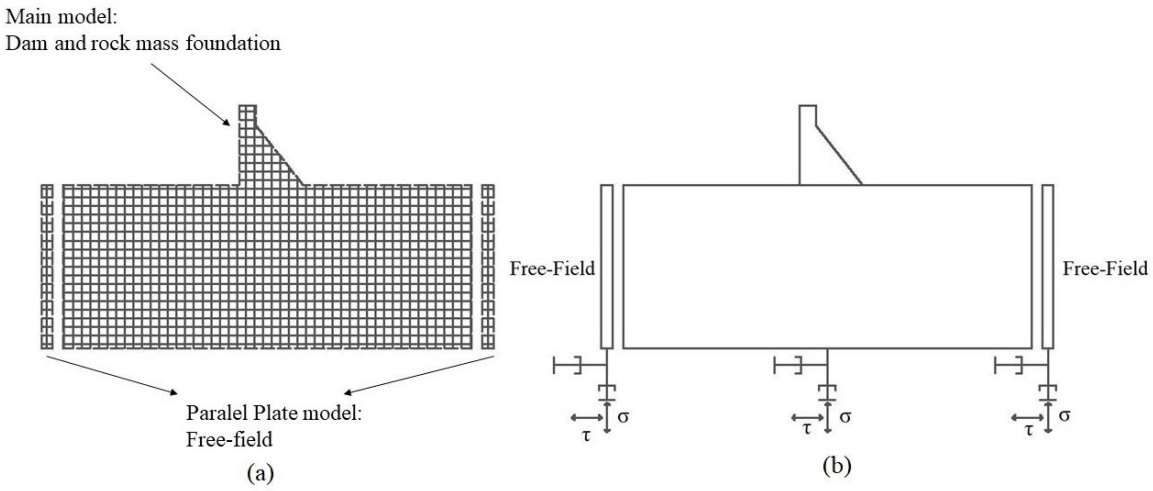

Figure 4.4 - Deformable rock mass foundation, free-field boundary conditions

4.4 Rayleigh damping

For dynamic analysis, Rayleigh damping is usually adopted given its simplicity and the control it allows over modal damping ratios. This formulation presents two coefficients, one associated to the mass matrix, [M], which is commonly designated by α, and the other one associated to the stiffness matrix, [K], commonly designated by β. The damping matrix, [C], is given by:

$$[\boldsymbol{C}] = \boldsymbol{\alpha}\,[\boldsymbol{M}] + \boldsymbol{\beta}\,[\boldsymbol{K}] \tag{4.12}$$

The mass proportional term corresponds physically to linear viscous dampers connecting the nodal points of the structure to external supports. The stiffness proportional term corresponds to linear viscous dampers connecting the nodal points of the structure (Hall, 2006).

The coefficients α and β can be defined based on the critical damping definition, that is:

$$\boldsymbol{c_{cr}} = \boldsymbol{2\,m\,\omega} \tag{4.13}$$

where c_{cr} is the critical damping, m is the mass of the structure and ω is the fundamental natural frequency. Thus, the relative damping ratio is,

$$\xi = \frac{c}{c_{cr}} = \frac{1}{2}\left(\frac{\alpha}{\omega} + \beta\,\omega\right) \tag{4.14}$$

where,

$$\alpha = \xi\,\omega = 2\,\pi\,\xi\,f \tag{4.15}$$

$$\beta = \frac{2\,\xi}{\omega} = \frac{1}{\pi}\,\frac{\xi}{f} \tag{4.16}$$

In Equations 4.15 and 4.16, ξ is the relative damping ratio and *f* is the frequency of the target structural mode. The fundamental mode of vibration associated to the lowest frequency is usually adopted. The program Parmac2d-FFlow has a calculation module that finds the eigenvalues and the eigenvectors corresponding to the vibration mode of a given structure.

Figure 4.5 shows the modal damping percentage in terms of the vibration frequency, for a 5 % damping ratio and a target frequency of 1.76 Hz. It can be observed that the mass proportional term highly damps modal responses with lower frequencies. For high frequencies, the mass proportional term has a small contribution. This, as shown in the case studies presented in chapter 5, can lead to higher shear sliding displacement values when compared to the ones obtained when Rayleigh damping is adopted (Monteiro Azevedo et al., 2012).

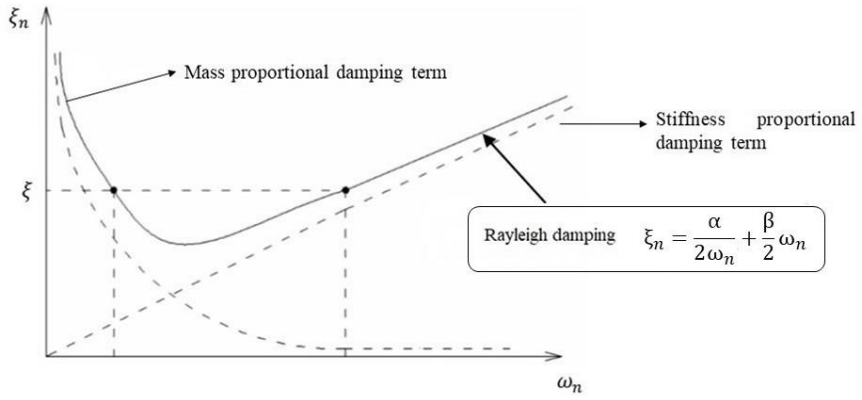

Figure 4.5 - Rayleigh damping

As pointed out by Hall, (2006), the mass proportional term is not a real physical mechanism, which can lead to erroneous damping forces when the damping formulation is made in global coordinates and the mass proportional term is present.

When an explicit procedure is adopted, analyses are usually performed with the mass proportional term, given that the stiffness proportional term requires, for stability reasons, a significant reduction of the critical timestep. As it will be shown, in stability scenarios it is important to study the effects of mass proportional damping and stiffness proportional damping separately, because either one of these factors may overdamp the main failure mode.

4.5 Safety factor criteria

Analysis of stresses in the dam body at design stage is traditionally based on the calculation of a local safety factor with the purpose of quantifying the safety margin in each point of the dam regarding the state of stress associated to a given failure envelope.

For the maximum principal positive stress (tensile stress), the Rankine criteria is adopted, while for the maximum shear stress, a Mohr-Coulomb constitutive law is admitted. The local safety factor, s_f, determined in each nodal point through extrapolation of the values evaluated in the Gauss points is given by:

$$\boldsymbol{s_f = min\left(\left(\frac{\sigma_t}{\sigma_1}\right)\ if\ \sigma_1 > 0\ ;\ \frac{C\ \cos\varphi}{R - \sigma_0 \sin\varphi}\right)} \tag{4.17}$$

where C [MPa] is the cohesion, φ is the friction angle, σ_t [MPa] is the tensile stress, σ_i [MPa] is the principal stress "i". The values R and σ_0 are functions of the principal stresses, σ_1 and σ_3, being given by:

$$\boldsymbol{R = \sqrt{\frac{(\sigma_1 - \sigma_3)^2}{4}}} \tag{4.18}$$

$$\boldsymbol{\sigma_0 = \frac{\sigma_1 + \sigma_3}{2}} \tag{4.19}$$

By defining the local safety factor, it is assumed that every component of the local stress state is increased to a point that the Mohr's circle is tangent to the failure envelope. A decrease of the cohesion and of the tensile strength tends to shift the failure envelope to a position tangent to the circle.

4.6 Application example with the Parmac2D-FFlow program

4.6.1 Model description

With the purpose of validating the free-field model and in order to verify whether the MDE loading was properly set, the program Parmac2D-FFlow was used to study the model behavior under MDE loading.

The dam geometry is the same as the one previously studied in chapter 3. The height of the dam is 15 m and a grout curtain and a drainage system are simulated in the dam foundation. The free-fields are also represented (Figure 4.6). A non-linear model is adopted only at the interface between the dam and the foundation. The analyses were carried out for an earthquake with a peak ground acceleration of 0.17 g using the horizontal and vertical acceleration records defined in chapter 5.

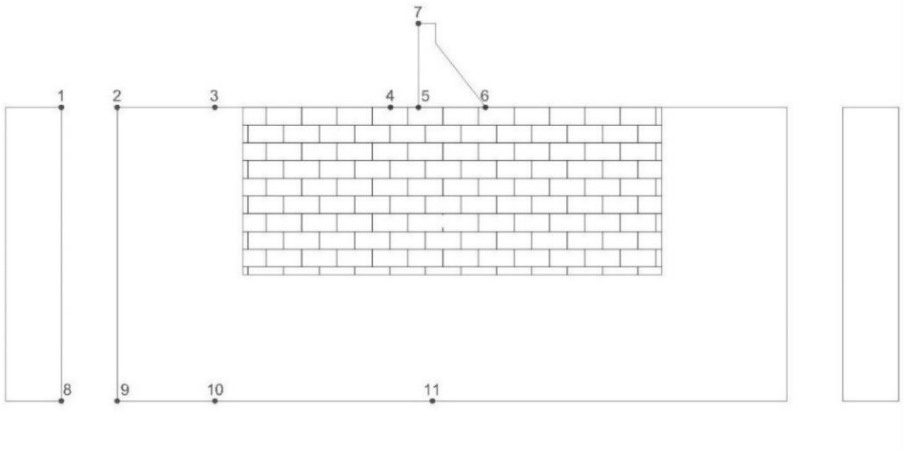

Figure 4.6 - Dam model highlighting the points where results are recorded during the seismic analysis

As can be seen in Figure 4.6, results during the seismic analysis are recorded in eleven points. The points where the velocities are compared are situated at the top of the free field (point 1) and at the top of the foundation, upstream from the dam, approaching the heel of the dam (points 2-5).

4.6.2 Analysis of results

The velocities obtained in 5 different points are presented from Figure 4.7 to Figure 4.11 and compared with the vertical and horizontal records of the applied MDE loading. The MDE loading lasts 5 seconds. The results on the top of the free-field and on the vicinity of this point are, as expected, exactly the same as those equivalent to the MDE loading. As the record point approaches

the dam's heel, a small deviation in the velocity recorded is expected. This is due the interaction between the foundation and the dam body.

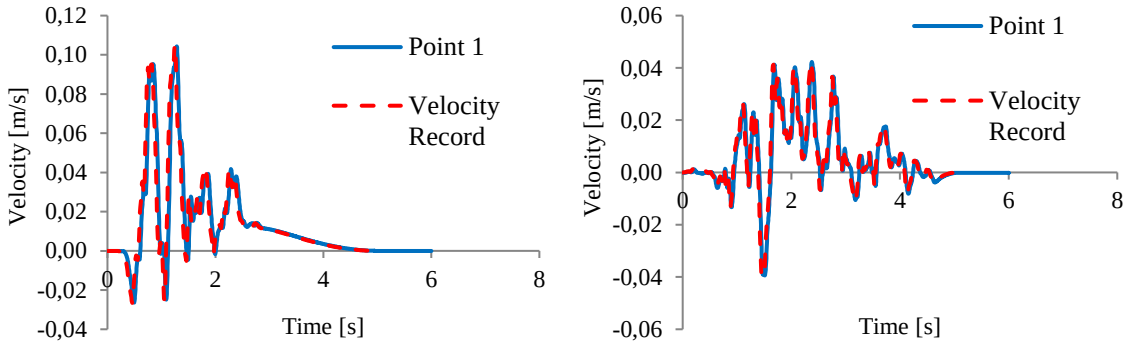

a) X direction b) Y direction

Figure 4.7 - Velocity results in point 1 for an earthquake with a PGA of 0.17 g and non-linear behavior of the dam/foundation interface

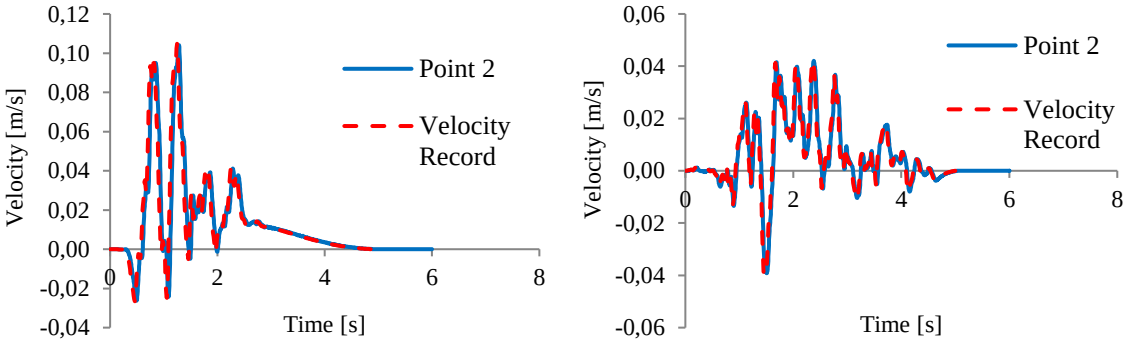

c) X direction d) Y direction

Figure 4.8 - Velocity results in point 2 for an earthquake with a PGA of 0.17 g and non-linear behavior of the dam/foundation interface

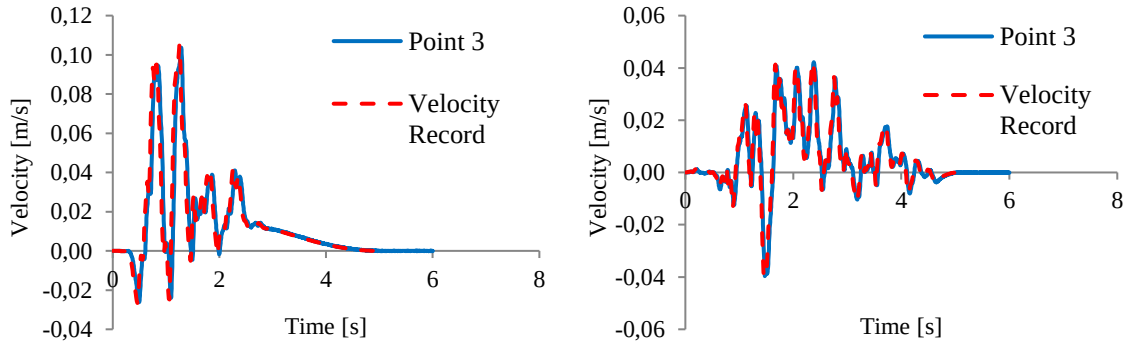

e) X direction f) Y direction

Figure 4.9 - Velocity results in point 3 for an earthquake with a PGA of 0.17 g and non-linear behavior of the dam/foundation interface

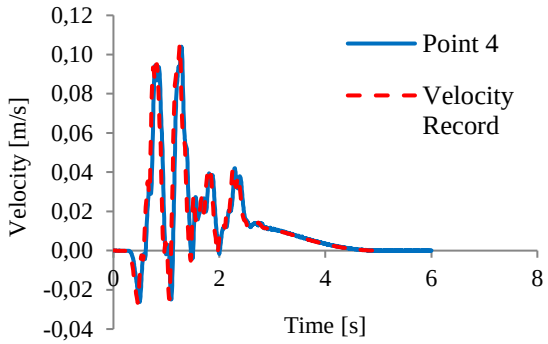

g) X direction

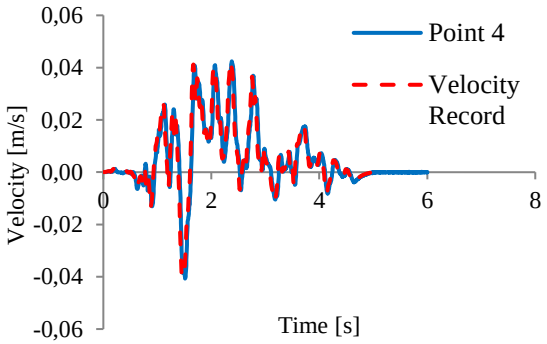

h) Y direction

Figure 4.10 - Velocity results in point 4 for an earthquake with a PGA of 0.17 g and non-linear behavior of the dam/foundation interface

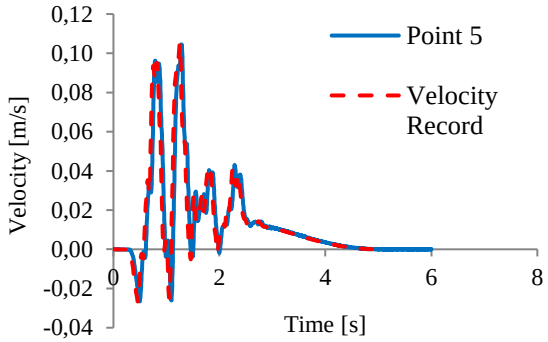

i) X direction

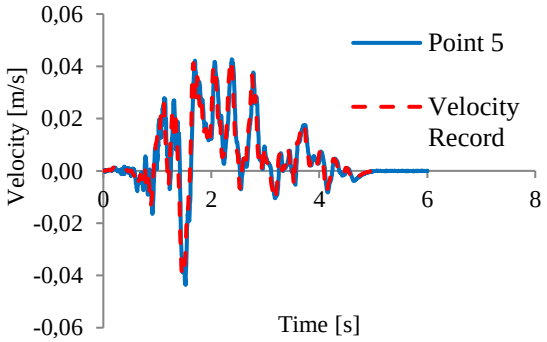

j) Y direction

Figure 4.11 - Velocity results in points 5 for an earthquake with a PGA of 0.17 g and non-linear behavior of the dam/foundation interface

5 NUMERICAL MODELLING OF THE SEISMIC BEHAVIOR OF GRAVITY DAM FOUNDATIONS

In order to study the hydrodynamic behavior of a concrete dam foundation under a shear sliding failure scenario through the concrete/rock interface, for the maximum design earthquake (MDE), two different dam models were analysed: a 15 m high dam (Model 1) and a 30 m high dam (Model 2). For each of these dams, the foundation model has horizontal and vertical discontinuities, like the ones described in chapter 3.4.1. Three different peak ground accelerations, PGA, were considered: 0.17 g (Ma), 0.26 g (Mb) and 0.34 g (Mc). For the vertical component, a 2/3 reduction factor was considered.

Two different modelling hypotheses were evaluated: (1) non-linear behavior only of the concrete dam structure/fractured foundation interface and (2) non-linear behavior of the concrete dam structure/fracture foundation interface and the fractured foundation. For each modelling hypothesis, two damping possibilities were considered: Rayleigh damping (K) and mass proportional damping only (M).

In every case studied, the rock mass hydraulic and mechanical characteristics are improved with grout and drainage systems, the water level upstream is equal to the dam's height and the water level downstream is zero.

For the models where it is only considered non-linear behavior of the interface between the dam and the foundation, a linear elastic hydromechanical analysis is first performed and then the characteristics of the interface are altered. For the cases where both the concrete/rock interface and the fractured foundation interfaces have non-linear behavior, an initial analysis is carried out where the foundation non-linear behavior is considered, followed by a second analysis where the concrete/rock interface is also considered.

The response of the different modelling hypotheses is compared. Comparisons regarding velocities in determined points, water pressure and normal stress in the joints are presented. The horizontal displacement at the crest of the dam and the shear sliding displacement at heel and toe of the dam are compared for both damping hypotheses. The interface stiffness parameters influence in the model's response is also evaluated for both modelling hypotheses.

The geometry of the dams studied was explained previously, in chapter 3.4.1 and is presented in Table 5.1.

Table 5.1 – Depth of the grout curtain and drainage boreholes

Model	Dam height (m)	Depth of the waterproof grout curtain (m)	Depth of drainage boreholes (m)
1	15	7.2	6.0
2	30	15.4	8.4

The mechanical and hydraulic models for the two dams studied are presented in Figure 5.1 and Figure 5.2. In the mechanical models, the adopted free-fields are present in the left and right sides of the foundation. The elastic foundation is included in the analysis because the program adopted only allows elastic free-fields.

No hydraulic model is considered at the dam interface construction joints given that the permeability factor of the dam structure is much lower than the permeability factor of the fractured foundation.

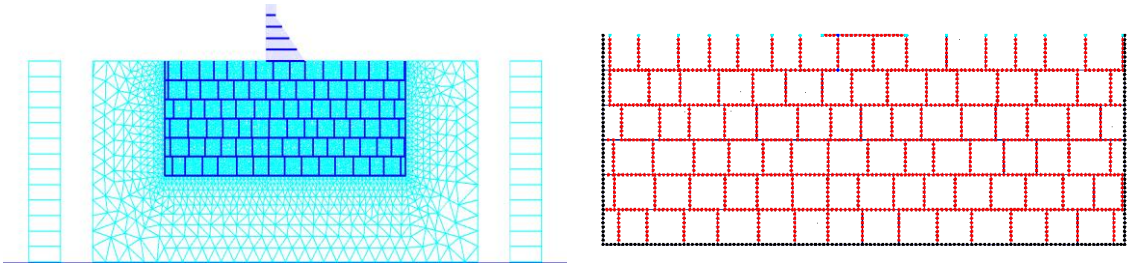

a) Mechanical model: interface elements, triangular plane elements, nodal points and free-field

b) Hydraulic model: seepage channels and hydraulic nodes

Figure 5.1 – Discretization of the hydrodynamic model of the 15 m high dam

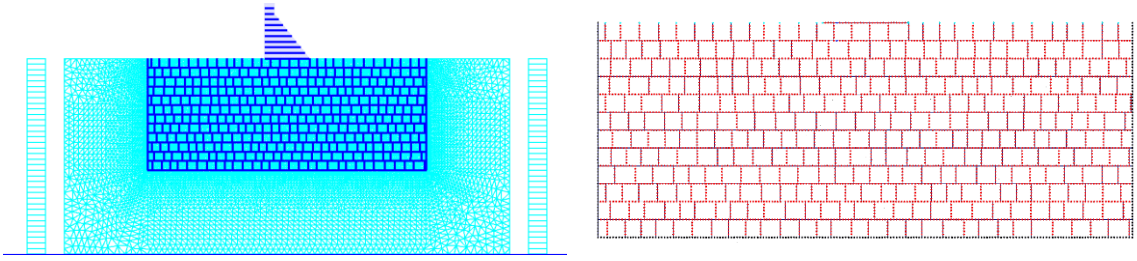

a) Mechanical model: interface elements, triangular plane elements, nodal points and free-field

b) Hydraulic model: seepage channels and hydraulic nodes

Figure 5.2 - Discretization of the hydrodynamic model of the 30 m high dam

Table 5.2 presents some data related to the mechanical and hydraulic models such as number of blocks, number of interfaces, number of hydraulic nodes and average edge length of the triangular elements.

Table 5.2 – Mechanical and hydraulic data

Model	Nº of deformable blocks	Nº of triangular shape elements	Nº of nodal points	Nº of interfaces	Nº of hydraulic nodes	Average edge length
1	104	11425	7622	1642	1520	0.6
2	382	22477	15753	3827	3374	0.6

In every model, the values of displacements, stresses and velocities were exported in some pre-defined points, shown in Figure 4.6, to asses and further understand the numerical response of the dam models studied.

5.1 Material properties

The numerical model consists of three different blocks: dam, fractured area of the dam foundation and homogeneous foundation. These blocks interact between each other through interfaces. The mechanical and hydraulic properties are the same for the two analysed models. Table 5.3 presents the normal and shear stiffnesses of the interfaces between materials. Table 5.4 presents the mechanical properties of the three different blocks.

Table 5.3 – Normal and shear stiffnesses of the interfaces between materials

Interfaces between materials	k_n [GPa/m]	k_s [GPa/m]
Construction joints	60.0	30.0
Dam/foundation joint	36.0	18.0
Foundation faults	36.0	18.0
Fractured/elastic foundation	30.0	15.0

Table 5.4 - Mechanical properties of the materials

Material	E [GPa]	ν	ρ [kg/m^3]
Dam's concrete	30.0	0.2	2400.0
Fractured foundation	18.0	0.2	2650.0
Continuous foundation	15.0	0.2	2650.0

As mentioned before, two calculation scenarios were admitted: i) non-linear behavior only of the dam/fractured foundation interface and ii) non-linear behavior of the dam/fractured foundation interface and of the fractured foundation. In both cases, the interface elements are simulated by a Mohr-Coulomb constitutive law model with a tensile cut-off criterion. For the concrete/foundation joint, the friction angle (φ) is 50º and the cohesion (C) and maximum tensile stresses (σ_t) are initially set equal to 3 MPa. Prior to the seismic calculation, the assumed values of cohesion and maximum tensile stress are set to zero. For the interfaces between blocks of the foundation, the friction angle is equal to 35º and both the cohesion and the maximum tensile stress are set to zero.

In a simplified manner, the elastic Young's modulus, the cohesion and the strength properties assumed for all the materials and interfaces are those normally used in a static analysis, amplified by a factor of 1.5.

The hydraulic properties of the seepage channels between interfaces, such as the water bulk modulus and permeability factor, are presented in Table 5.5.

Table 5.5 – Hydraulic properties of the seepage channels

Seepage channel (SC)	K_w [GPa]	k_{CE} [$\times 10^8$ MPa^{-1}s^{-1}]
SC concrete/rock mass	2.1	0.8300
SC rock mass/rock mass	2.1	0.4150
SC concrete/rock mass in the grout curtain's area	2.1	0.3270
SC rock mass/rock mass in the grout curtain's area	2.1	0.1653

The value of the hydraulic opening (a_0) adopted in the calculation is 0.1668 mm. The value of the residual aperture is $a_0/3$ and the value of the maximum aperture is $5a_0$. The grout curtain reduces the permeability factor of the seepage channels it intersects. As for the drainage system, the water pressure is automatically altered to one third of the water pressure upstream from the dam. Due to the short duration of the seismic action, the water pressures are kept constant during the MDE loading and thus the fluid flow coupling is not performed.

5.2 Fundamental frequency and velocity history record

For the MDE, two acceleration records were adopted for the vertical and for the horizontal components, Figure 5.3. They were defined based on a fault model, Carvalho, (2007), for a peak

ground acceleration of 0.17 g. The records were then scaled for the several peak ground acceleration values analysed.

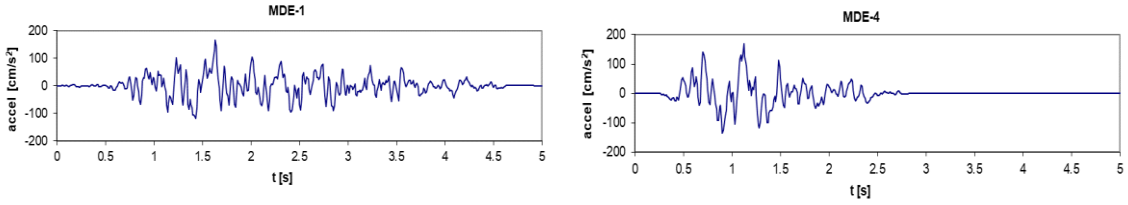

a) Horizontal component (0.17 g) b) Vertical component (0.17 g)

Figure 5.3 - Accelerograms for maximum design earthquake (horizontal and vertical components)

For the dynamic analysis, a Rayleigh damping centered in the fundamental modal response frequency was adopted. For this reason, it is required to perform a modal analysis in order to find the numerical model fundamental frequency. Table 5.6 presents the fundamental frequencies for each model analysed. These results were obtained using the program Parmac2D-FFlow, considering a massless foundation and adopting the Westergaard added mass at the upstream face. In addition to the fundamental frequency, to completely define all Rayleigh damping constants, it is important to specify the critical damping ratio, which was considered equal to 5 % in every model. In the eigenvalue analysis, a linear elastic model was adopted in all interfaces. Because the dam corresponding to model 2 is bigger than model 1, the vibration frequency is lower for model 2, due to the fact that it inversely depends on the mass.

Table 5.6 – Fundamental frequency

Mode 1	Model 1	Model 2
Vibration frequency [Hz]	13.30	6.82

5.3 Boundary conditions

In the mechanical model, the lateral boundaries and the base of the model are fixed, so the displacements in every direction are zero. In the rock mass surface, both upstream and downstream of the dam, and on the upstream face of the dam, pressures simulating the hydrostatic water pressure are applied.

Regarding the hydraulic boundary conditions, zero permeability was assumed along the bottom and along the sides of the models. In the hydraulic nodes located at the rock surface, upstream of the dam, the pressure values were set according to the water level.

At the lateral boundaries of the model, a free-field is imposed and at the bottom of the model, non-reflecting boundaries are adopted (Lemos et al., 1999). The dynamic input was applied as shear and pressure stress waves, given the corresponding velocity components.

5.4 Calculation procedure

The analysis is divided into three stages:

1) In a first stage, a mechanical analysis is carried out, determining the effect of the self-weight of the dam considering a ratio between the horizontal and the vertical effective stresses *in situ* equal to 0.5.

2) In a second stage, the hydrostatic water pressures upstream and downstream are set according to the reservoir levels and a coupled hydromechanical analysis is performed. The permeability factor of the seepage channels intersected by the grout curtain is reduced and the water pressure on the hydraulic nodes close to the drainage line are set accordingly. The interface behavior of the concrete/rock and fractured rock interfaces are defined according to the already referred calculation scenarios.

3) In the last stage, the seismic analysis is performed by adding the Westergaard masses in every nodal point of the upstream face of the dam in the direction perpendicular to the upstream surface. After the seismic analysis, the values of displacement, water pressure, velocities and normal stress in pre-defined points are retrieved for further analysis.

5.5 Analysis of results

5.5.1 Foundation behavior

In the analysis of the dam models, two cases were adopted as good starting points for the shear sliding failure scenario through the concrete/rock interface for the maximum design earthquake (MDE).

In the first case, non-linear behavior is adopted just at the concrete/rock foundation and the foundation is assumed to be linear elastic. This option is commonly adopted at the design stage. In the second case, non-linear behavior is adopted at both the concrete/rock foundation interface and at the fractured rock interfaces. This would be the option that should be taken if information regarding the rock faults were available.

The effect of the foundation behavior on the dams response is studied by analysing the results output from the program Parmac2D-FFlow such as velocities, water pressure, normal effective stresses, and shear displacements. The results obtained with different foundation behaviors are compared and conclusions are taken.

5.5.1.1 Velocity

By recording the velocities in both directions in a point at the rock surface at the fractured area of the foundation, it is possible to assess if the consideration of a fractured rock does lead to an extra damping mechanism. Figure 5.4 and Figure 5.5 show the velocity recorded for both directions in point 4 (Figure 4.6), at the fractured foundation surface. The results are compared for both the elastic, interface model (1), and the fractured foundation, interface model (2). Only the results for a PGA value of 0.34 g and for both dam models 1 and 2 of are shown.

As showed in Figure 5.4 and Figure 5.5, the fact that the foundation is considered to be fractured does not have a significant effect on the registered ground velocities, which means that for the models considered the opening and closing of the discontinuities during the MDE for the non-linear model do not have a significant contribution to the damping mechanism. For this reason, the same velocity register can be used on both foundation scenarios, as the non-linear behavior of the interfaces does not have a significant influence in the attenuation of the imposed velocity fields.

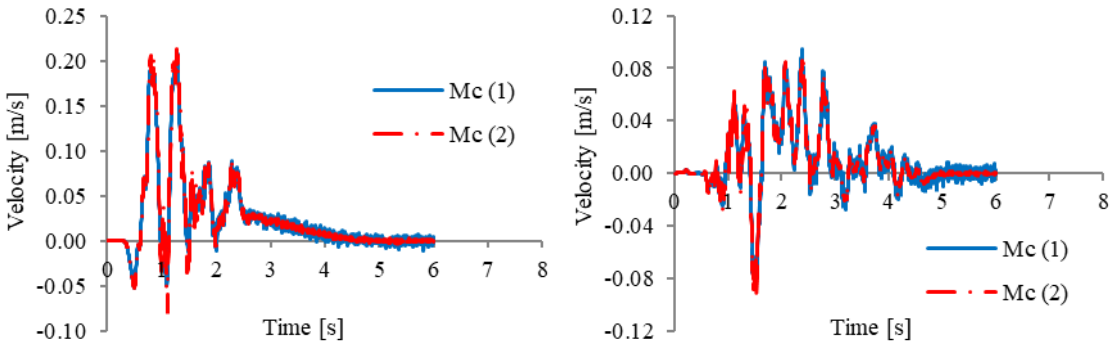

a) X direction b) Y direction

Figure 5.4 – Velocity recorded in point 4 for a PGA of 0.34 g (Mc) and for model 1

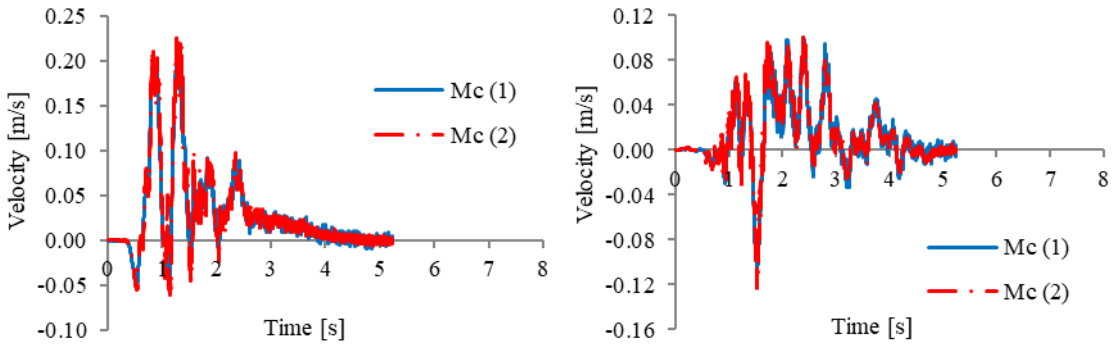

a) X direction b) Y direction

Figure 5.5 - Velocity recorded in point 4 for a PGA of 0.34 g (Mc) and for model 2

5.5.1.2 Water pressure

The water pressure distribution along the dam base represents the uplift pressure acting on a dam and is always taken into consideration when designing a dam because of its destabilizing effect. It is important to study the water pressure distribution for the two interface models because these results depend on the aperture of the discontinuities which may be different for each scenario.

The water pressure distribution along the dam base before the dynamic analysis is presented in Figure 5.6 a) for dam model 1 and in Figure 5.6 b) for dam model 2 for the two foundation models adopted, (1) and (2). The effect of the drainage system can be clearly identified in Figure 5.6 by the pressure reduction at a distance from the dam heel equal to approximately 1/6 of the dam's height. As mentioned, at the drainage line the head is equal to 1/3 of the head upstream of the dam.

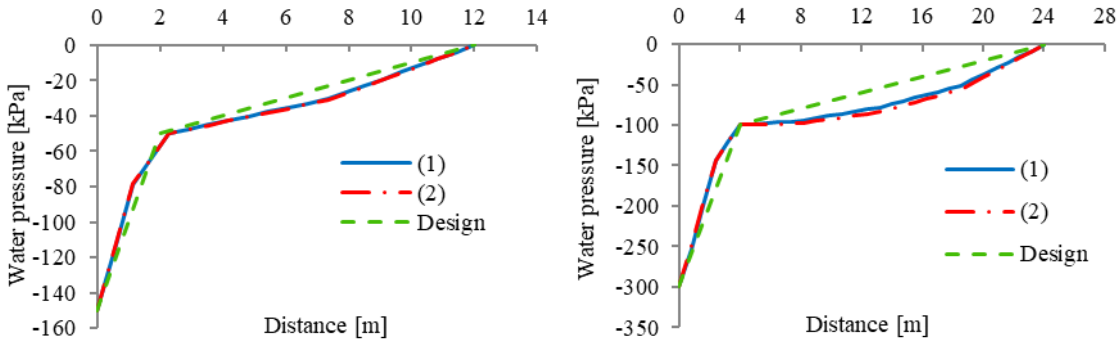

a) Dam model 1 b) Dam model 2

Figure 5.6 - Water pressure along the dam base for two interface models and for two dam heights

It is also possible to verify that the water pressure values at the dams heel and toe are defined by the reservoir level upstream and downstream of the dam, respectively. The reservoir level upstream

of the dam is equal to the dam's height, which is 15 metres for model 1 and 30 metres for model 2. Figure 5.6 also shows that the pressure distribution results obtained for interface model (1) are very similar to the results for interface model (2), following the known bilinear uplift distribution that is usually adopted at the design stage. The uplift bilinear design pressure curve with a water pressure in the drainage line equal to 1/3 of the difference between the upstream and downstream values, is in agreement with data obtained in piezometric readings taken in the foundations of a number of dams from both Tennessee Valley Authority and US Bureau of Reclamation (Casagrande, 1961).

5.5.1.3 Normal effective stress

The normal effective stress in the interface between the concrete dam and the rock mass foundation is an important parameter because it is directly related with the possible shear failure that can occur, according to the adopted Mohr-Coulomb failure model.

Figure 5.7 presents the normal effective stress along the dam base for the two interface models, (1) and (2) and for the dams with different heights. It can be verified that the effective normal stresses are associated to a compressive stress state, as expected, due to the self-weight of the dam.

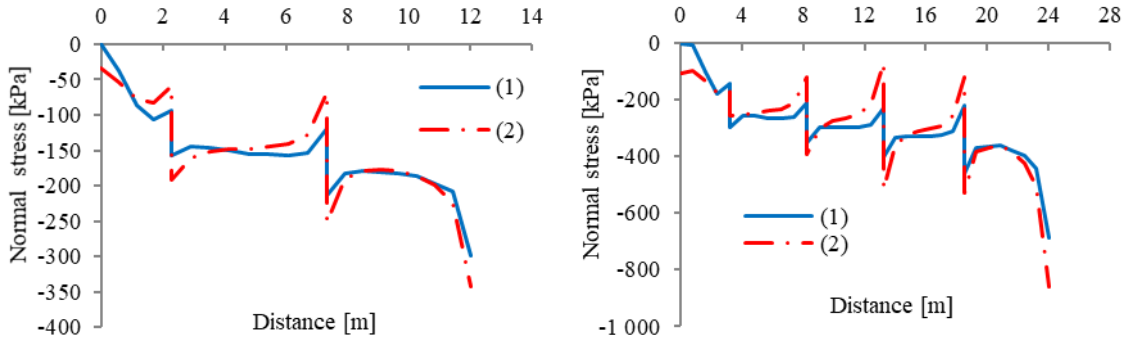

a) Dam model 1 b) Dam model 2

Figure 5.7 -Normal effective stress distribution along the dam/foundation interface before the seismic analysis

Results show that the stress distribution follows the same trendline for both interface models and both dams, 15 m high and 30 m high. The effective normal stress at the dam heel is zero for model (1), indicating that, already before the seismic analysis, openings occur in that zone. As for the dam toe, the effective normal stress results are higher for model (2). The discontinuities that occur at the normal effective stress are due to the discrete nature of the model.

As previously mentioned, shear sliding due to the seismic action is related to the normal effective stress distribution. The fact that models (1) and (2) have different stress distributions will lead to different behaviors under seismic action. The fact that in model (1) the dam is already decompressed at the dam heel may indicate that shear sliding will be favored but the response under seismic loading is highly non-linear and for this reason it is difficult to anticipate which model may lead to higher shear sliding displacements.

It should be highlighted that the normal effective stress diagram area is equal to the self-weight of the dam minus the uplift pressure and for this reason, the effective normal stress values are higher for the highest dam.

Figure 5.8 compares the results of the effective normal stress along the dam base before and after the seismic action. The peak values for the analysis after the earthquake are higher than before because of the vertical component of the acceleration, which increases the effective normal stress.

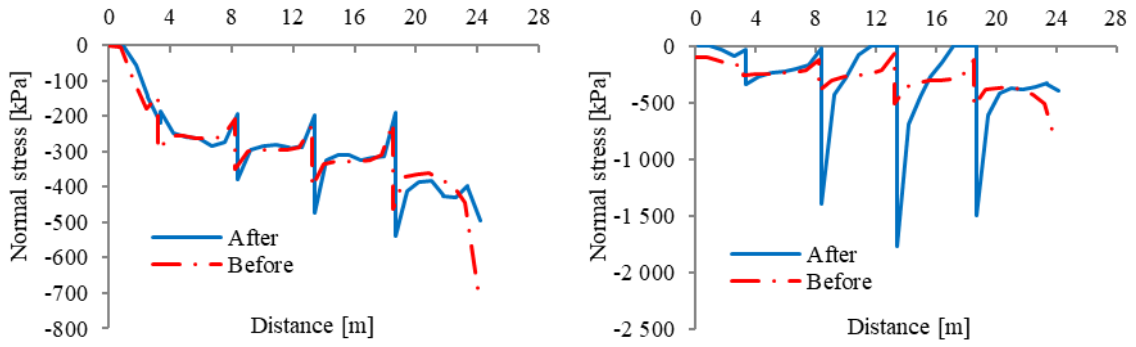

a) Interface model (1) b) Interface model (2)

Figure 5.8 - Comparison between the effective normal stress before and after the seismic analysis for the dam model 2 and a 0.34 g (Mc) earthquake

5.5.1.4 Shear sliding displacement

The shear sliding at the dam heel and toe for both dam heights are analysed for three different PGA values, Ma, Mb and Mc and for both models, (1) and (2). Figure 5.9, Figure 5.10 and Figure 5.11 show the results for the dam model 1 and Figure 5.12, Figure 5.13 and Figure 5.14 for the dam model 2.

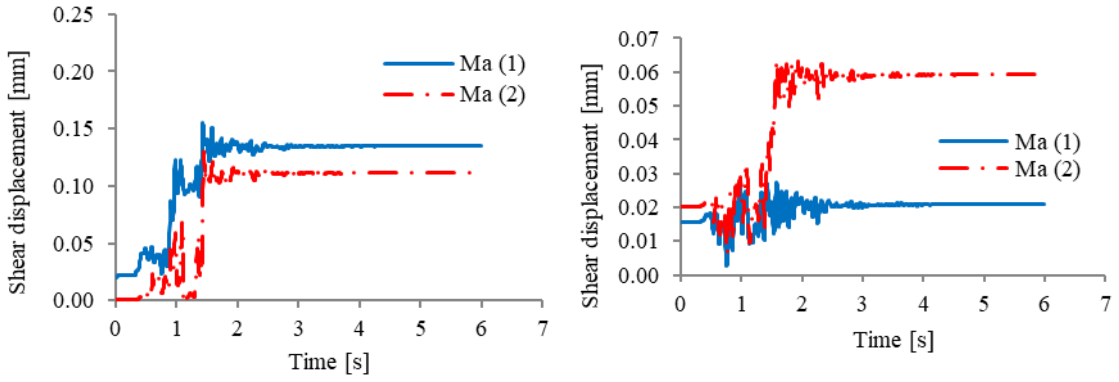

a) Dam heel b) Dam toe

Figure 5.9 - Shear sliding displacement at the dam's heel and toe for the dam model 1 and a PGA of 0.17 g

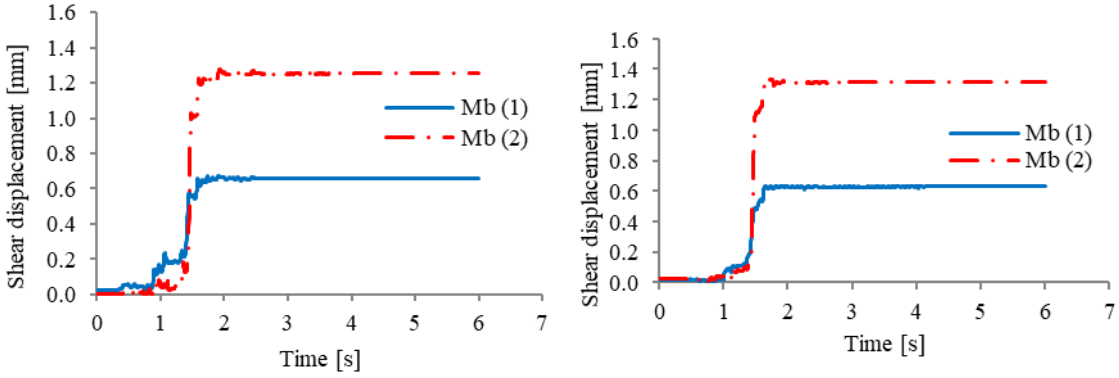

a) Dam heel b) Dam toe

Figure 5.10 - Shear sliding displacement at the dam's heel and toe for the dam model 1 and a PGA of 0.26 g

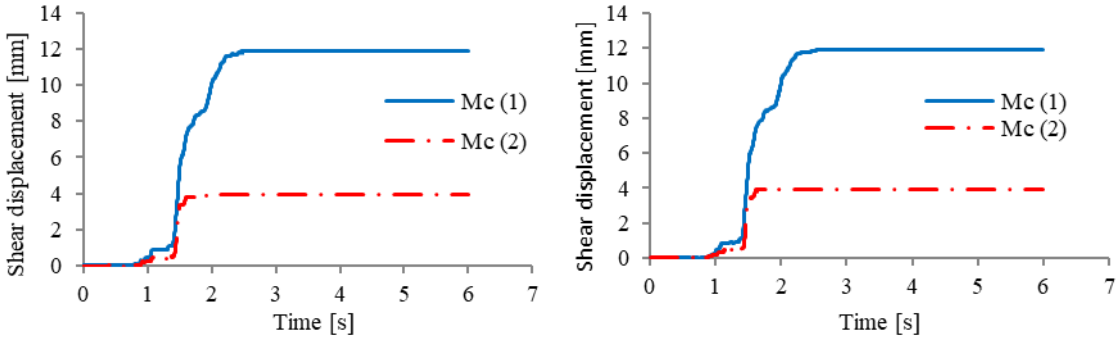

a) Dam heel b) Dam toe

Figure 5.11 - Shear sliding displacement at the dam's heel and toe for the dam model 1 and a PGA of 0.34 g

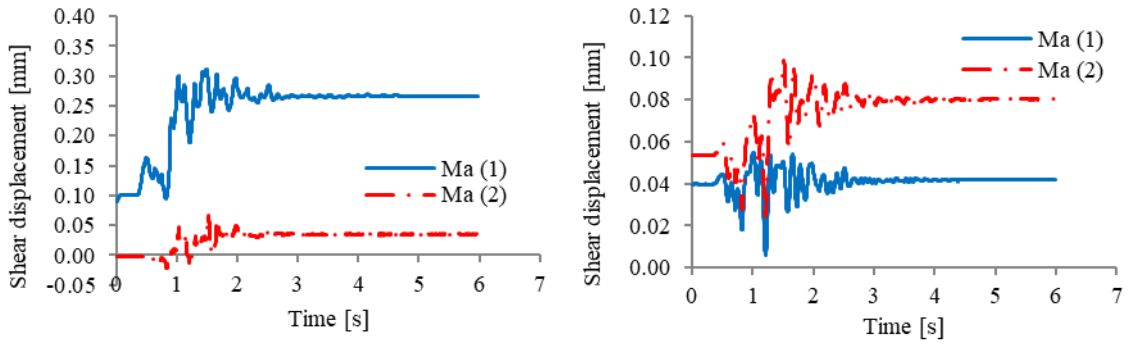

a) Dam heel b) Dam toe

Figure 5.12 - Shear sliding displacement at the dam's heel and toe for the dam model 2 and a PGA of 0.17 g

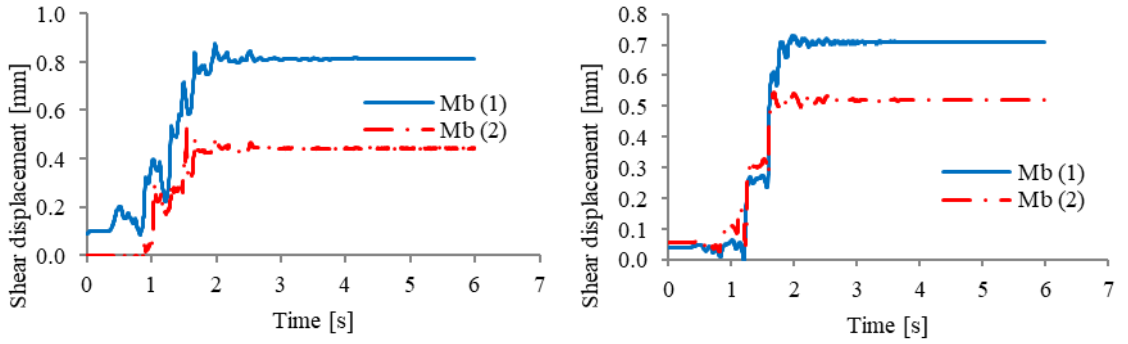

a) Dam heel b) Dam toe

Figure 5.13 Shear sliding displacement at the dam's heel and toe for the dam model 2 and a PGA of 0.26 g

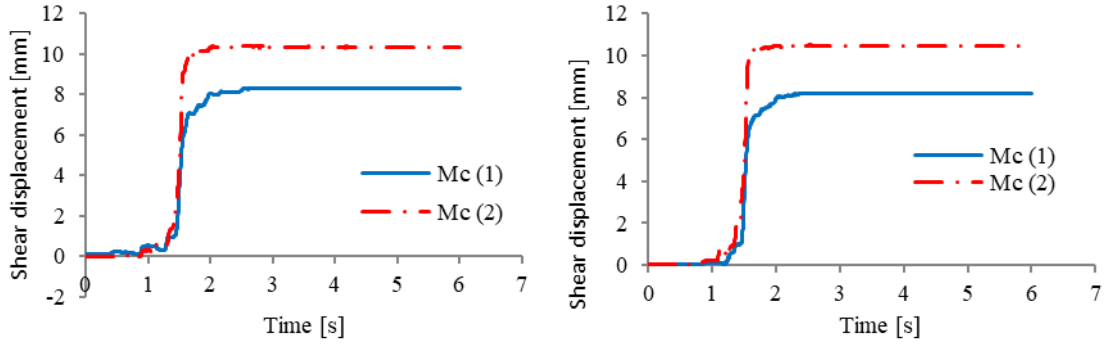

a) Dam heel b) Dam toe

Figure 5.14 - Shear sliding displacement at the dam's heel and toe for the dam model 2 and a PGA of 0.34 g

In Figure 5.10 it is possible to observe that, for the 15 m high dam, the shear sliding results obtained under a seismic loading with a 0.26 g PGA are greater when the non-linear behavior of the fractured

foundation is considered. For a seismic loading with a 0.34 g PGA, the highest shear sliding displacement occurred for the linear elastic foundation model (1).

For the 30 m high dam, the shear sliding displacement results for the seismic loading equivalent to a 0.26 g PGA, presented in Figure 5.13, are higher when the foundation behaves elastically (1). For the seismic loading with a 0.34 g PGA, the highest shear sliding displacements values occur when the non-linear fractured foundation behavior is adopted (2).

As shown in the figures previously presented, shear sliding usually occurs almost instantaneously as soon as the Mohr-Coulomb criterion is not verified. The shear sliding displacements under seismic loading are, as expected, very similar at the dam heel and toe, for both PGA and for both foundation behavior models. The jumps that occur in the shear displacement response at the dam interface are mostly associated to a rigid body motion of the dam body.

Note that the maximum shear sliding displacement value of 12 mm that is registered to occur at the dam model 2 indicates that this dam withstands a maximum design earthquake with a PGA of 0.34 g without compromising its safety. The small amplitude value that is registered also validates the small displacement hypothesis that is adopted in the calculations. If shear displacements higher than 5 % of the edge length were registered, the calculation algorithm would need to handle large displacements (Farinha et al., 2017).

Figure 5.15 presents the results of the maximum shear sliding displacement at the dams toe, for both foundation models and for all the adopted PGA values. It is possible to observe that for the higher PGA value, Mc, the results in the dam model 1 are higher for interface model (1) than for interface model (2), as shown in Figure 5.11 b).

The numerical results show that it is not possible to anticipate which foundation behavior will lead to higher shear sliding displacements under seismic loading, see also Figure 5.16 and Figure 5.17. It would be expected that a non-linear interface model for the fractured rock would be more conservative, but, as shown, the response is highly non-linear and influenced by the dam height and by the adopted PGA.

The shear sliding displacement at the dam toe for the three different PGA values and for both dam models is presented in Figure 5.16 and Figure 5.17.

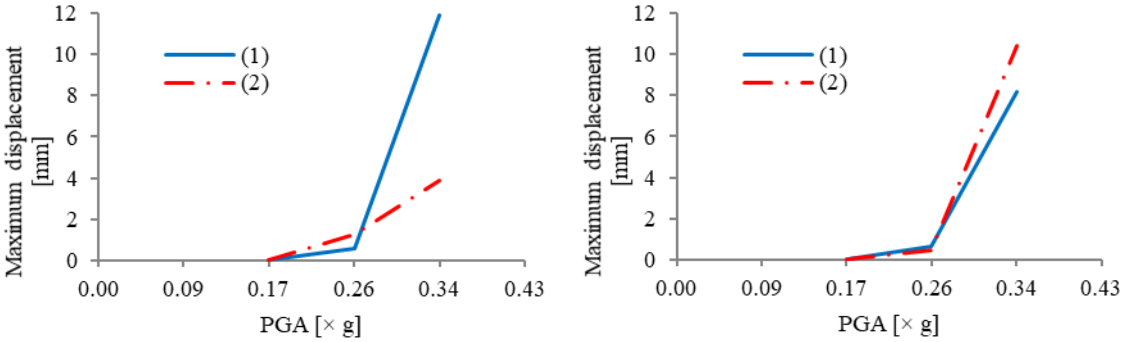

a) Dam model 1 b) Dam model 2

Figure 5.15 – Maximum displacements for three PGA values and for both interface models at the dams toe

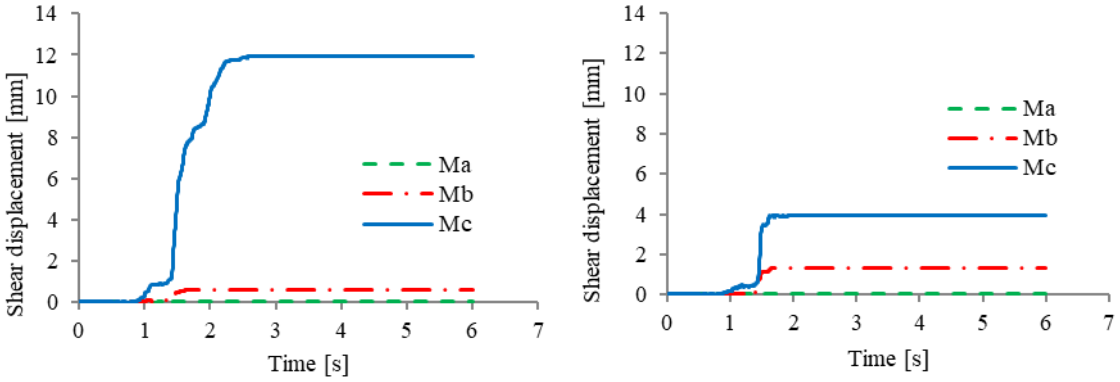

a) Interface model (1) b) Interface model (2)

Figure 5.16 - Shear sliding displacement at the toe of dam model 1

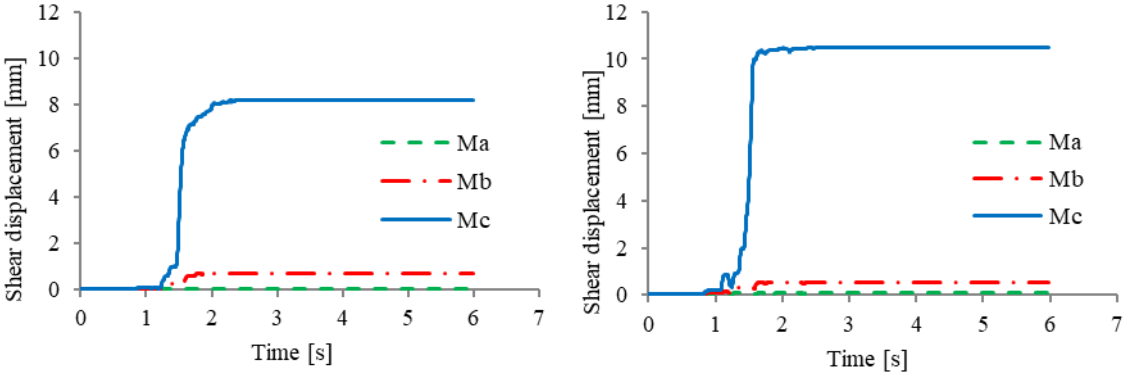

a) Interface model (1) b) Interface model (2)

Figure 5.17 - Shear sliding displacement at the toe of dam model 2

Figure 5.18 shows the time history of shear sliding and normal effective stress at the dam heel for both interface models and for the three adopted PGA values, Ma, Mb and Mc. It can be identified that shear sliding occurs at the time when the values of effective normal stress are zero, which may lead to an instantaneous instability as soon as the Mohr Coulomb criterion is not verified at the concrete/rock interface integration points.

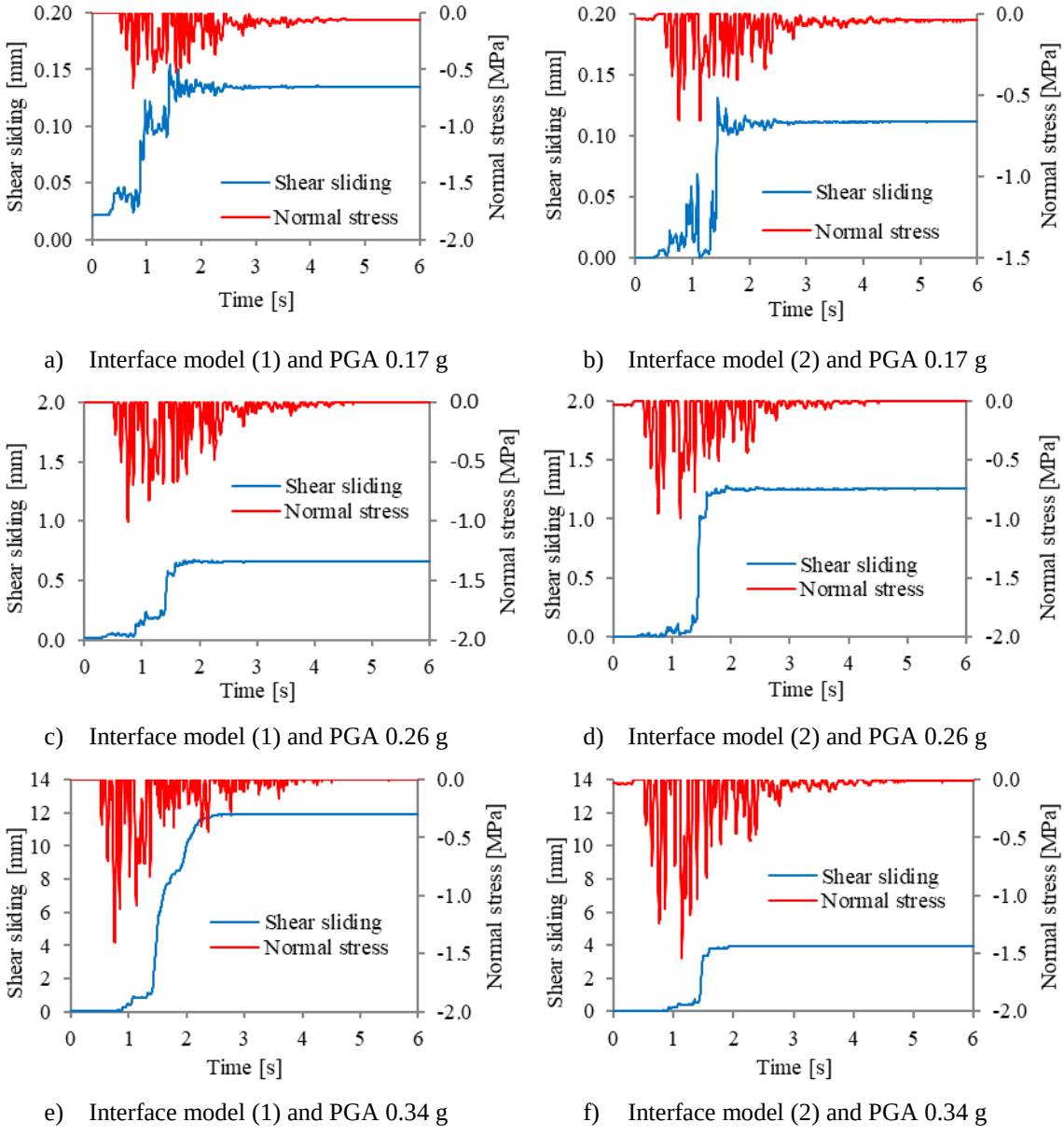

a) Interface model (1) and PGA 0.17 g

b) Interface model (2) and PGA 0.17 g

c) Interface model (1) and PGA 0.26 g

d) Interface model (2) and PGA 0.26 g

e) Interface model (1) and PGA 0.34 g

f) Interface model (2) and PGA 0.34 g

Figure 5.18 - Time history of shear displacement and normal stress at the heel of dam model 1

5.5.1.5 Maximum values

In order to fully characterize the normal effective stress and the shear sliding displacement behavior at the dam/foundation interface, the maximum and minimum values of the displacements (aperture and sliding) and stresses (normal stress and shear stress) were analysed for the two dams of different height, assuming a non-linear constitutive law at the interface and in the fractured foundation and considering mass proportional damping.

The results for the minimum and maximum displacements and stresses are shown in Table 5.7 and Table 5.8, for dam model 1 and for dam model 2, respectively. As expected, the displacements and stresses increase for the higher PGA values. The absolute values are higher for the 30 m high dam. It is possible to observe that the maximum normal tensile stresses are, for both cases, equal to 0 because, as known, the stresses at the dam/foundation interface must be compressive.

Table 5.7 – Minimum and maximum displacement and stresses for different peak ground accelerations for dam model 1

Peak ground acceleration	Displacement [mm]				Stress [MPa]			
	Aperture		Sliding		Normal		Shear	
	min	Max	min	Max	min	Max	min	Max
Ma (2)	-0.02	0.15	0.00	0.13	-0.66	0.00	-0.22	0.63
Mb (2)	-0.03	0.49	-0.01	1.33	-1.08	0.00	-0.34	1.19
Mc (2)	-0.04	0.77	-0.02	3.96	-1.62	0.00	-0.51	1.68

Table 5.8 - Minimum and maximum displacement and stresses for different peak ground accelerations for dam model 2

Peak ground acceleration	Displacement [mm]				Stress [MPa]			
	Aperture		Sliding		Normal		Shear	
	min	Max	min	Max	min	Max	min	Max
Ma (2)	-0.03	0.18	-0.02	0.10	-1.18	0.00	-0.37	1.24
Mb (2)	-0.06	0.58	-0.04	0.55	-2.24	0.00	-0.55	2.27
Mc (2)	-0.15	0.95	-0.04	10.5	-5.43	0.00	-0.91	2.91

The analysis of the minimum and the maximum values can also be performed for the dam's body. In this case, the stress acting in the dam is studied, as well as the safety factor. The analysis was carried out considering a non-linear constitutive law at the interface and in the fractured foundation and assuming mass proportional damping only.

The higher the safety factor, the safer the structure is against a seismic action. The greater safety factors are for the lower PGA values, both maximum and minimum values (Table 5.9 and Table 5.10).

Table 5.9 – Minimum and maximum safety factors and stresses for different peak ground accelerations for dam model 1

Peak ground acceleration	Safety factor		Stress [MPa]	
	min	Max	min	Max
Ma (2)	26.8	324.4	-1.1	0.1
Mb (2)	6.9	122.7	-1.5	0.4
Mc (2)	2.4	60.2	-1.6	1.3

Table 5.10 - Minimum and maximum safety factors and stresses for different peak ground accelerations for dam model 2

Peak ground acceleration	Safety factor		Stress [MPa]	
	min	Max	min	Max
Ma (2)	11.2	360.7	-2.0	0.3
Mb (2)	6.2	106.2	-2.3	0.5
Mc (2)	0.9	30.3	-4.2	3.1

5.5.2 Effect of the normal stiffness

In the soft contact approach adopted in this study, the joint element is also considered to be able to deform. The joint elastic properties may be chosen through a trial-and-error procedure in such a way that the overall deformability is within the expected range and that the joint normal displacement is negligible when compared to the adopted average finite element size (Hart, 1995).

Interface properties can also be derived from laboratory testing or by back calculation, knowing the deformability and the joint structure of the rock mass and the deformability of the intact rock. Values for normal stiffness of rock joints can range from 10 to 100 × 10^{-3} GPa/m for joints with soft clay infilling to over 100 GPa/m for tight joints in granite and basalt (Hart, 1995).

The adopted stiffness values are within the range of the values used in several research studies regarding discrete element applications (Farinha, 2010; Bureau, Keller, & McClelland, 2005; Barla, Bonini, & Cammarata, 2004; Itasca, 2004). A parametric study was also carried in order to assess the influence of the interface elastic values, (normal stiffness (*kn*) and shear stiffness (*ks*)) on the overall response. In order to do so, three different sets of normal and shear stiffnesses were

considered for the dam/foundation interface elements for the rock mass discontinuities: half of the reference stiffness values (0.5 *k)* and the double of the reference stiffness values (2 *k*). The reference stiffness values are the ones presented in Table 5.3.

5.5.2.1 Water pressure

In Figure 5.19 and Figure 5.20 the water pressure results are presented for each interface model along the base of the 15 m high dam and the 30 m high dam, for each adopted interface scenario. The results presented show that the water pressure distribution at the dam/rock interface is not influenced by the stiffness parameter.

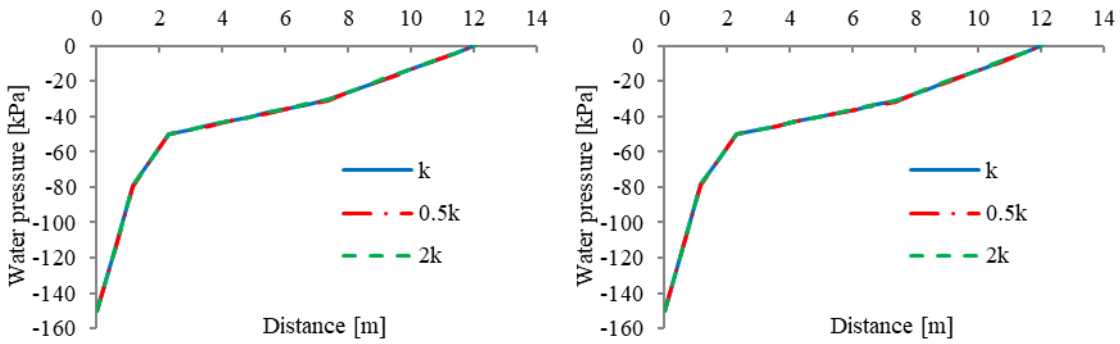

a) Interface model (1) b) Interface model (2)

Figure 5.19 – Dam model 1: Water pressure along the dam base for different interface models and different interface normal stiffnesses

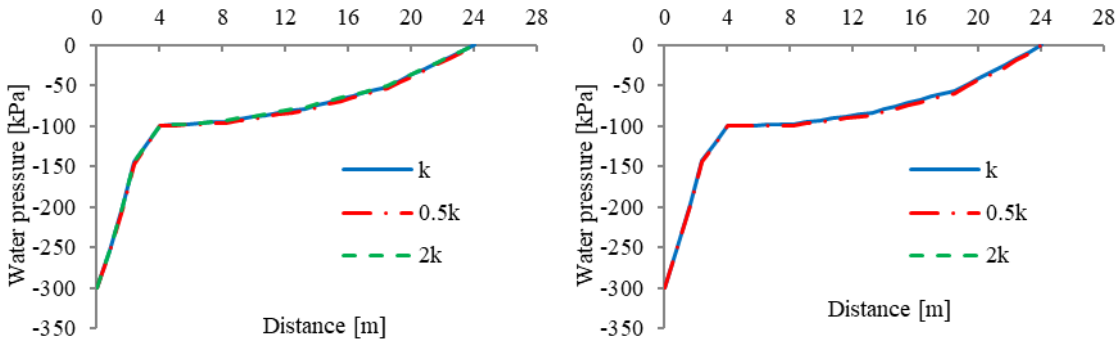

a) Interface model (1) b) Interface model (2)

Figure 5.20 – Dam model 2: Water pressure along the dam base for different interface models and different interface normal stiffnesses

5.5.2.2 Normal effective stress

The effect of the adopted stiffness parameter on the normal effective stress was also assessed for each interface model, (1) and (2), and for both dam heights. The results presented in Figure 5.21 and Figure 5.22 show that the influence of the stiffness parameter for the adopted range is also negligible.

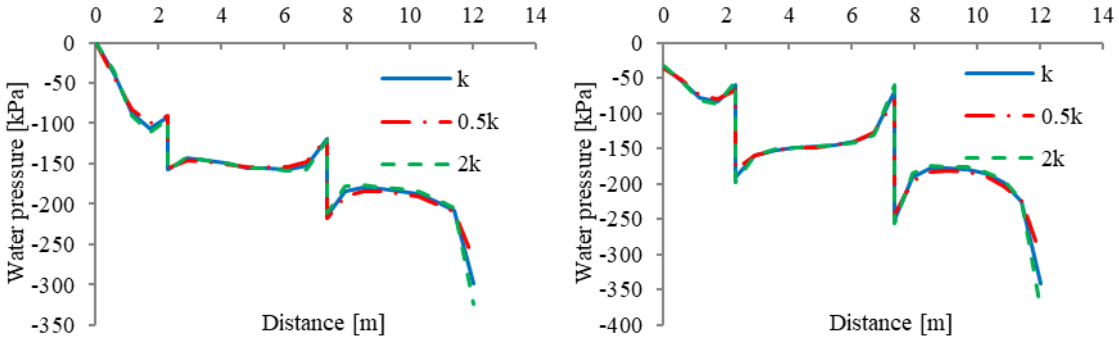

a) Interface model (1) b) Interface model (2)

Figure 5.21 – Dam model 1: Normal effective stress distribution along the dam/foundation interface for different interface models and different normal stiffnesses

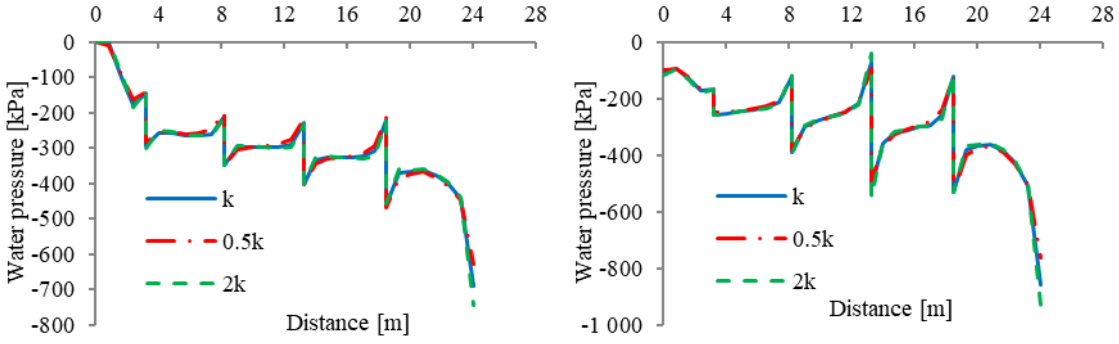

c) Interface model (1) d) Interface model (2)

Figure 5.22 – Dam model 2: Normal effective stress distribution along the dam/foundation interface for different interface models and different normal stiffnesses

5.5.2.3 Horizontal and shear sliding displacements

The calculated horizontal displacements at the dam crest and the shear sliding displacements are presented in Figure 5.23, Figure 5.24 and Figure 5.25 for dam model 1 and in Figure 5.26, Figure 5.27 and Figure 5.28 for dam model 2. Only the peak ground acceleration Mc was adopted.

The results presented show that the stiffness parameter has some influence on the shear displacement response. Also due to the highly non-linear process that occurs during seismic loading, it is not possible to predict which set of stiffness parameters will lead to a higher shear sliding. When the non-linear interface model is considered at the foundation, the highest displacement occurs for the highest stiffness value, for both dams, but when an elastic foundation is considered this is no longer verified. The numerical results show that it is always necessary to carry out a parametric study of the stiffness parameters given their influence on the overall response under seismic loading.

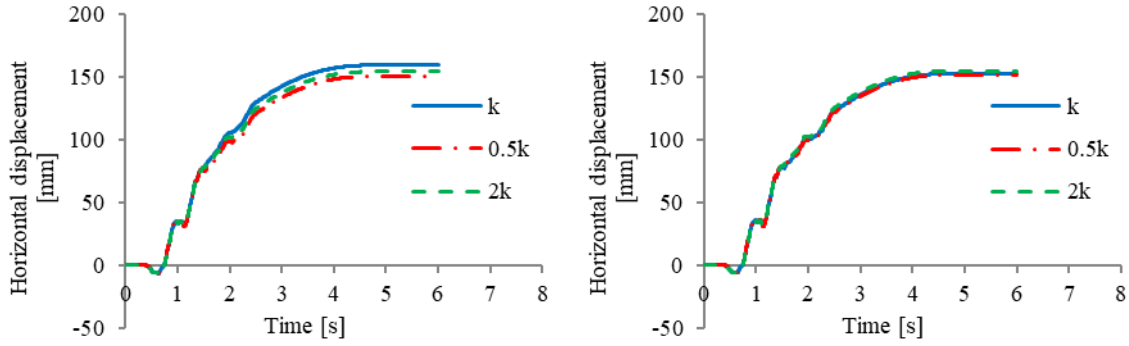

a) Interface model (1) b) Interface model (2)

Figure 5.23 – Dam model 1: Horizontal displacement at the crest of the dam

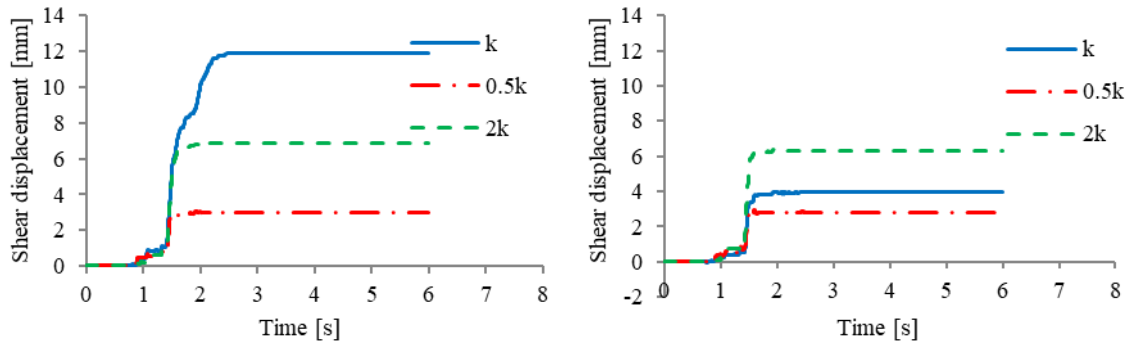

a) Interface model (1) b) Interface model (2)

Figure 5.24 – Dam model 1: Shear sliding displacement at the heel of the dam

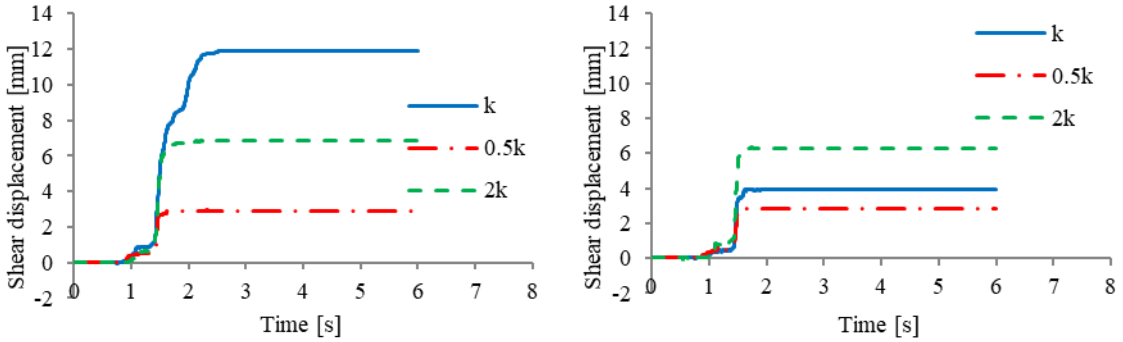

a) Interface model (1) at the dam toe b) Interface model (2) at the dam toe

Figure 5.25 – Dam model 1: Shear sliding displacement at the toe of the dam

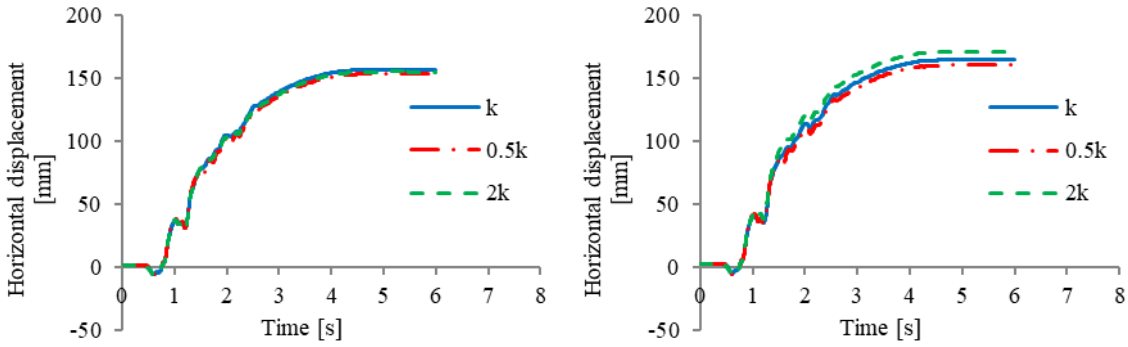

a) Interface model (1) b) Interface model (2)

Figure 5.26 – Dam model 2: Horizontal displacement at the crest of the dam

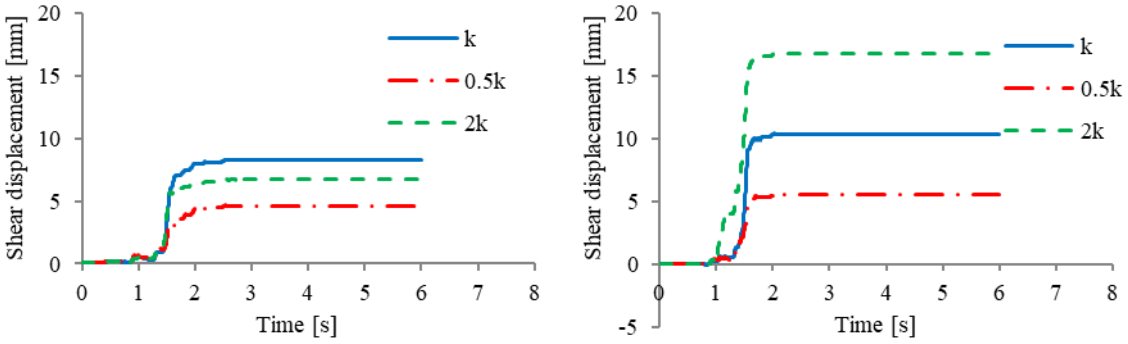

a) Interface model (1) b) Interface model (2)

Figure 5.27 - Dam model 2: Shear sliding displacement at the heel of the dam

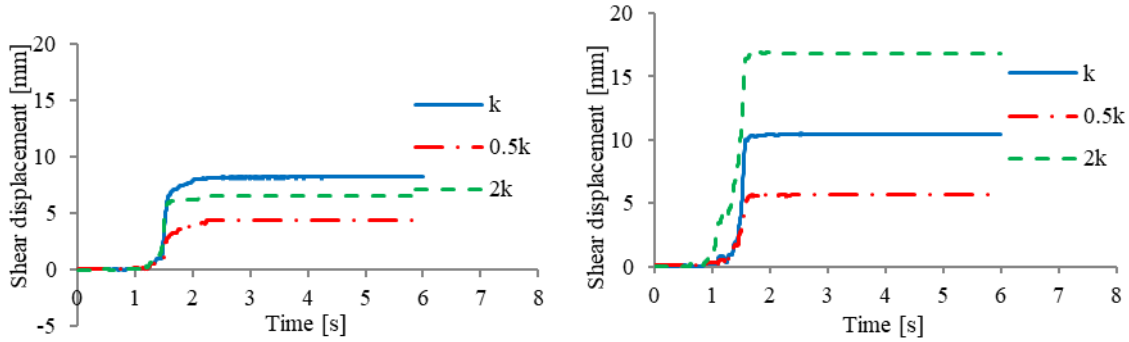

a) Interface model (1) b) Interface model (2)

Figure 5.28 - Dam model 2: Shear sliding displacement at the toe of the dam

Figure 5.29 and Figure 5.30 show the maximum shear sliding displacements at the toe of each dam obtained for the three PGA values and for the three normal interface stiffness values adopted. The numerical results corroborate the values from Figure 5.23 to Figure 5.28: for the elastic foundation (1), the highest shear sliding displacement occurs for the reference normal interface stiffness value, *kn*, followed by the double of the same value, 2 *kn* and by 0.5 *kn*. When the non-linear foundation model is adopted (2), the highest maximum shear displacement occurs when the highest stiffness value is adopted.

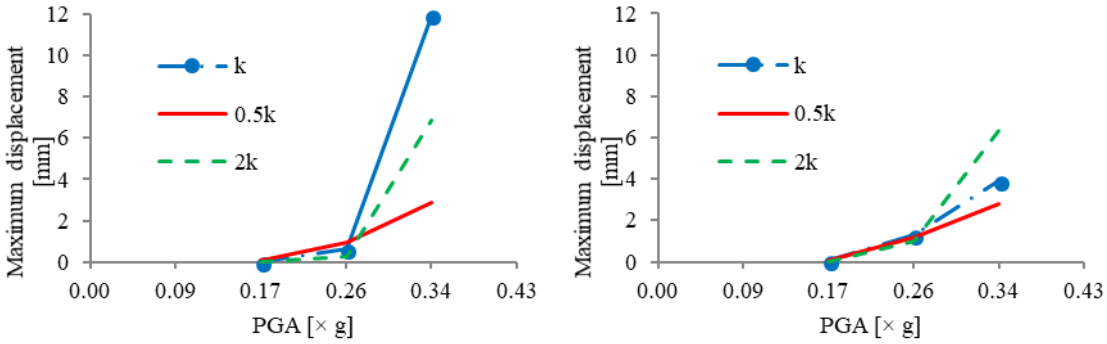

a) Interface model (1) b) Interface model (2)

Figure 5.29 – Maximum shear displacement at the toe of dam model 1

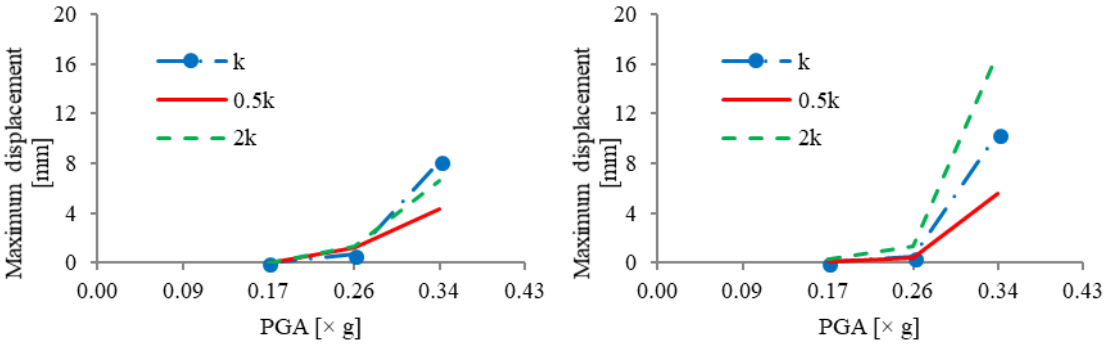

a) Interface model (1) b) Interface model (2)

Figure 5.30 - Maximum shear displacement at the toe of dam model 2

5.5.3 Rayleigh damping effect

In this section two different damping approaches are compared: Rayleigh damping and mass proportional damping only. Rayleigh damping considers both mass and stiffness proportional terms. In all cases, the damping constants, α and β are defined in order to have a critical damping ratio of 5 % at the fundamental response frequency, Table 5.6. The damping is only considered in the dam and in the fractured foundation. In the elastic foundation no damping is considered.

When an explicit solution procedure based on the central difference is adopted, mass proportional damping is usually assumed due to computational reasons, as the critical timestep needs to be further reduced when stiffness proportional damping is adopted. Given that Rayleigh damping is computationally very demanding, only the 15 m high dam, model 1, was studied. For this dam, the critical timestep with mass proportional damping simulation is equal to 7.7×10^{-6} s, and for the Rayleigh damping simulations a critical value of 2.5×10^{-7} s is required. Due to this increase factor of around 30, the simulations vary from around 4 hours, with mass damping only, to around 2.5 days on a Intel Core i7 @ 2.93 Hz when proper Rayleigh damping is considered.

The results comparing the shear sliding displacements under seismic loading obtained with Rayleigh damping and mass proportional damping only are presented from Figure 5.31 to Figure 5.34. Both foundation models are assessed, (1) and (2), for the three PGA values adopted: 0.17 g, 0.26 g and 0.34 g.

Given the Rayleigh damping curves, it can be concluded that when the most important failure mechanism is associated with rigid body motion the mass proportional term is more effective and when the failure mechanism is associated with a high stiffness mechanism such as rocking, the stiffness proportional term will be more influential.

The results obtained clearly show that it is not possible to anticipate which damping approach will lead to the maximum shear sliding displacement value under MDE loading. The main mechanism that triggers failure mechanism can change from low frequency, where mass proportional damping leads to smaller shear displacement value, to high frequency, where stiffness proportional damping is more effective. The results presented also show that at the design stage at least some numerical analyses should be performed with Rayleigh damping in order to assess the shear sliding displacement value that can occur for a given PGA value, Figure 5.31 c).

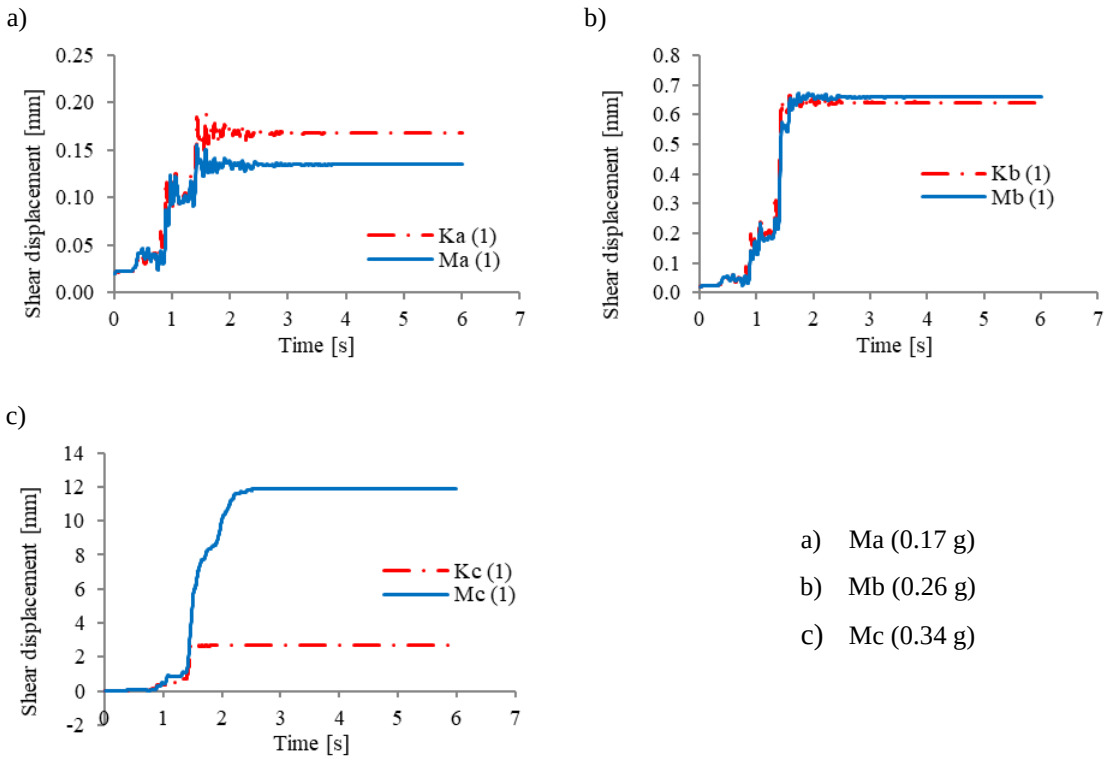

Figure 5.31 – Elastic foundation (1) shear displacement at the heel of the dam for Rayleigh damping and mass proportional damping

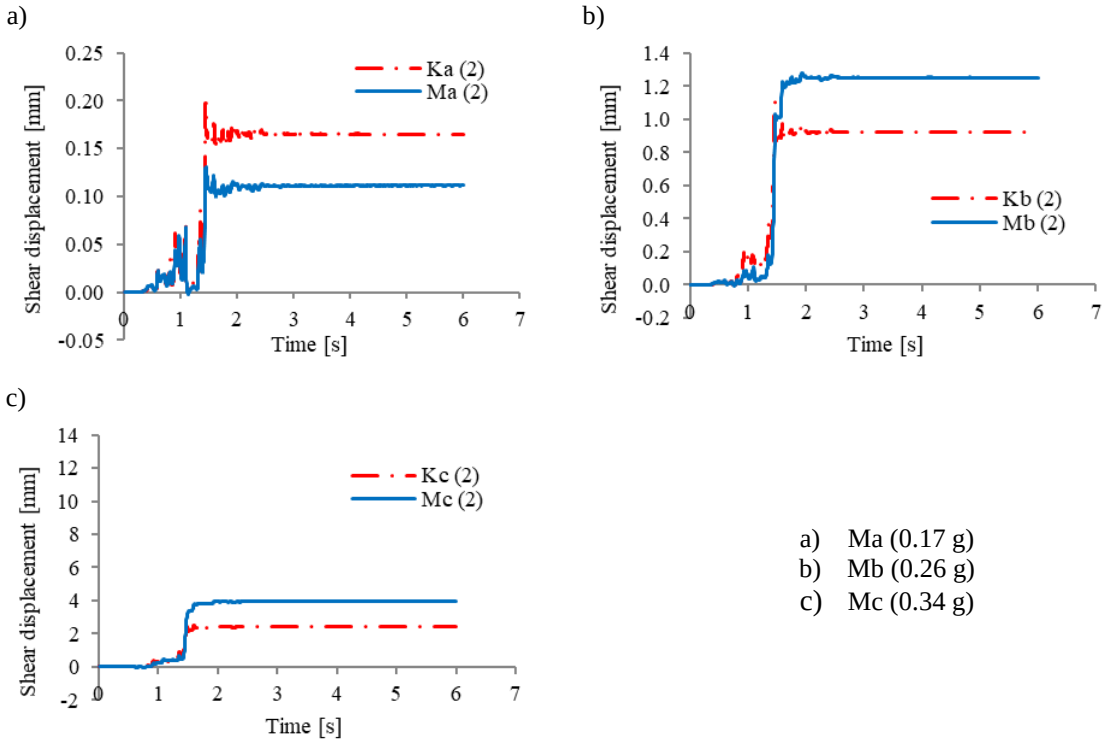

Figure 5.32 - Non-linear fractured foundation (2) shear displacement at the heel of the dam for Rayleigh damping and mass proportional damping

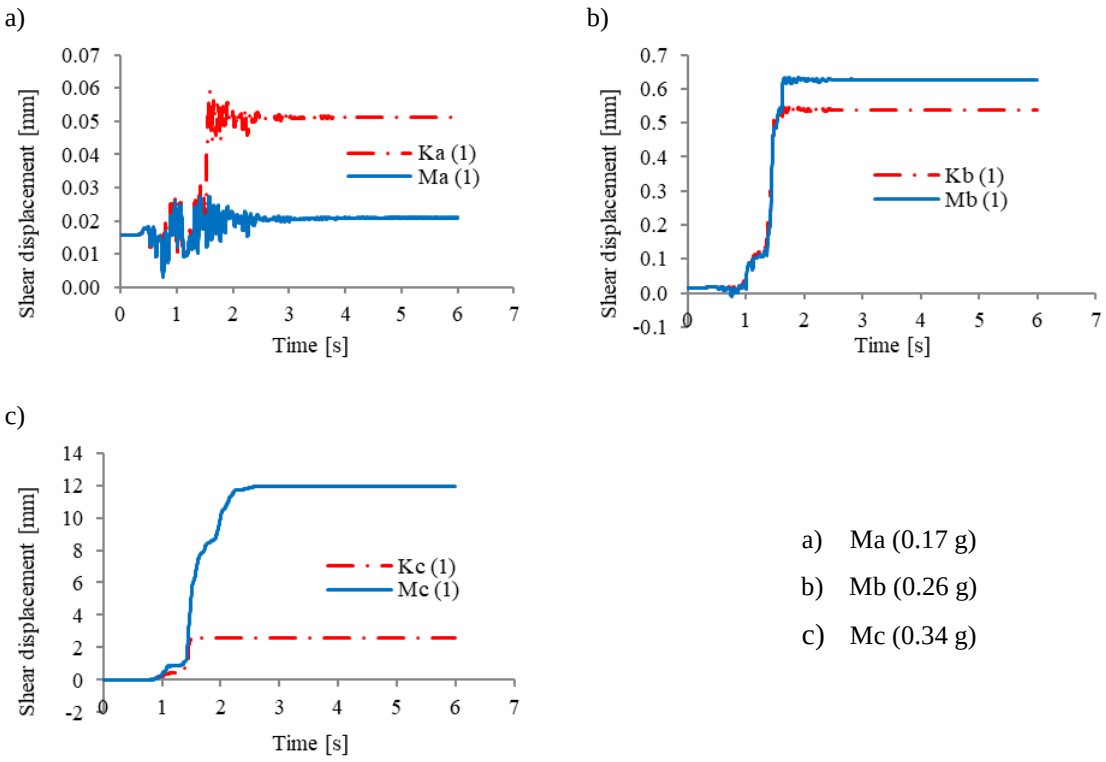

Figure 5.33 - Elastic foundation (1) shear displacement at the toe of the dam for Rayleigh damping and mass proportional damping

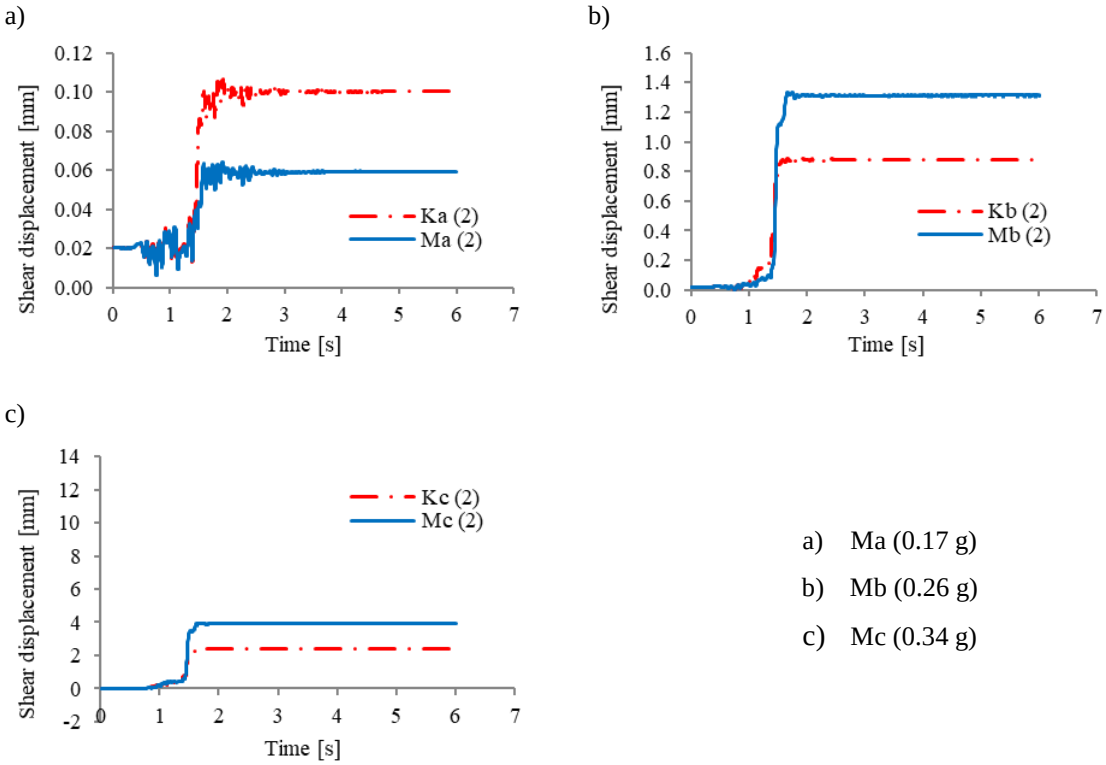

Figure 5.34 - Non-linear fractured foundation (2) shear displacement at the toe of the dam for Rayleigh damping and mass proportional damping

6 CONCLUSIONS

6.1 Summary and conclusions

The objective of this research was to assess concrete gravity dam stability for a shear sliding failure scenario under maximum design earthquake (MDE) loading, taking into consideration the hydromechanical behavior of the dam foundation.

The influence of explicitly considering the non-linear behavior of a fractured foundation, including the hydromechanical behavior, was assessed. The results presented show that it is not possible to anticipate whether a linear elastic foundation model leads to smaller or higher shear sliding displacements under MDE loading.

Analysis was carried out with dams of different height and foundations with the same discontinuity geometry. The results show that different dam geometries and different peak ground acceleration (PGA) values can lead to trends in the registered shear sliding displacement values, although it is not possible to anticipate the response. The results obtained clearly indicate that, if a fractured foundation is identified at design stage, both foundation models, elastic foundation and non-linear fractured foundation, should be carried out and the maximum displacement values should be considered for stability assessment.

A parametric study was also carried out in order to assess the influence of the dam/foundation interface stiffness values on the shear sliding displacement. Results presented lead to the conclusion that the interface elastic properties should be chosen with care. These properties may be derived from laboratory testing or by back calculation knowing the deformability and the joint structure of the rock mass and the deformability of the intact rock, or by using values proposed in the literature. The study that was carried out indicate that several parametric analysis should be done with at least a multiplying factor of two to four in order to assess shear sliding stability.

The effect of considering different damping approaches was also studied for the dam model 1. The study was not carried out for the dam model 2 due to computational costs associated with stiffness proportional damping, as the critical timestep needs to be strongly reduced when compared with the mass proportional damping. The results presented clearly show that a reduced number of simulations should be carried out with a Rayleigh damping approach, adopting the stiffness

proportional damping. As shown, it is not possible to anticipate which damping approach leads to higher shear displacement values. If mass proportional damping is adopted and the failure mechanism is strongly associated with rigid body motion, the shear sliding displacement value is lower than when Rayleigh damping is adopted. However, if the shear failure mechanism is associated with high frequency (rocking for example) the stiffness proportional damping is more effective and the shear sliding displacements is reduced.

6.2 Further developments

There are further possibilities for research in the topic presented in this thesis, such as:

- Perform similar analysis with different rock mass foundation discontinuity geometries;
- Consider additional dam geometries, for example 70 m and 100 m high gravity dams, in order to increase the results database;
- Adopt real seismic accelerations registers, which have been recorded in the vicinity of operating dams;
- Model the dynamic interaction between dam and water reservoir using a Lagrangian fluid formulation and compare the results with those obtained with the simplified Westergaard added mass approach adopted here.
- Implement and validate a numerical solution based on implicit numerical procedures, in order to reduce the computational times associated with the explicit procedure, especially when Rayleigh damping is considered.

REFERENCES

Anderson, C., Mohorovic, C., Mogck, L., Cohen, B., & Scott, G. (1998). *Concrete dams. Case histories of failures and nonfailures with back calculations. US Department of the Interior. USBR. DSO-98-05*.

Barla, G., Bonini, M., & Cammarata, G. (2004). Stress and seepage analyses for a gravity dam on a jointed granitic rock mass. In *Proceedings of the First International UDEC/3DEC Symposiums*. Bochum, Germany, 29 September -1 October 2004.

Barton, N., Bandis, S., & Bakhtar, K. (1985). Strength, deformation and conductivity coupling of rock joints. *International Journal of Rock Mechanics and Mining Sciences*, *22*(3), 121–140. https://doi.org/10.1016/0148-9062(85)93227-9

Barton, N., & de Quadros, E. F. (1997). Joint aperture and roughness in the prediction of flow and groutability of rock masses. *International Journal of Rock Mechanics and Mining Sciences*, *34*(3–4), paper No. 252.

Bozovic, A. (1989). Selecting seismic parameters for large dams. *Committee on Seismic Aspects of Dam Design*, *Bulletin 7*, 1–78. https://doi.org/Bulletin 72

Bretas, E. M. (2012). *Desenvolvimento de um modelo de elementos discretos para o estudo de barragens gravidade em alvenaria. Ph.D Thesis*. Universidade do Minho. Portugal.

Brown, S. R. (1987). Fluid flow through rock joints: the effect of surface roughness. *Journal of Geophysical Research: Solid Earth*, *92*(B2), 1337–1347.

Bureau, G., Keller, T. O., & McClelland, S. W. (2005). Nonlinear seismic analysis of Sweetwater main dam. In *Proceedings of the 25th USSD Annual Meeting and Conference*. Salt Lake City, USA, 6-10 June 2005, USSD.

Carvalho, A. (2007). *Modelação estocástica da acção sísmica em Portugal continental. Ph.D Thesis*. Instituto Superior Técnico. Portugal.

Casagrande, A. (1961). Control of seepage through foundations and abutments of dams. *First Rakine Lecture. Geotechnique*, *XI*(3), 161–182.

Cervera, M., Oliver, J., & Faria, R. (1995). Seismic evaluation of concrete dams via continuum damage models. *Earthquake Engineering and Structural Dynamics*, *24*(9), 1225–1245.

Darbre, G. R. (2004). Swiss guidelines for the earthquake safety of dams. In *Proceedings of the*

13th World Conference on Earthquake Engineering. Vancouver, Canada, 1-6 August 2004.

Farinha, M. L. B. (2010). *Hydromechanical behaviour of concrete dam foundations. In situ tests and numerical modelling. Ph.D Thesis*. Instituto Superior Técnico. Portugal.

Farinha, M. L. B., Monteiro Azevedo, N., & Candeias, M. (2017). Small displacement coupled analysis of concrete gravity dam foundations: static and dynamic conditions. *Rock Mechanics and Rock Engineering*, *50*(2), 439–464. https://doi.org/10.1007/s00603-016-1125-7

Hall, J. F. (2006). Problems encountered from the use (or misuse) of Rayleigh damping. *Earthquake Engineering and Structural Dynamics*, *35*(5), 525–545. https://doi.org/10.1002/eqe.541

Hart, R. D. (1995). An introduction to distinct element modeling for rock engineering. In *Analysis and Design Methods* (pp. 245–261). Elsevier.

ICOLD. (2016). Bulletin 148: Selecting seismic parameters for large dams, guidelines. *Committee on Seismic Aspects of Dam Design, International Commision on Large Dams*.

INAG. (2001). *Curso de exploração e segurança de barragens*. *Instituto da Água, Lisboa*.

Itasca. (2004). UDEC - Universal distinct element code, version 4.0, User's Manual. *Itasca Consulting Group. Minneapolis, USA.*

Lemos, J. V, Cundall, P. A., & Dasgupta, B. (1999). Earthquake analysis of concrete gravity dams on jointed rock foundations. *Distinct Element Modelling in Geomechanics. AA Balkema, Rotterdam*, 117–143.

Louis, C. (1969). *A study of groundwater flow in jointed rock and its influence on the stability of rock mass. Ph.D Thesis*. University of Karlsruhe (in Germany), English translation, Imperial College Rock Mechanics Research Report nº10, London, UK.

Louis, C., & Maini, Y. N. (1970). Determination of in situ hydraulic parameters in jointed rock. In *Proceedings of the 2nd International Congress on Rock Mechanics* (Vol. I, pp. 235–245). Belgrade, USA, 21-26 September 1970.

Lysmer, J., & Kuhlemeyer, R. L. (1969). Finite dynamic model for infinite media. *Journal of the Engineering Mechanics Division*, *95*(4), 859–878.

Monteiro Azevedo, N. (2003). A rigid particle discrete element model for the fracture analysis of plain and reinforced concrete. Ph.D Thesis. Heriot-Watt University. Scotland.

Monteiro Azevedo, N., Bretas, E. M., & Lemos, J. V. (2012). Shear sliding of gravity dams for maximum design earthquake analysis. In *15th World Conference on Earthquake Engineering*

(15WCEE) (pp. 1–10). Lisbon Portugal. 24-28 September 2012.

Monteiro Azevedo, N., & Farinha, M. L. B. (2015). Um modelo hidromecânico para análise de fundações de barragens gravidade em betão. *Geotecnia*, *133*(March 2015), 05–33.

Olsson, R., & Barton, N. (2001). An improved model for hydromechanical coupling during shearing of rock joints. *International Journal of Rock Mechanics and Mining Sciences*, *38*(3), 317–329. https://doi.org/10.1016/S1365-1609(00)00079-4

Portuguese National Committee on Large Dams. (1992). *Large dams in Portugal*. Lisbon, Portugal.

Priscu, R., Popovici, A., Stematiu, D., & Stere, C. (1985). *Earthquake engineering for large dams*. John Wiley and Sons, Inc., Bucarest.

Snow, D. T. (1965). *A parallel plate model of fractured permeable media*. *Ph.D Thesis*. University of California. USA.

Westergaard, H. M. (1933). Water pressures on dams during earthquakes. *Transactions ASCE*, *98*, 418–432.

Wieland, M. (2012). Seismic design and performance criteria for large storage dams. In *Proceedings of the 15th World Conference on Earthquake Engineering*. Lisbon, Portugal, 24-28 September 2012.

Wieland, M. (2014). Seismic hazard and seismic design and safety aspects of large dam projects. In *Perspectives on european earthquake engineering and seismology* (pp. 627–650). Zurich, Switzerland. https://doi.org/10.1007/978-3-319-07118-3

Wieland, M. (2016). Safety aspects of sustainable storage dams and earthquake safety of existing dams. *Engineering*, *2*(3), 325–331. https://doi.org/10.1016/J.ENG.2016.03.011

Wilson, E. L., & Khalvati, M. (1983). Finite elements for the dynamic analysis of fluid-solid systems. *International Journal for Numerical Methods in Engineering*, *19*(11), 1657–1668.

Wyllie, D. C., & Mah, C. (2004). *Rock slope engineering*. CRC Press, New York.

Internet pages

"Dam Safety: Stability and Rehabilitation of "Smaller" Gravity Dams" http://www.hydroworld.com/articles/hr/print/volume-30/issue-6/articles/dam-safety-stability-and-rehabilitation-of-smaller-gravity-dams.html. Visited in February 2018 (http://aemstatic-ww2.azureedge.net/content/dam/etc/medialib/new-lib/hydroreview/print-articles/volume-30/issue-6/14945.res/_jcr_content/renditions/pennwell.web.375.244.jpg)

"Dams generate hopes and fears". https://www.swissinfo.ch/eng/dams-generate-hopes-and-fears/30373166. Visited in April 2018 (https://www.swissinfo.ch/image/30361050/3x2/640/426/df922d4731fe7b65eaaf213f9adc4b72/Ht/9935460-30361066.jpg)

"Jinping Hydropower Station constructed partly by CGGC goes into full production". https://www.chinadaily.com.cn/m/gezhouba/2014-12/05/content_19033422.htm. Visited in April 2018 (https://www.chinadaily.com.cn/m/gezhouba/attachement/jpg/site1/20141205/286ed488c7d515ebb8480b.jpg)

"Roselend Dam". https://structurae.net/structures/roselend-dam. Visited in April 2018 (https://files1.structurae.de/files/photos/1927/france_2008/dsc_1020.jpg)

"Studying seismic activity: 'Epicentre zone shifting towards Warna reservoir" Koyna dam. http://indianexpress.com/article/india/studying-seismic-activity-epicentre-zone-shifting-towards-warna-reservoir-4950512/. Visited in April 2018 (http://images.indianexpress.com/2017/11/reservoir.jpg)

"The Dam that could not break" Austin 1911. pabook2.libraries.psu.edu/palitmap/AustinDam.html. Visited in February 2018 (http://pabook2.libraries.psu.edu/palitmap/AustinDamFront.jpg)

Barragens de Portugal. "Pocinho." Visited in November 2017 (http://cnpgb.apambiente.pt/gr_barragens/gbportugal/index.htm)

ICOLD. "Dams." Visited in November 2017 (http://www.icold-cigb.net.)

USSD. "Dam & Levee Education." Visited in November 2017 (https://www.ussdams.org/)

APPENDIX 1 – VERIFICATION AND VALIDATION OF THE PARMAC2D-FFLOW PROGRAM

In order to verify and validate the model adopted in the numerical work presented in the thesis, different structures were analysed, considering both mechanical and hydraulic effects. Hence, three different structures were analysed in the earlier stages of this thesis, with the main objective of studying the main subjects of this work.

The numerical results obtained with the Parmac2D-FFlow program were compared with the known analytical solutions. This study enabled not only to learn how to work with this structural analysis program, such as preparing data files, run the program and analyse the results, but also to get familiarised with the parameters that are considered in the mechanical calculations.

A1.1 Cantilever

Numerical model description

Figure A.1 shows the adopted geometry for the cantilever model. Its length is equal to 10 metres and its thickness is unitary. The initial block model was generated using the program UDEC (Itasca, 2004).

In terms of boundary conditions, the cantilever was considered fixed in the bottom, in both global directions. As shown in Figure A.1, the cantilever was considered in an upward position and was assumed that a force of 25 kN/m, equivalent to its self-weight, is applied in the -x direction.

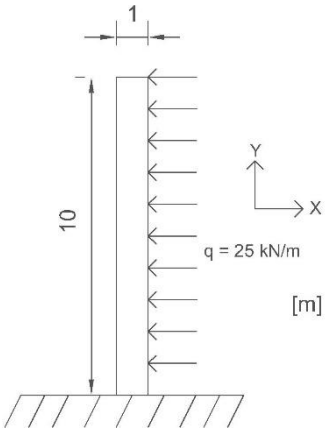

Figure A.1 - Model geometry of a cantilever

The mechanical characteristics adopted for the cantilever are presented in Table A.1

Table A.1 - Mechanical characteristics considered for the cantilever

Young's modulus E (GPa)	30.0
Poisson's ratio υ	0.15
Concrete density ρ_c (kg/m^3)	2.5
Gravity acceleration g (m/s^2)	10.0

In order to verify the performance of the calculation program, Parmac2D-FFlow, the results of displacements (δ), stresses (σ) and, in dynamic cases, the natural frequency (ω), are compared. The domain was discretized by triangular plane finite elements with an average edge length of 0.1 m.

The numerical model of the cantilever used in the program Parmac2D-FFlow, presented in Figure A.2 a), has 1946 triangular elements corresponding to a total of 1084 nodal points. Figure A.2 b) presents the deformed shape of the cantilever with the self-weight applied in the global -x direction.

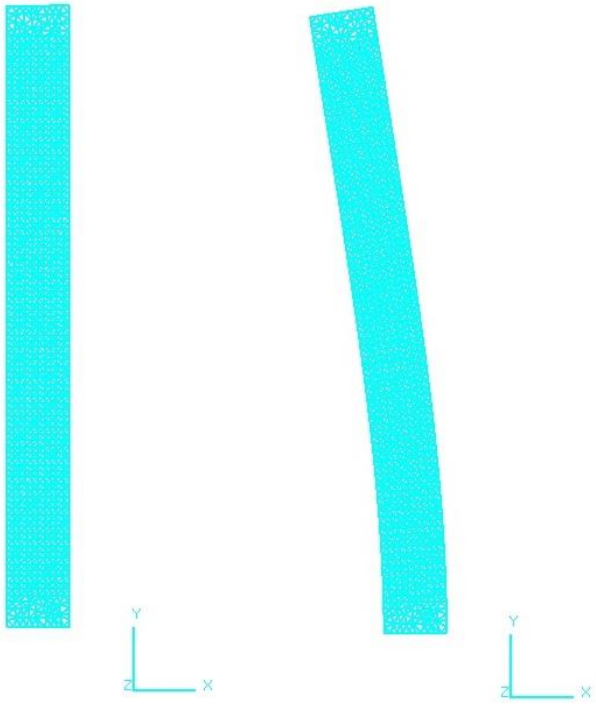

a) Undeformed shape b) Deformed shape

Figure A.2 - Cantilever numerical model

Analytical solution

From the beam theory, the displacement at the free end of the cantilever is given by:

$$\boldsymbol{\delta = \frac{1\ p\ l^4}{8\ E\ I}} \tag{A.1}$$

where *p* represents the applied uniform load (kN/m), *l* represents the length of the cantilever (m), *E* represents the Young's modulus (kPa) and *I* represent the moment of inertia (m^4).

Also, from the beam theory, the stresses at a given cross-section can be calculated using:

$$\boldsymbol{\sigma = \frac{M}{A\ z}} \tag{A.2}$$

where *M* is the bending moment (kNm), *A* is the cross-section area (m^2) and *z* is the distance from the compressed or tensioned fiber to the neutral axis.

The first natural frequency of a cantilever beam is given by:

$$\boldsymbol{\omega = 1.875^2 \sqrt{\frac{E\ I}{\rho\ A\ L^4}}} \tag{A.3}$$

where ρ is the material density (kg/m^3).

Another way to calculate the natural frequency is through the analysis of the displacement response over time in order to quantify the period (T), measured in seconds. The natural frequency in Hz is then given by the inverse of the period:

$$\boldsymbol{\omega = \frac{1}{T}} \tag{A.4}$$

Analysis of results

In this section, the analytical solutions are compared to the results obtained using Parmac2D-FFlow, in order to validate the model.

Table A.2 presents the displacement at the cantilever free end obtained numerically and the known analytical value based on the beam theory, equation A.1. The same table shows that the displacement results obtained using Parmac2D-FFlow are, as expected, similar to the analytical values. As also known from the finite element theory, the smaller the edge length adopted in the triangular plane element discretization, the closer the numerical results will be to the values obtained analytically.

Table A.2 - Displacement at the free end of the cantilever

Parmac2D-FFlow solution δ (mm)	11.9
Analytical Solution δ (mm)	12.5

The fundamental frequency was calculated using two different approaches: using equation A.3 or performing a time/displacement analysis by applying to the cantilever the self-weight in the global -x direction. The horizontal displacement over time is presented in Figure A.3.

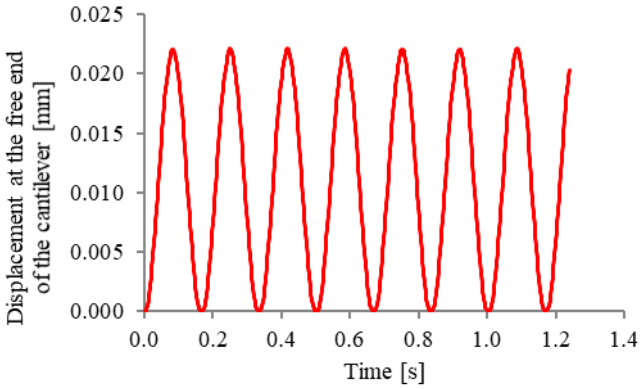

Figure A.3 - Displacement-time response

The period is the distance from two maximum or minimum points in the chart. This distance was measured in Figure A.3 and it was concluded that the period is equal to 0.173 s. Table A.3 presents the natural frequency values obtained numerically using Parmac2D-FFlow and the analytical value. Also presented is the natural frequency calculated using the Parmac2D-FFlow eigenvalue module.

Table A.3 - Results of the natural frequency for the cantilever

Parmac2D-FFlow solution (rad/s)	5.72
Analytical solution (rad/s)	5.59
Displacement/Time response solution(rad/s)	5.78

The fundamental frequency obtained using Parmac2D-FFlow, following an eigenvalue analysis, is higher than the analytical solution obtained using equation A.3. A better prediction would be obtained if the edge plane element length were reduced. Table A.3 also shows that the technique of finding the fundamental frequency through the analysis of the displacement response over time leads to a reasonable value.

A1.2 Frame

Numerical model description

Figure A.4 shows the adopted geometry for the frame model. Its length is equal to 12 metres and its height is 10 metres. The thickness of both the pillars and the beam is unitary. The initial block model was generated using the program UDEC.

The frame's pillars are made of material 1 and the beam is made of material 2. In terms of boundary conditions, two different situations are considered for the connection between the frame beam and the pillars: i) fixed and ii) simple supported. The numerical results are compared with analytic solutions.

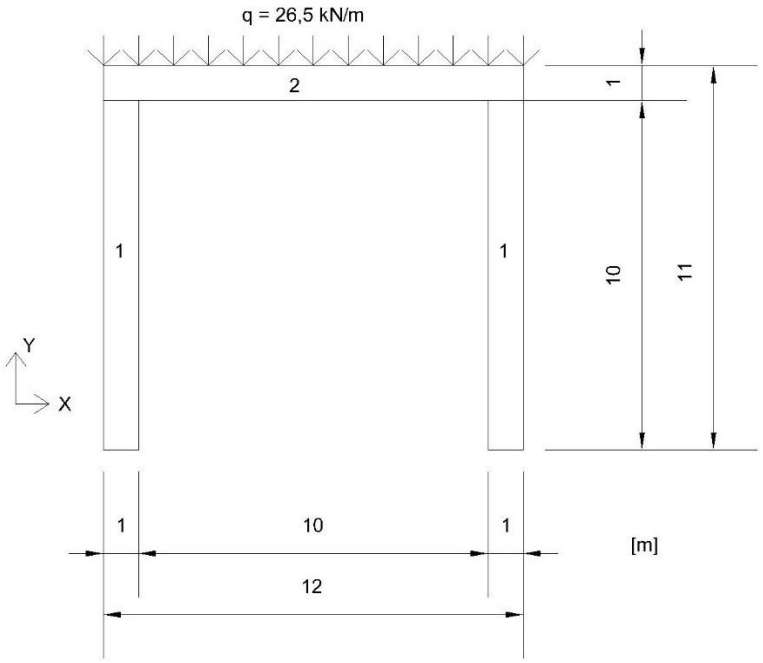

Figure A.4 - Model geometry of the frame

For the interface elements, a non-linear Mohr-Coulomb constitutive model with a tensile cut-off criteria was adopted. The normal and shear stiffnesses of the interfaces between the pillars and the beam are presented in Table A.4. The friction angle is equal to 35º and the cohesion and the maximum tensile stress are both equal to 2 MPa. It is important to highlight that the relation between these stiffnesses comes from the relation between the Young's modulus (E) and the shear modulus

(G), where G is equal to 0.4E, considering a general Poisson's coefficient equal to 0.2. Therefore, the shear stiffness is equal to 0.4 of the normal stiffness.

Table A.4 - Normal and shear stiffness of the interfaces

Interfaces between elements	*kn* [GPa/m]	*ks* [GPa/m]
Frame pillars/beam	40.0	16.0

As previously mentioned, the frame is composed by two different materials. The pillars are made of material 1 and the beam is made of material 2. Because the gravity acceleration is zero in the pillars, the load is applied on the beam in the -y direction and it is equivalent to the self-weight. The mechanical characteristics adopted for material 1 and material 2 are presented in Table A.5.

Table A.5 - Mechanical characteristics considered for the frame

Material	Material 1	Material 2
Young's modulus E (GPa)	20.0	40.0
Poisson's ratio υ	0.20	0.20
Density ρ (kg/m^3)	2.65	2.65
Gravity acceleration g (m/s^2)	0	10.0

In order to verify the performance of the calculation program, Parmac2D-FFlow, the results of displacements (δ) and stresses (σ) are compared. The domain was discretized by triangular plane finite elements with an average edge length of 0.1 m.

The numerical model of the frame used in the program Parmac2D-FFlow, presented in Figure A.5 a), has 6234 triangular elements corresponding to a total of 3470 nodal points and 20 interfaces between materials. Figure A.5 b) presents the deformed shape of the frame with the self-weight as the only load applied in the beam in the -y global direction.

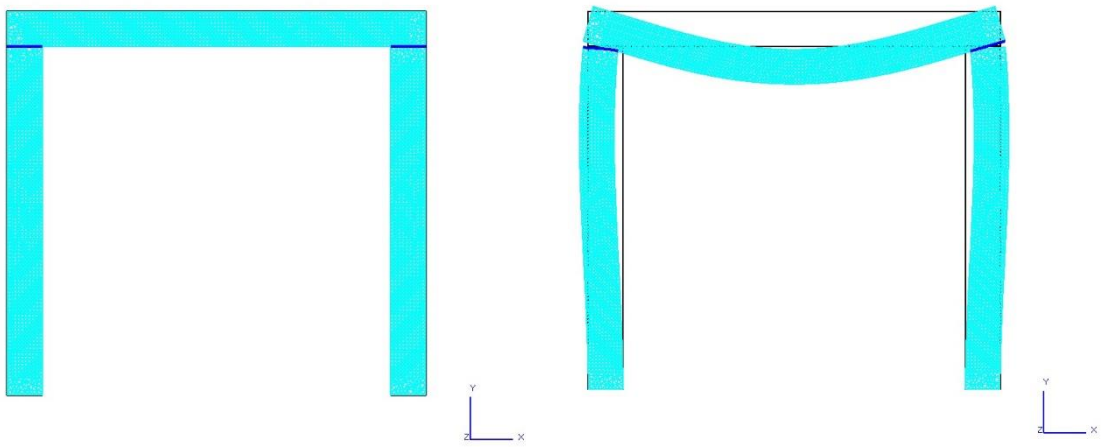

a) Frame undeformed shape b) Frame deformed shape

Figure A.5 - Frame numerical model

In Figure A.5 it is possible to observe the two interfaces connecting the pillars and the beam which, as previously mentioned, have a specified cohesion and maximum tensile stress. Figure A.6 presents an enlarge view of connection between one pillar and the beam.

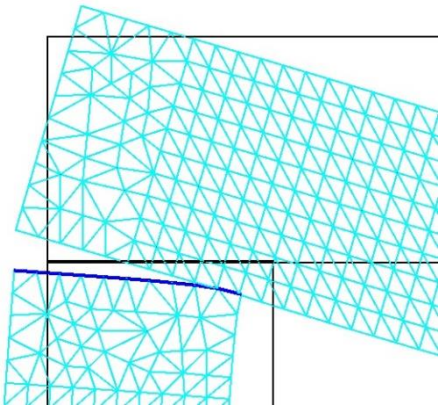

Figure A.6 - Interface between the pillar and the beam

Analytical solution

The displacement is computed at mid-span of the beam for the two models considered. In Figure A.7: a) both supports fixed and b) both supports pinned.

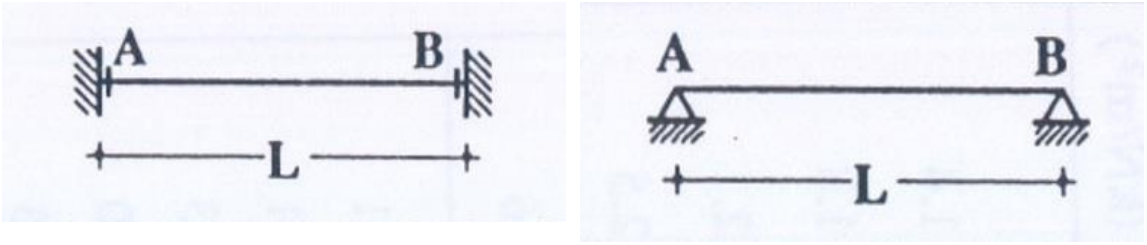

a) Double fixed beam b) Simply supported beam

Figure A.7 - Two models for the beam connection

When the beam is double fixed, the displacement from the beam theory is given by A.5 and when the beam is simply supported, the displacement from the beam theory is given by A.6.

$$\boldsymbol{\delta = \frac{1\ p\ l^4}{384\ E\ I}} \tag{A.5}$$

$$\boldsymbol{\delta = \frac{5\ p\ l^4}{384\ E\ I}} \tag{A.6}$$

where *p* represents the load applied (kN/m), *l* represents the length of the beam of the frame (m), *E* represents the Young's modulus (kPa) and *I* represent the moment of inertia (m^4).

From the beam theory, the stresses at a given cross-section can be calculated using:

$$\boldsymbol{\sigma = \frac{M}{A\ z}} \tag{A.7}$$

where *M* is the bending moment (kNm), *A* is the cross-section area (m^2) and *z* is the distance from the compressed or tensioned fiber to the neutral axis.

Analysis of results

In this section, the analytical solutions are compared to the results obtained using Parmac2D-FFlow, in order to validate the model.

Table A.6 presents the displacement at mid-span of the frame beam obtained numerically and the known analytical value based on the beam theory. As known from the finite element theory, the smaller the edge length adopted in the triangular plane element discretization, the closer the numerical results will be to the values obtained analytically.

Table A.6 - Displacement solutions at mid-span of the beam

Parmac2D (mm)	Analytic (mm)	
0.97	Double Fixed	Simply Supported
	0.43	2.15

As expected, the analytical solution obtained considering the beam with fixed supports is smaller than the solution obtained considering the beam simply supported. In equations A.5 and A.6 the rigidity is given by EI and it is inversely proportional to the displacement. Because a real structure is generally not fixed nor simply supported, the displacement solution obtained in Parmac2D-FFlow is a value between the two analytical solutions. This means that the real structure can be modeled using spring supports with stiffness varying between the fixed (EI = ∞) and simply supported (EI = 0) situations.

The stresses were calculated at mid-span of the beam, where the bending moment is maximum. The analytical stress results are presented in Table A.7. It is important to outline that, because the bending moment is positive, the stresses in the upper fiber of the section are compressed (negative) and the stresses in the lower fiber of the section are tensioned (positive). The same signs are observed in the results obtained from Parmac2D-FFlow.

Table A.7 - Stress solutions at mid-span of the beam

Stress solutions	Upper fiber	Lower fiber
Analytical (kPa)	-954	954
Parmac2D (kPa)	-1712	1687

Figure A.8 presents the stress field in the whole frame structure in the x direction. At mid-span of the beam, the stresses in the upper fibber are negative, in blue, and the stresses in the lower fibber are positive, in red.

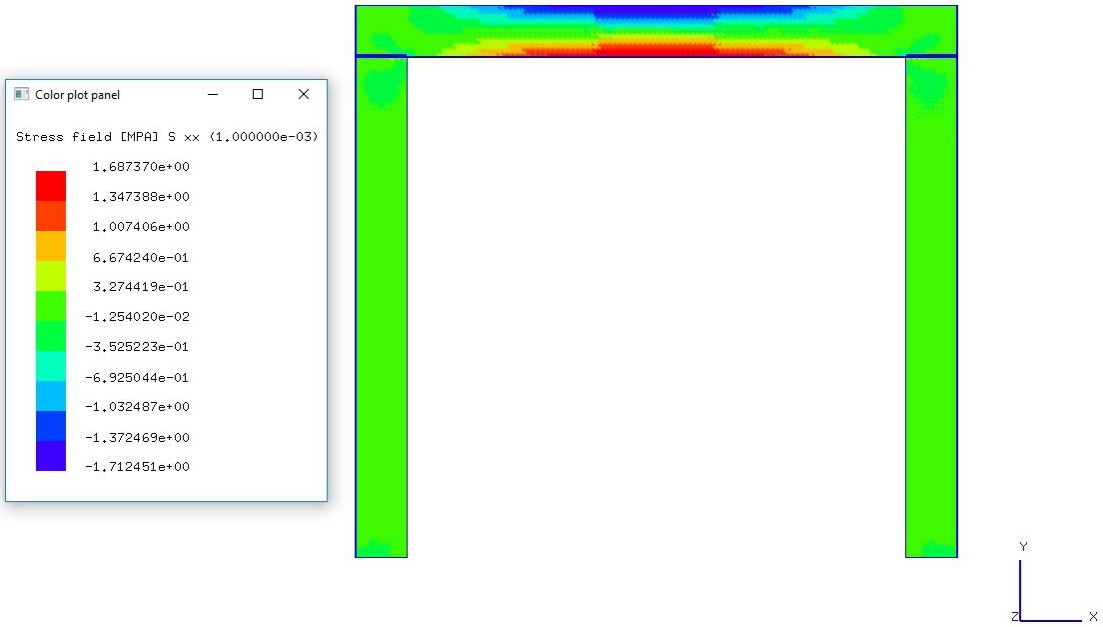

Figure A.8 - Stress field in the x direction

The analytical solution is calculated considering that the beam is simply supported. If the stresses were calculated considering that the beam was double fixed, the bending moment at mid-span would decrease, causing the stresses to decrease too.

Because the average length of the edge of the triangle element is equal to 0.1 m and the interface is 1 m long, each interface has 10 triangle elements and 11 nodes. Figure A.6 shows that, in the deformed shape, not every node of the interface is in contact with both the beam and the pillar. This loss of contact occurs because the interface tensile resistance is zero.

A1.3 Seepage along a horizontal discontinuity

Numerical model description

In order to validate the hydromechanical model, three cases are studied, using the same basic geometry. Four impervious blocks are considered, as shown in Figure A.9. The total length of the structure is 20 m and the height is equal to 10 m. Blocks are separated by a horizontal discontinuity, through which water can flow, and by two impervious vertical discontinuities. The initial block model was generated using the program UDEC.

For the first model, the self-weight is the only load applied and the permeability coefficient is homogeneous. The second model considers a possible heterogeneity below the central block by changing the permeability coefficient to twice the permeability factor previously adopted (Kce = 1.66×10^{-5}). The third model considers that there is an extra vertical load applied on top of the central block, equal to its self-weight.

Figure A.9 a) presents the geometry adopted for the first and second models. The difference between these models is that, in the second model the permeability coefficient is different. Figure A.9 b) presents the adopted geometry and loads for the third model. The load applied is equivalent to the self-weight of the block made of material 3.

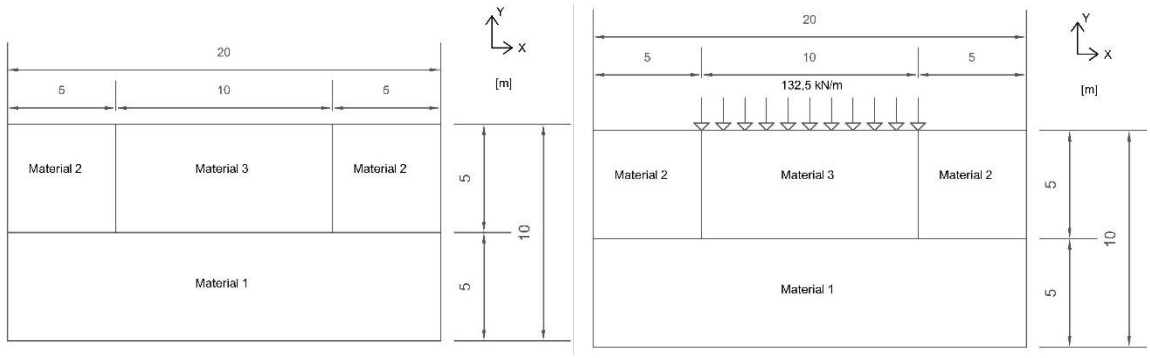

a) Model geometry and materials (first and second models)

b) Model geometry, materials and load applied (third model)

Figure A.9 - Model geometry

Considering the mechanical model, the vertical and horizontal displacements are equal to zero in the base of the model (base of the block made of material 1). In every other nodal point of the

model, the horizontal displacements and the rotations are fixed. Thus, the vertical discontinuities present only relative shear displacements.

The mechanical, interface and hydraulic characteristics considered are common for the three models. The blocks are made from three different materials. Material 1 is for the lower block, simulating a foundation, material 2 is for the left and right-side blocks and material 3 is for the central block. The mechanical characteristics adopted for all the materials are presented in Table A.8. Acceleration due to gravity is assumed to be 10.0 m/s^2.

Table A.8 - Material properties

Material	Material 1	Material 2	Material 3
Young's modulus E [GPa]	20.0	20.0	5.0
Poisson's ratio ν	0.18	0.2	0.2
Density ρ [kg/m^3]	2.65	2.4	2.65

For the interface elements, a non-linear Mohr-Coulomb constitutive model with a tensile cut-off criteria was adopted. The normal and shear stiffnesses for these elements are presented in Table A.9.

Table A.9 - Normal and shear stiffnesses of the interfaces

Interfaces between materials	*kn* [GPa/m]	*ks* [GPa/m]
Vertical interfaces	30.0	12.0
Horizontal interfaces	60.0	24.0

The hydraulic model considers that the hydraulic node on the left border has a piezometric head equal to 5 m and the piezometric head of the hydraulic node on the right border is equal to 0, causing seepage from the left to the right sides of the horizontal discontinuity.

Table A.10 presents the hydraulic characteristics of the horizontal discontinuity for model 1 and model 3. In model 2, the permeability coefficient is considered as twice of that assumed in the other two models, being equal to 1.66×10^{-5}.

Table A.10 - Hydraulic characteristics of the horizontal discontinuity

Seepage channel (SC)	k_w [GPa]	k_{CE} [$\times 10^8$ $MPa^{-1}s^{-1}$]	a_0 (mm)	a_{max} (mm)	a_{min} (mm)
Horizontal discontinuity	2.1	0.830	0.1668	$5 \times a_0$	$1/3 \times a_0$

In order to verify the performance of the calculation program, Parmac2D-FFlow, the results of the water pressure and flow were analysed, considering the influence of the horizontal discontinuity hydraulic aperture and permeability. The domain was discretized by triangular plane finite elements with an average edge length of 0.2 m.

The numerical model used in the program Parmac2D-FFlow, presented in Figure A.10, has 3486 triangular plane elements, corresponding to a total of 1949 nodal points and 101 interfaces between materials. The hydraulic model has 68 hydraulic nodes and 67 seepage channels. These values are common for the three models. Figure A.10 a) presents the mechanical model and Figure A.10 b) presents the hydraulic model.

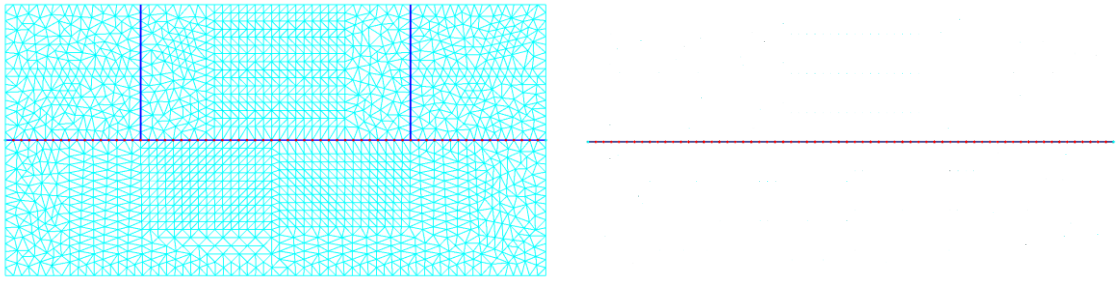

a) Mechanical model b) Hydraulic model

Figure A.10 - Numerical models of the horizontal discontinuity and the blocks

Figure A.11 a) presents the deformed shape of the blocks with the self-weight as the only load applied in the -y global direction. Because the block made of material 3 is heavier than the blocks made of material 2, the deformation is greater in the central block. Figure A.11 b) presents the deformed shape for model 3, in which there is a load applied on the top the central block equivalent to its self-weight.

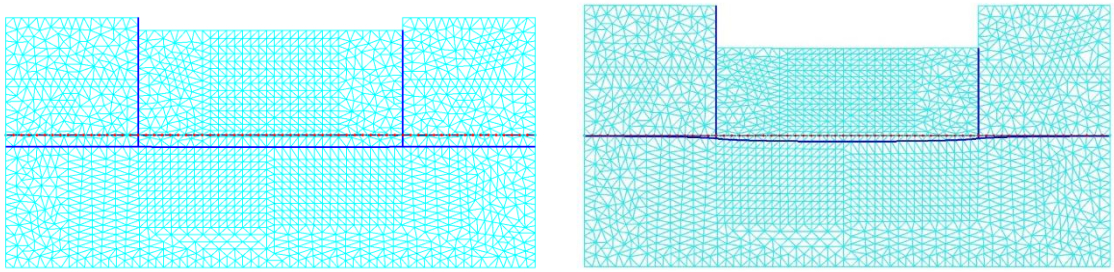

a) Deformed shape (first and second model) b) Deformed shape (third model)

Figure A.11 - Deformed shape of the blocks (magnified 1000 times)

Calculation procedure

The main goal is to analyse the influence that the permeability of a certain material has on the water pressure and flow.

In the first phase, the program performs a simple mechanical calculation only with vertical loads corresponding to the self-weight. Then, the program performs a coupled hydromechanical calculation. In model 3, the increase in vertical load applied on top of the central block is only considered in the second phase of the analysis.

Analysis of results

Figure A.12 presents the water pressure values along the horizontal interface for the three different models considered. The values obtained allow us to conclude that, for the first model, the water pressure decreases linearly along the interface, where the value on the left far end is equal to the imposed water pressure, 50 kPa, and in the right far end the water pressure is zero.

The hydraulic aperture of the seepage channels is the sum of the aperture at nominal zero normal stress plus the mechanical normal displacement resulting from the vertical loads applied. The initial aperture is set for every model and is constant, while the mechanical aperture varies, causing a slight variation in the aperture of the seepage channels. The flow that goes through the model is equal to 9.66×10^{-7} $m^3/s/m$.

For the second example, the water pressure does not follow a linear variation, resulting from different permeability factors assigned to the horizontal discontinuity. The flow that goes through the model is equal to 1.29 $\times 10^{-6}$ $m^3/s/m$. The flow that goes through model 3 is equal to 7.64 $\times 10^{-7}$ $m^3/s/m$. Because of the extra vertical load, the hydraulic aperture below the central block decreases and, therefore, the flow decreases as well.

For the third example and contrary to the previously model, the water pressure in the interface assigned to the central block decreases at a faster rate, because of the increase of vertical load in this section. The initial and final values of water pressure still correspond to the imposed water pressure in the calculation program, 50 kPa and 0 kPa, respectively.

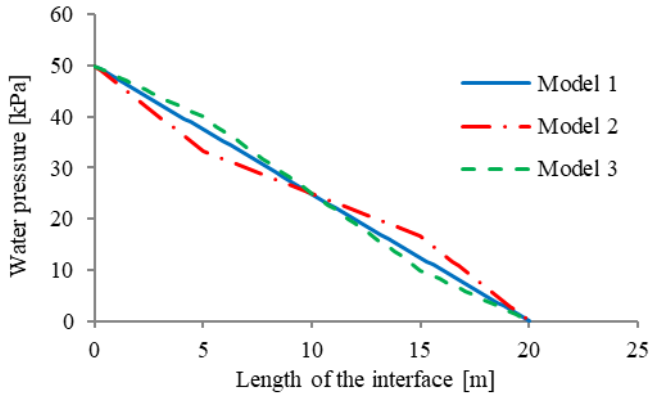

Figure A.12 - Water pressure variation along the horizontal interface for the three models

Figure A.13 presents the hydraulic aperture variation along the horizontal interface for the first model, where the self-weight is the only load applied and the permeability coefficient is homogeneous. It is easy to distinguish three different areas with different hydraulic apertures, being possible to conclude that the hydraulic aperture of the horizontal discontinuity in the area below the central block is smaller than the aperture below the left block, because the density of the central block is greater. The third distinct area corresponds to the hydraulic aperture values below the right block. In the transition zone between the central and the right block, the hydraulic aperture value increases to similar values to the other transition zone, between the left and central block, where it decreases at a similar rate. The negative values of the hydraulic aperture correspond to a closing of the aperture.

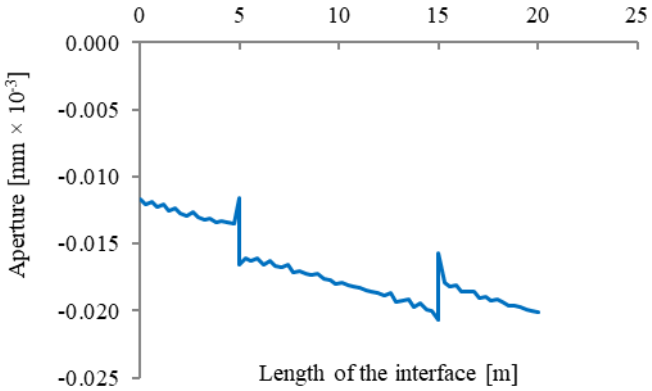

Figure A.13 - Hydraulic aperture variation along the horizontal interface for model 1

The chart of the hydraulic aperture for model 2 is similar to the chart of the hydraulic aperture for model 1, because the aperture values depend on the water pressure and the vertical loads applied, which are maintained the same for both models

As mentioned before, one of the factors that influence the variation in hydraulic aperture is the vertical load applied. Model 3 has an increase in the vertical load on top of the central block, corresponding to material 3 self-weight, which causes an abrupt decrease in the aperture, as shown in Figure A.14. Because the calculation program is a finite element method program, in the areas where there is a transition between materials, peak of values are observed.

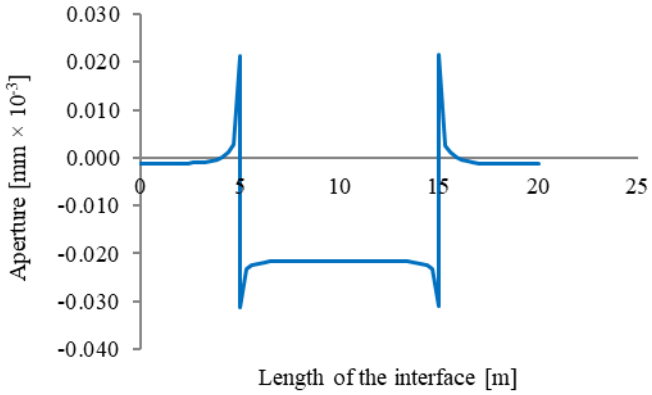

Figure A.14 - Hydraulic aperture variation along the horizontal interface for model 3